

Edge Stretch Performance of 6DR1 Aluminum in Typical Automotive Blanking Conditions

by

Nicholas Robert Kalweit

**A thesis submitted in partial fulfillment of the
requirements for the degree of
Master of Science in Engineering
(Mechanical Engineering)
in the University of Michigan-Dearborn
2017**

Master's Thesis Committee:

**Professor HongTae Kang, Co-Chair
Professor Ghassan Kridli, Co-Chair
Associate Professor German Reyes-Villanueva
Professor Pankaj Mallick**

ACKNOWLEDGEMENTS

I would first like to thank my thesis co-advisors Professor Ghassan Kridli and Professor HongTae Kang of the College of Engineering at the University of Michigan. They were a constant source of worthwhile guidance whenever I needed it most throughout the evolution of this paper.

I would also like to thank the experts at Ford Motor Company including Dr. Andrey Ilinich and Dr. George Luckey of Research and Development, as well as Dr. Evangelos Liasi of Stamping Engineering. The valuable mentorship I received from them was indispensable in the development of the ideas in this paper.

I must express great appreciation to my parents for supporting the years of study and research I devoted that culminated in this paper. I could not have accomplished what I have today without them.

Last, but certainly not least, I must express profound gratitude to my partner Genevieve Flaspohler for her unwavering support in my ambitions to explore the intricacies of graduate school, and perhaps most importantly for imparting great forms of wisdom and intellect on me that has reverberated in everything I have accomplished in this paper, and beyond.

TABLE OF CONTENTS

ACKNOWLEDGEMENTS.....	ii
LIST OF FIGURES	v
LIST OF TABLES.....	x
LIST OF APPENDICES.....	xi
ABSTRACT.....	xii
CHAPTER	1
I. Introduction.....	1
II. Literature Review.....	5
III. Materials and Methodology	15
3.1 Introduction.....	15
3.2 Material.....	15
3.3 Methodology.....	17
3.3.1 Specimen shape and dimensions.....	17
3.3.2 Trimming operation	18
3.3.3 Tensile testing procedure	20
3.3.4 EDM trimming baseline.....	20
3.3.5 Data analysis procedure	21
IV. Investigative Study #1: Optimal upper trim tool edge geometry.....	22
4.1 Introduction.....	22
4.2 Methodology	23
4.2.1 Trimming parameters.....	23
4.2.2 Design of experiment (DOE).....	24
4.2.3 Design vs. actual geometry of trim tool edges.....	25
4.3 Results.....	25
4.3.1 Total elongation data analysis.....	25
4.3.2 Multivariate, linear regression model	27
4.3.3 Probability distribution of optimal parameters	30
4.4 Conclusion	31
V. Investigative Study #2: Galling Study	33
5.1 Introduction.....	33
5.2 Methodology.....	33

5.2.1	Trimming parameters.....	34
5.2.2	Design of experiment (DOE).....	35
5.2.3	Design vs. actual geometry of trim tool edges.....	35
5.3	Results.....	36
5.3.1	Microscopic gall measurement procedure	36
5.3.2	Incremental edge damage	37
5.3.3	Observations of natural galling.....	38
5.3.4	Total elongation data analysis.....	43
5.3.5	Multivariate, linear regression model	44
5.3.6	Probability distribution of optimal parameters	47
5.4	Conclusion	48
VI.	Investigative Study #3: Lower trim tool gap study.....	50
6.1	Introduction.....	50
6.2	Methodology.....	51
6.2.1	Trimming parameters.....	51
6.2.2	Design of experiment (DOE).....	52
6.2.3	Design vs. actual geometry of trim tool edges.....	52
6.3.	Results.....	53
6.3.1	Microscopic gap measurement	53
6.3.2	Incremental edge damage	54
6.3.3	Total elongation data analysis.....	54
6.3.4	Multivariate, linear regression model	55
6.3.5	Probability distribution of optimal parameters	59
6.4	Conclusion	61
VII.	Conclusion	62
7.1	Summary	62
7.2	Implications.....	63
7.3	Limitations	63
7.4	Future work.....	63
REFERENCES	65

LIST OF FIGURES

Figure 1:	Schematic cross-sectional view of conventional trimming components and operation of a blanking die. (a) Blank panel before pad and upper trim tools make contact. (b) Partially trimmed blank panel after pad makes contact with part side and trim tools initiate shearing. (c) Fully trimmed blank where part is separated from offal.	2
Figure 2:	Microscopic images of sheared edge of aluminum sheet metal trimmed with typical blanking conditions and annotated with typical geometrical effects of shear trimming. Multiple perspectives of trimmed edge are shown: (a) side view, (b) isometric view, and (c) front view.....	2
Figure 3:	(a) Laboratory 0.9 mm 6DR1 aluminum sample trimmed with conventional sharp trimming conditions at 50x magnification. (b) Production 0.9 mm 6DR1 aluminum blank trimmed with dull upper at 50x microscopic cross-sectional.	3
Figure 4:	Comparison of true stress vs. true strain tensile testing data for 6DR1 aluminum and BH210 steel. Note that 6DR1 aluminum has flat stress-strain curve at medium to high strain. Stress and strain values are extrapolated with power law equation beyond total elongation from standard tensile test.	16
Figure 5:	Dimensions (in mm) of the half-dog bone specimen. Thickness was 0.9mm.	17
Figure 6:	Three baseline trimming conditions (a) clearance (% of sheet thickness), (b) support (degrees of offal rotation), and (c) trimming direction relative to material direction. 18	
Figure 7:	(a) Experimental press side view showing main operational trimming tools: pad, lower & upper trim, and support block. Press has pad closed on a half-dog bone specimen and the upper trim tool is in motion downward to complete a trimming operation. Shims behind the lower trim tool control clearance by positioning the lower trim tool relative to a fixed upper trim tool. (b) (c) & (d) shows microscopic images of partially trimmed aluminum sheet metal at the onset of fracture, showing different levels of offal rotation due to offal support with urethane blocks: (b) high , (c) low, and (d) no support.....	19
Figure 8:	Original and elongated (immediately before fracture) half-dog bone length used to calculate total elongation.	20
Figure 9:	Mean elongation of EDM samples in the three directions. Intervals represent the 95% confidence interval on the mean elongation value.....	20
Figure 10:	Multiple microscopic view of upper and lower trim tool edge imprints in 0.9mm blank in production blanking die, showing variation in tool sharpness. (a) Upper trim tool edge imprints. (b) Lower trim tool edge imprints.....	22
Figure 11:	Investigated trimming parameters. Clearance (a), Support (b), Shape (c), Direction (d).....	23
Figure 12:	(a) Experimental press side view (b) isometric view of trimming operation without pad or support shown.	24
Figure 13:	Both images represent the 0.00R trim tool edge by design. (a) Top view, microscopic image with actual measured trim tool edge geometry defined by contrast of lighting. (b) CMM contour tracing results showing cross-section edge profile.....	25

Figure 14: Elongation data for radius upper trim tool with high support trimming conditions. Mean EDM elongation shown as reference line in red. Interval lines represent 95% confidence interval on the mean elongation value.....	26
Figure 15: Elongation data for radius upper trim tool trimming with low support conditions. Mean EDM elongation shown as reference line in red. Interval lines represent 95% confidence interval on the mean elongation value.....	26
Figure 16: Cross-sectional metallographic images of trimmed edge from two trimming conditions showing the large geometrical imperfections in the low supported condition: (a) 0.04R – 50% clearance – High Support and (b) 0.04R – 50% clearance – Low Support.....	27
Figure 17: Scatterplot of elongation vs. radius of upper trim tool with regression lines: left pane high support, right pane low support. Only transverse direction (TD) data is shown. Data not fitted at 50% clearance, low support.	28
Figure 18: Main effect plot generated by regression model showing that radius of upper trim tool and clearance are significant and negatively proportional to elongation.....	29
Figure 19: Microscopic pictures of trimmed edge at 10% clearance, DD, and high support showing variability in damage to the grain structure of the sheared edge. Radius in the upper trim tool was (a) 0.04R (b) 0.08R (c) 0.14R (d) 0.45R. The largest distribution of damage was clearly visible for dullest edge at R0.45 in (d).	30
Figure 20: (a) Histogram of optimal radius elongation data with fitted 3-parameter Weibull distribution. (b) The corresponding probability plot with lower and upper bound 95% confidence intervals.	31
Figure 21: Gall marks occurring in the trimmed edge of production trimmed aluminum panels.	33
Figure 22: Investigated trimming parameters. Clearance (a), Support (b), Shape (c), Gall Depth (d), and Direction (e).....	34
Figure 23: (a) Experimental press side view (b) isometric view of trimming operation without pad or support shown, galling plate identified.....	35
Figure 24: Top view, microscopic image with actual measured trim tool edge geometry defined by contrast of lighting showing 0.25R trim tool edge by design.	36
Figure 25: Microscopic view of trimmed edge with gall mark from galling tool. Measurement of gall depth was performed with microscopic images for every half-dog bone specimen.	36
Figure 26: Interval plot of four incremental damage trimming conditions with 95% confidence interval for the mean shown. Elongation results show that 10%-0.00R-No Support condition produced the highest response and 30%-0.25R-Support condition produced the lowest response.	37
Figure 27: Microscopic pictures of trimmed half-dog bone edge, looking down the trim edge for each of the four major trimming conditions. (a) Shows the average edge quality of 10% - 0.08R – No Support trim condition with no natural galling occurring. (b) Shows the average edge quality of 30% - 0.08R – No Support trim condition with no natural galling occurring. (c) Shows the average edge quality of 10% - 0.33R – High Support trim condition with no natural galling occurring. (d) Shows the average edge quality of 30% - 0.33R – High Support trim condition with natural gall marks occurring. (e) Microscopic picture of artificial and natural galling occurring in the 30% - 0.33R – High Support trim condition, specifically showing how natural gall depth exceeded the artificial gall depth.	38

Figure 28: Visualizations of profilometer measurement data of half-dog bone sample trimmed edge at 10% - 0.08R/No Support condition. (a) 3D mesh plot and (b) contour plot clearly shows the effective gall mark penetrates entire trimmed surface.	40
Figure 29: Visualizations of profilometer measurement data of half-dog bone sample trimmed edge at 30% - 0.08R/No Support condition. (a) 3D mesh plot and (b) contour plot shows the effective gall mark partially penetrates the trimmed surface, approximately 75% of the total thickness. The partial gall penetration is due to the rollover and the angle of the fracture zone which eventually exceeds the galling depth and creates an unaffected zone.	40
Figure 30: Visualizations of profilometer measurement data of half-dog bone sample trimmed edge at 10% - 0.33R/High support condition. (a) 3D mesh plot and (b) contour plot shows the effective gall mark partially penetrates the trimmed surface, approximately 50% of the total thickness. The partial gall penetration is due to the rollover and the angle of the fracture zone which eventually exceeds the galling depth and creates an unaffected zone.	41
Figure 31: Visualizations of profilometer measurement data of half-dog bone sample trimmed edge at 10% - 0.33R/High support condition. (a) 3D mesh plot and (b) contour plot shows the effective gall mark partially penetrates the trimmed surface, approximately 30% of the total thickness. The partial gall penetration is due to the rollover and the angle of the fracture zone which eventually exceeds the galling depth and creates an unaffected zone. Natural gall marks are present, and can exceed the artificial gall mark both in depth and length.	41
Figure 32: (a) Half-dog bone tensile specimen with significant gall marks located by black marker lines and (b) identical tensile specimen after tensile test showing fracture initiation occurred at previously identified gall mark.	42
Figure 33: Pie chart percentile breakdown of fracture initiation location at four main trimming conditions: Rows represent four Clearance – Shape/Support conditions and columns represent four intended gall depths (in inches). Each pie chart is categorized by fracture location: “Artificial” represents fracture at galling tool location, “Natural ” represents fracture at a measured and identified notch outside the galling tool location, and “Other” represents fracture at unmeasured location outside the galling tool location.	43
Figure 34: Elongation data for all measured gall depths (micro-meters). Each panel represents a combination of support/upper trim tool shape and rolling direction conditions. Data points are categorized by clearance. Mean EDM elongation shown as reference line in red.	44
Figure 35: Scatterplot of elongation vs. gall depth with regression lines from regression model. Each panel represents shape/support trimming condition. Data within each panel categorized by clearance.	45
Figure 36: Main effect plot of individual trimming conditions, generated by regression model. 46	
Figure 37: (a) Histogram of optimal gall elongation data with fitted probability distribution (3-parameter Weibull). (b) The corresponding probability plot with lower and upper bound 95% confidence interval.	47
Figure 38: (a) DOP drawn shell with pre-mature split and (b) CAD model of trim tool inserts for blanking window opening with designed gaps shown.....	50

Figure 39: Five major categories of trimming conditions. Clearance (a), Support (b), Shape (c), Lower trim tool gap (d), and Direction (e).	51
Figure 40: (a) Experimental press side view (b) Isometric view of laboratory trim tools with the gap in the lower tool and arrows indicating trimming operation.	52
Figure 41: (a) Trim tool with radius geometry shown with two arrows that represent the two directions that microscopic pictures were taken and measured. (b) Top view, microscopic image with actual measured trim tool edge geometry defined by contrast of lighting showing 0.25R trim tool edge by design.	53
Figure 42: Microscopic view of gap width witness in the trimmed half-dog bone specimen with three measurements along the gap width shown.	53
Figure 43: Interval plot of four main trimming conditions with 95% confidence interval for the mean shown. Elongation results show that 10%-0.04R-No Support condition produced the highest response and 30%-0.14R-Support condition produced the lowest response.	54
Figure 44: Scatter plot of total elongation and gap distance based of trimming conditions. Panel columns represent rolling direction: (a) DD, (b), TD, and (c) LD. Rows of panels represent clearance and shape/support conditions.	55
Figure 45: Scatterplot of elongation vs. gap distance with regression lines from regression model. Each panel represents shape/support trimming condition. Data within each panel categorized by clearance.	56
Figure 46: Main effect plot of individual trimming conditions, generated by regression model.	57
Figure 47: Microscopic images of trimmed edge at gap location for each of the four major trimming conditions: (a) 10% - 0.04R – No Support, (b) 30% - 0.04R – No Support (c) 10% - 0.14R – High Support, and (d) 30% - 0.14R – High Support. Gap distance for all images were at maximum value of 0.004”	58
Figure 48: Percentage of fracture initiation located at gap in lower trim tool in half-dog bone specimen, shown in red, compared to random location outside gap.	59
Figure 49: (a) Histogram of optimal gall elongation data with fitted probability distribution (3-parameter Weibull). (b) The corresponding probability plot with lower and upper bound 95% confidence interval.	60
Figure 50: Total elongation (%) for EDM'd edge at different locations along coil in diagonal direction (DD).	69
Figure 51: Results of forward stepwise linear regression analysis for the radius upper trim steel shapes. Significant terms were considered when p-value <0.05.	70
Figure 52: Tabulated results of the final linear regression model for the radius upper trim steel shapes including ANOVA table, R ² value, and regression equations.	71
Figure 53: Diagnostic graphs of the residuals from the final linear regression model for the radius upper trim steel shapes.	72
Figure 54: Results of forward stepwise linear regression analysis for the radius upper trim steel shapes. Significant terms were considered when p-value <0.05.	73
Figure 55: Tabulated results of the final linear regression model for the radius upper trim steel shapes including ANOVA table, R ² value, and regression equations.	74
Figure 56: Diagnostic graphs of the residuals from the final linear regression model for the radius upper trim steel shapes.	75
Figure 57: Results of forward stepwise linear regression procedure for the radius upper trim steel shapes. Significant terms were considered when p-value <0.05.	76

Figure 58: Tabulated results of the final linear regression model for the radius upper trim steel shapes including ANOVA table, R^2 value, and regression equations. 77

Figure 59: Diagnostic graphs of the residuals from the final linear regression model for the radius upper trim steel shapes. 77

LIST OF TABLES

Table 1:	Novelis manufacturer data for coil material used in this study: (a) Coil identification including heat date to T4 temper, (b) mechanical properties for 6DR1 aluminum at front and back of coil, and (c) chemical composition (weight percent maximum, unless shown as a range) balance Al. LD/DD/TD refer to the angle of the trim line relative to material rolling direction.	16
Table 2:	DOE matrix	24
Table 3:	Comparison of design and actual measured geometry in trim tool edges for radius shapes.....	25
Table 4:	Elongation limits for optimal radius trimming conditions and various levels of risk	31
Table 5:	DOE matrix	35
Table 6:	Comparison of design and actual measured geometry in trim tool edges	36
Table 7:	Elongation limits for optimal radius trimming conditions and various levels of risk	48
Table 8:	Description of all conditions in full factorial DOE.....	52
Table 9:	Comparison of design and actual measured geometry in trim tool edges	53
Table 10:	Elongation limits for optimal radius trimming conditions and various levels of risk	60

LIST OF APPENDICES

Appendix A.....	69
Appendix B.....	70
Appendix C.....	73
Appendix D.....	76

ABSTRACT

This work investigates the edge stretch response of 6DR1 aluminum sheet trimmed at various conditions typical in blanking die operation. Three investigatory trimming parameters were studied in the experiment: upper trim edge shape, galling depth, and gap distance in the lower trim tool. Additionally, three other trimming parameters were included in various combinations to each of the investigatory parameters studied: clearance, sample orientation with respect to the rolling direction, and offal support. A sharp lower trim tool edge was maintained for all trimming conditions, as well as blanking die trimming standards of 90° trim angle and no shear angle were strictly adhered to. Electro discharge machined (EDM) custom tensile test specimens, referred to as half-dog bone specimens, were trimmed in a laboratory trimming die with various settings and edge-stretch was measured by total elongation of the trimmed specimens in a tensile test. A regression analysis was performed to determine statistically significant trimming parameters. Optimal trimming conditions were identified by fitting a range of levels for each trimming parameter that maximized elongation to a probability distribution, which provided feasibility from an engineering perspective. Statistical metrics, namely the mean and standard deviation of the distribution, were utilized to identify a robust lower limit expectation of elongation response with optimal trimming conditions. Clearance between upper and lower trim tools had the most significant influence on elongation: as clearance increased, elongation response decreased. Optimal clearance was defined as equal to or less than 30%. As upper trim tool radius increased, elongation response decreased. Optimal radius was defined as equal to or less than 0.14 mm. Galling had a significant reduction effect on elongation, where gall marks with increased penetration depth and length exhibited larger reductions in edge stretch response. Optimal gall depth was defined as equal to or less than 50 μm . Gap distance in the lower trim tool had no statistically significant effect on edge stretch. Measured elongations for optimal trimming conditions followed a left-skewed Weibull distribution with greater statistical probability of low elongation to failure than that predicted with a normal distribution.

CHAPTER I

Introduction

Shearing of ductile metals in automotive applications is a complex process which combines large plastic deformation and ductile fracture mechanics. The history of research on shearing ductile metals involves experimental, analytical, and numerical methods to investigate and optimize the quality of the trimmed edge. In early studies, steel was the most commonly investigated material. However, recently the automobile industry has adopted initiatives in light-weighting vehicles to improve fuel efficiency, and therefore aluminum has rapidly become an important focus of study. The study of material edge stretch (the measure of a material's ability to subsequently stretch after trimming operations) is an important factor to consider when determining optimal trimming conditions that maximize sheared edge quality, especially in automotive stamping processes where edge stretch is a common result of forming sheet metal. There is not a comprehensive understanding of the relationship between some important trimming parameters common in stamping processes (i.e. radius of upper trim tool, galling, and tool defects) and the corresponding edge stretch performance, especially in modern 6000 series aluminum. This is the main motivation for this investigation.

Typical shearing operations in automotive sheet metal stamping are blanking, piercing, and trimming. In contrast to other operations, such as stamping and bending where the aim is to deform the sheet plastically, these operations lead to the total rupture of the metal [1]. The focus of this paper is on blanking die operations. Blanking is a subset of trimming, where 90° trim angle and no shear angle are maintained in traditional blanking processes, although trimming is often referred to when discussing blanking parameters and mechanisms. To avoid confusion in terminology throughout this paper, unless given appropriate distinction, the use of trimming remains in context of traditional blanking operations. The conventional trimming process implemented in blanking is schematically illustrated in Figure 1 and involves three major die components: pad, upper trim tool, and lower trim tool. After the blank is placed in the die, the pad is lowered to clamp the blank and prevent its rotation during the trimming process, seen in Figure 1 (a). Then the upper trim tool

moves vertically down to contact the blank and begin the trim process, seen in Figure 1 (b). Finally, the upper trim tool continues downward until the blank is completely trimmed, and the offal is removed as scrap, seen in Figure 1 (c).

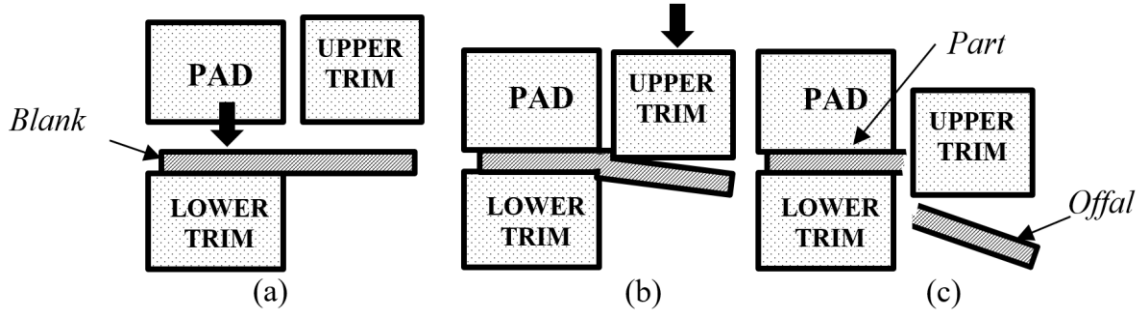


Figure 1: Schematic cross-sectional view of conventional trimming components and operation of a blanking die. (a) Blank panel before pad and upper trim tools make contact. (b) Partially trimmed blank panel after pad makes contact with part side and trim tools initiate shearing. (c) Fully trimmed blank where part is separated from offal.

The quality of the sheared edge, which considers geometrical imperfections and plastic strain damage, is controlled by several important parameters: trim angle, shear angle, pre-strain, clearance (distance between upper and lower trim tools), offal support, tool edge geometry, and trimming direction relative to the rolling direction. Typical sheared edge geometries are described according to Figure 2 using multiple microscopic images at various perspectives.

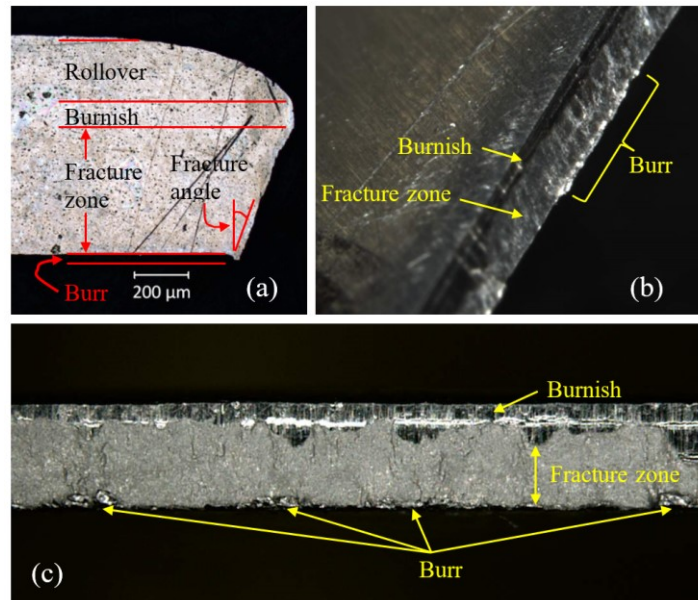


Figure 2: Microscopic images of sheared edge of aluminum sheet metal trimmed with typical blanking conditions and annotated with typical geometrical effects of shear trimming. Multiple perspectives of trimmed edge are shown: (a) side view, (b) isometric view, and (c) front view.

These sheared edge geometries are the result of four main stages. (1.) During initial contact, the upper and lower trim tools indent the blank, pulling down material from the upper surface into the die opening causing rollover. (2.) After continued travel of the upper trim tool, shear deformation takes place, creating the smooth burnished area due to contact with upper trim tool, and the sheared area continues to reduce causing working hardening. (3.) Ductile failure occurs near the cutting edge of the upper and lower trim tool and propagates through the blank thickness, creating a rough fracture zone. (4.) Depending on the nature of the fracture propagation, a burr or sliver can occur once separation of part and offal is complete.

In any shear trimming process, material along the sheared edge accumulates large amounts of damaging plastic deformation and geometrical imperfection. The extent of damage due to plastic deformation depends on the trimming conditions. This can clearly be seen by comparing metallographic cross-sectional images of the sheared edge for a lab sample trimmed with more optimal conditions, shown in Figure 3 (a), with a production blank trimmed with less than ideal trimming conditions, shown in Figure 3 (b). A damaged, highly strained edge can be a premature fracture initiation point, where material will stretch less before failing when compared to material with an undamaged edge.

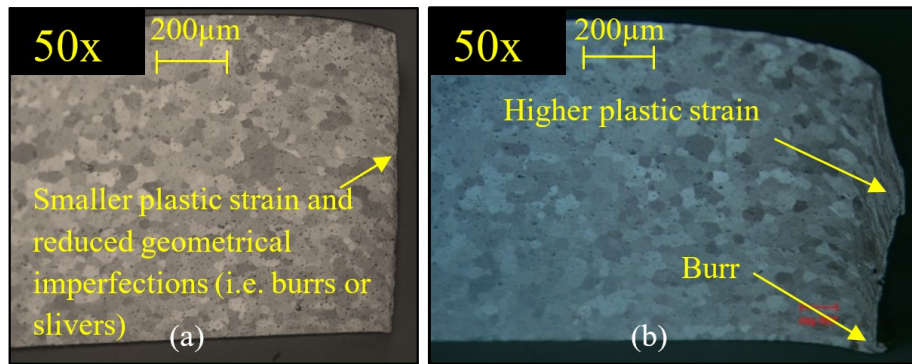


Figure 3: (a) Laboratory 0.9 mm 6DR1 aluminum sample trimmed with conventional sharp trimming conditions at 50x magnification. (b) Production 0.9 mm 6DR1 aluminum blank trimmed with dull upper at 50x microscopic cross-sectional.

The damage inherent in any shear trimming operation is an important factor to consider when designing blanking dies for aluminum automotive body parts, where aluminum coils are trimmed into blanks and the blanks are drawn into the designed part shape. In particular instances, the draw stage will apply stretching forces along previously trimmed edges (which is referred to as edge stretch or elongation). Among the numerous potential trim line developments in blanking, the inner closed loop sheared edges are typically the focus for evaluating panel formability due to high

potential for large magnitudes of edge stretch along the closed loop in subsequent forming operations. In general, due to the damage inherent in the trimming process, the edge-stretch of a trimmed blank will be less than what the nominal material properties predict.

In this thesis, three investigated trimming parameters were defined and studied: upper trim tool sharpness, galling depth, and lower trim tool gap distance. These parameters were selected because they are common in production blanking operations and exist in different magnitudes based on manufacturer standards, yet the explicit effects of these parameters on aluminum material edge stretch has not been studied. Therefore, the high level objectives of this study are to:

1. Find and analyze the aluminum edge stretch response of the three investigated trimming parameters (upper edge sharpness, galling depth, and lower gap distance) in combination with other baseline trimming conditions (clearance, material direction, and support),
2. Statistically determine a robust range of optimal trimming conditions that maximize material edge stretch.

In order to achieve these objectives, it was necessary to design an experiment that accurately replicates sheet metal blanking conditions and subsequent edge stretch mechanics. The experiment involved building modular trimming tools that replicated all three investigated trimming parameters, implementing a standardized tensile test to measure material edge stretch, and applying statistical tools to understand significant effects of edge stretch response.

CHAPTER 2

Literature Review

The earliest work pertaining to the subject of trimming sheet metal in shearing processes started in the early 1900's when a shearing process for several materials was developed experimentally by Izod [2] and Anthony [3]. Empirical research in the area of shearing continued through the mid-1900's with empirical approaches that demonstrated the possibility to interrupt shearing and blanking experiments, thereby study damage due to the blanking process. A popular paper by Chang and Swift [4] was among the first to provide detailed experimental information, like autographic punch force vs. punch displacement diagrams for several ductile metals in relation to various clearances. A later paper by Johnson and Slater [5] experimentally studied temperature, clearance (1-9%), and strain rate effects on the force and energy required in blanking. Findings included that the energy required for blanking increased at a large rate as clearance decreased below 5%, where especially high energy was needed for low clearances (~1%). The energy required for blanking at clearances greater than 5% seemed to decrease at a much lower rate, eventually flattening out near 9%.

Initial efforts to analytically understand fracture mechanisms during shearing process were derived by Noble and Oxley [6], where simple stress analysis techniques were used to identify the maximum hydrostatic stress in the deformed region of the specimen and that crack initiation occurs in those highly strained regions. Jouri and Jones [7] studied the empirical relations that relate deformation of aluminum and mild steel specimens to the impact energy of a drop mass, effectively determining that the punch penetration and amount of energy required to initiate crack to complete severance was higher for steel compared to aluminum. Using data from earlier works by Chang and Swift [4] as well as Johnson and Slater [5], Atkin [8] proposed a simple shear model to investigate the parameters at the maximum blanking load and postulated that the existence of a peak blanking load must be attributed to a plastic load instability and not fracture since cracks initiated after peak blanking load. Atkins applied the model and found two major trends: (1) As clearance increased, peak blanking load decreased and the maximum punch penetration at peak

blanking load increased due to material rotation. (2) The greater the material strain hardening exponent, n , the greater the maximum punch displacement and sheared zone width, while the lower the maximum shear strain at plastic instability point¹. Zhou and Wierzbicki [9] provided further work by developing a plane strain tension zone model of the shear zone that assumed large shear deformation present in blanking could be viewed as large tensile deformation, and found the maximum shear force and plastic work in blanking were within 10% of the experimental results of punch force vs. displacement diagrams. Slip line theory outlined by Johnson et al. [10] provided an analytical approach to calculate shearing loads required to cause plastic flow². Slip line theory makes several assumptions, such as plane strain, rate-independent, rigid- perfectly plastic³, and incompressible solid. Jimma [11] provided a plane strain theoretical analysis of the blanking process using slip line theory and found upper and lower limit on punch force at various clearances and punch penetrations. In summary, while these analytical models made it possible to approximately predict the maximum blanking force, punch penetration, and strain in the material, it was still not possible to predict the shape of the sheared surface due to the large complexity of the stress states and fracture mechanics involved in the blanking process.

The complete blanking process appeared to be too complex to fully describe with an analytical approach, so instead numerical finite element methods were utilized to simulate the blanking process. Difficulties arose since large, localized deformations present in the shear blanking process produced excessive element distortion in the numerical model. Another difficulty of the numerical approach is accurately predicting the ductile fracture, where either deletion or separation of elements must be utilized. The mechanism of ductile fracture in metals is widely known to follow a distinct order of events: nucleation, growth, and coalescence of voids at microscopic defects [12]. A range of fracture criteria have been studied by McClintock [13], Cockcroft and Latham [14], and Rice and Tracy [15]. These fracture criteria reflect the local damage accumulated in the material due to void growth. McClintock [13] studied cylindrical voids, while Rice and Tracey [15] studied spherical voids and found that in plastic materials there is a very strong inverse dependence of fracture strain on hydrostatic tension, where void growth rates are amplified by

¹ This effect was due to the fact that large values of n allow for greater capacity of work hardening that would diffuse the strain over a wider region, increasing the sheared zone width and allowing more punch displacement, while decreasing peak shear strain.

² Slip lines are defined as discontinuities in stress and velocity that occur across an infinitely thin line within the material. Two extremum principles establish an upper and lower limit to actual blanking loads that can be obtained using a statically admissible stress field and kinematical admissible velocity field, respectively.

³ A rigid-perfectly plastic solid is a hypothetical solid which, under any stress system, would be rigid when stressed below the yield point, that is, the elastic moduli are infinitely large, and exhibits no strain hardening after yielding.

hydrostatic tension. Numerical methods have shown that hydrostatic state of stress (also referred to as triaxiality⁴) occur in the sheared material near the trimming tool edge of blanking operations, leading to fracture initiation [16] [17] [18]. Several numerical simulations were used to simulate the blanking process in order to accurately predict fracture initiation and sheared edge geometry. Initial numerical studies correlated plain strain numerical simulation with experiments using a range of blanking force, penetration depth, sheared edge geometry, clearances, and materials, finding general qualitative correlation with experimental sheared edge geometry [18] [19] [20] [21] [22]. The most consistent correlation found by these studies was that increasing clearance led to multiple effects: more tool penetration depth necessary for fracture initiation, decreased blanking force, and increased geometrical effects to the trimmed edge like rollover and burr.

In summary of the reviewed literature so far, the evolution of the study of trimming sheet metal in shear included empirical, analytical, and numerical methods. The subsequent discussion of the reviewed literature addresses specific trimming parameters and the effect they have on the properties of the sheared edge.

Clearance is the distance between the upper and lower trim tools, usually reported as percentage of material thickness. Faura et al. [23] using numerical simulation with AISI 304 and Hamblin [24] using experimental punch-die experiments with 0.6% carbon steel investigated optimal clearances by minimizing the blanking force, maximizing geometrical quality in the sheared edge, and maintaining robustness to variations of tool wear. Findings showed that optimum clearance was near 10%. Initial studies by Chang and Swift [4] experimentally showed that increasing clearance increased the zone where plastic flow occurred. Hu et al. [25] used numerical FEA of half-dog bone specimens and found that increasing clearance qualitatively increased the amount of plastic deformation in the sheared edge; however quantitative magnitude is less clear. More quantitative measures were performed by Wang et al. [22] using plane strain numerical simulation of conventional hole blanking conditions in AHSS where increasing clearance increased the plastic deformation damage in the shear affected zone.

Slivers are thin, floating pieces of residual material that becomes dislodged from bulk material during the trimming process. Li [26] found that at appropriate cutting angles the surface quality becomes insensitive to the blade sharpness, and almost zero slivers and burrs are produced for large clearances and extremely dull blades. However, a later paper by Golovashchenko [17]

⁴ Triaxiality is defined as the ratio of hydrostatic and equivalent (von Mises) stress

suggested that slivers still occurred with trimming angles in a production environment and often cutting angle is dictated by part geometry, therefore applying trimming angles can add to die complexity and cost. Golovashchenko [17] with experimental microscopic imaging and Hu et al. [18] with a numerical simulation independently showed that crack initiation starts a small distance from the edge of the upper trim tool. This area was subject to high plastic deformation and hydrostatic stress state (due to high compressive pressure from the trimming edge), and was the location where a tongue-like formation can be created which can turn into a sliver.

Burrs are geometrical imperfections in the sheared edge and eliminating them from the blanking process is important to part quality. Li [26], Golovashchenko [17], and Golovashchenko and Ilinich [27] found that increasing clearance led to an increase of burr height. From these studies, the clearance at which burrs appear cannot be reliably inferred because clearance was not rigorously managed (claims of 5% and 10% clearances are clearly not held in the microscopic pictures). A more reliable study with improved experimental tools by Hu et al. [18] compared sheared edge quality in plane strain numerical simulation and experimental measurements of 6000 series aluminum, and found that increasing clearance beyond 21% led to increasing sheared edge rollover and significant burr size.

The effect of punch radius on sheared edge quality has also been studied. Hambli [24] and Li [26] studied the effect of punch radius on the evolution of the blanking force and the geometry of the sheared profile in steel, and found that increasing punch radius (0.00-0.25mm) led to increased burr height. Hu et al. [28] using numerical simulation aluminum hole expansion test found that increasing the punch radius from 0.02mm – 0.24mm qualitatively increases the amount of plastic deformation areas in the shear affected zone; however quantitatively the magnitude is less clear. Wang et al. [22], using plane strain numerical simulation of advanced high strength steel hole blanking tests, found that punch tool wear can greatly increase residual damage in the shear affected zone.

Most studies mentioned so far implemented the conventional trimming condition: sharp upper tool, sharp lower trim tool, and no support to prevent rotation of the offal. Golovashchenko [17] discovered that the conventional wisdom, that fracture initiation and propagation from both upper and lower sharp die edges should meet in middle, was only happening at low clearances (2-10%) where the strain distribution was symmetrical. However, at larger clearances, asymmetry in fracture initiation and propagation from trim edge was discovered; the crack from upper shearing

edge was more significant than crack at lower shearing edge. Golovashchenko hypothesized this asymmetry was caused by offal rotation, which caused additional tensile stress near the upper edge and compressive stress at the lower edge. Because most metals have higher ductility in a compressive stress state than in a tensile state, this effect would favor fracture initiation from the upper edge. Following this logic, Golovashchenko proposed an advanced trimming method to eliminate burrs and slivers from the asymmetrical, dual mechanism of fracture, where there would be a preference for fracture to occur on the lower sheared edge so the burr stays with the offal. The advanced trimming condition incorporated a “dull” R0.1mm upper trim tool, sharp lower trim tool, and a supporting force on the offal to prevent rotation during trimming operation, therefore promoting fracture to initiate from the lower shearing edge and propagate in the opposite direction to the material flow. This trimming technique was effective at eliminating burr formation on the part and sliver generation over a large range of clearances (2%-107%). Later studies by Golovashchenko and Ilinich [27] confirmed with steel alloys that increasing clearance in the advanced trimming condition restrained burr formation compared to conventional trimming conditions. In a following paper by Golovashchenko et al. [29] the mechanics of the advanced trimming method were supported with experimental and plane strain numerical simulation of advanced high strength steel that confirmed the change in fracture initiation point and the reduction in burr size when a dull upper, offal support, and sharp lower was used. A later study by Hu et al. [18] with plane strain numerical simulations of 6000 series aluminum confirmed that the advanced trimming technique matched the original findings in [29]. In a related finding by Hu et al. [28] where numerical simulations discovered that the hole piercing process was different from the straight edge trimming process in that the former has the axis-symmetric membrane constraint on the scrap button, while in the latter case, the scrap side was free to move without scrap support. It was concluded that in curved line trimming, there was inherent axisymmetric membrane constraint that acts to resist offal rotation, which reduced the onset of burrs similar to a physical supporting mechanism in the advanced trimming condition.

At this point, studies have only focused on optimizing sheared edge quality using experimental, analytical and numerical methods. However, no study yet mentioned has addressed the subsequent stretching operation of the trimmed edge, referred to as edge stretch or elongation. Initial studies into trimmed edge stretch indicated that aluminum sheet formability can be drastically reduced, up to 50%, as a result of poor blanking conditions [30].

Multiple experimental tests have been developed as a metric for determining material edge stretch, the most common being the hole expansion test or HET (circumferential trimming followed by a hole expansion operation) and the half-dog bone tensile test (straight-line trimming followed by a tensile test). Although both tests were intended to measure the material edge stretch, they did not yield the same results. For identical material at clearance of 15%, Golovashchenko and Ilinich [27] found that the half-dog bone specimen total elongation was approximately 33%, but Konieczny and Henderson [31] found HET elongation was approximately 55%. Chiriac [32] further explained this phenomenon with DP780 steel by indicating that the strain distribution along the perimeter of the hole during the HET can be substantially non-uniform and multiple localizations can occur. This might be why the hole expansion ratio was larger than the total elongation in half-dog bone tensile test where only one localization zone occurs.

The effect of burr size on material edge stretch has been studied in various cases. Experimental results by Le [33] studied the edge stretch of aluminum across a wide range of trimming parameters to show that geometrical imperfections in the form of burrs decrease edge stretch of trimmed aluminum: the larger the burr size, the lower the total elongation. Similar results were found for AHSS by Golovashchenko and Ilinich [27], as well as Chintamani and Sriram [34] where increasing burr size reduced material edge stretch. The effect of burrs on edge stretch from a fracture mechanics perspective was experimentally studied by Wang and Golovashchenko [35] where the edge stretchability of sheared aluminum sheet was studied across a wide range of trimming parameters by locally measuring strain with a circle grid analyzer. From observing these results, it can be inferred that when burrs are present, fracture initiates from the burr tip substantially earlier than would happen through the localization mechanism of fracture of standard tensile samples, therefore leading to reduced edge stretch compared to sheared edge without burr.

The effect of clearance on edge stretch has been found to be significant as reported in several studies. Chintamani and Sriram [34] as well as Konieczny and Henderson [31] performed hole expansion tests with various steels and showed that increasing clearance resulted in lower hole expansion ratio. Similarly, experimental results using half-dog bone specimens of aluminum by Le [33] and advanced high strength steel by Golovashchenko and Ilinich [27] found that increasing clearance led to lower total elongation. Hu et al. [25] implemented numerical simulations on the trimmed edge stretchability of aluminum and showed that small clearances (<10%) seemed to exhibit shear type failure (45° shear band) and larger elongations. Large clearances (>20%) tended

to show splitting type failure (perpendicular to trimmed edge) and lower elongations. Hu et al. [25] used numerical FEA of half-dog bone specimens and found that smaller clearances distributed a more uniform plastic strain distribution across the tensile specimen, which delays localization in the form of shear type failures, leading to higher edge stretch. Although smaller clearances seemed to increase edge stretch due to lower levels of plastic damage, there might be a limit to reducing clearance and expecting higher magnitudes of edge stretch. The well-known fine blanking process implements clearances less than 1% of material thickness and generates optimal sheared surface quality and dimensional accuracy. However, the process has been shown to exhibit extremely high levels of equivalent plastic strain in a concentrated shear zone in the sheared edge [16]. Lee et al. [36] compared the hardening effect on the fine blanked edge with the conventional blanked edge and found that the former process attains a hardness 1.7 times the original metal and the latter is only 1.3 times. This may be evidence that the deformation by the fine blanking process is more localized and severe than the conventional process, therefore affecting future stretching operations. Yu et al. [37] worked on developing an improved model for ductile fracture initiation criteria and propagation method by numerical simulation while investigating clearance and tool radii on the quality of sheared edge. The numerical results showed that decreasing clearance to around 1% of the sheet thickness led to an increase of stress variables (principle and mean stress) in the sheared edge.

The amount of plastic deformation in the trimmed edge seemed to be directly correlated with edge stretch response of trimmed specimens: an increase of plastic deformation likely reduces the material edge stretch response. Experimental results by Le [33] where aluminum half-dog bone specimen edge stretch was studied across ranges of prestrain (which effectively increased the baseline cumulative plastic deformation in sheared edge) and found that increasing prestrain prior to trimming process resulted in a reduction of edge stretch. Since previous findings discussed indicated that as increase of clearance and punch radius led to an increase of plastic deformation damage in the shear affected zone, it could be reasonable to conclude that increases of these trimming parameters could decrease edge stretch.

Edge stretch response from conventional compared to advanced trimming conditions has been studied for multiple materials. As previously discussed, the advanced trimming condition has been reliably successful at delaying burr formation at a wide range of clearances, which results in an increase in edge stretch response compared with conventional trimming conditions where burrs

are present. Unlike advanced trimming conditions, burrs arise in conventional trimming conditions when clearances are above 20% and largely contribute to reductions in edge stretch response [18]. Therefore, edge stretch findings generally support that at larger clearances, conventional trimming processes exhibit lower edge stretch results, most likely due to the significant burr present [27] [30] [35]. However, at smaller clearances, the difference between the edge stretch response of advanced and conventional trimming conditions seemed to be either statistically insignificant or the advanced condition seemed to perform worse. Golovashchenko and Ilinich [27] used straight edge trimming of AHSS half-dog bone samples and found that the advanced trimming method maintained higher elongation over higher clearance range (15%-35%) compared to conventional trimming; however, in a lower clearance range (<15%), the difference in edge stretch seemed inconclusive. Furthermore, Ilinich et al. [38] used straight edge trimming of DP500 half-dog bone specimens and found that the edge stretch for advanced trimming conditions was lower than conventional trimming conditions at low clearances, especially in the transversely trimmed direction. In the previously discussed results of Golovashchenko [30] as well as Wang and Golovashchenko [35] where higher edge stretch was found in AA6111-T4 sheet for advanced trimming parameters at all clearances, the clearance was not rigorously controlled (overshooting clearance exaggerated burr size, leading to underestimated edge stretch in conventional conditions). Additionally, in the case of Golovashchenko's [30] results, only one trimming direction was used. Studies show that trimming angle relative to rolling direction makes a significant effect on material edge stretch and would be necessary to make robust conclusions on edge stretch response to specific trimming parameters [33] [35] [38]. At lower clearances (near 10%) the distribution of plastic deformation in the sheared edge might be greater using advanced trimming conditions compared to conventional conditions because in the absence of burrs, the majority of damage would be caused by the dulled upper in the advanced trimming condition. Hu et al. [18] used plane strain numerical simulation and experimental methods to compare sheared edge quality of conventional and advanced trimming conditions, qualitatively confirming that for similar clearances the amount of plastic deformation and size of the shear affected zone is larger with the advanced trimming condition. In consideration of the aforementioned observations in the literature, the difference in the edge stretch response at low clearances (<10%) between the advanced and conventional trimming conditions seemed inconclusive.

In summary of the reviewed literature, the material edge stretch response of trimmed sheet metal in shear has been found to be directly affected by trimming conditions which cause a range of geometrical imperfections and plastic deformation in the sheared edge. Previous research widely supports that an increase in cumulative damage to the sheared edge (plastic deformation and geometrical imperfections) leads to a decrease in material edge stretch. More specifically, findings show that increasing clearance leads to increases in plastic deformation and geometrical imperfections like burrs, ultimately reducing edge stretch response. Additionally, findings showed that at low clearances (<10%), conventional trimming seemed to exhibit an inconclusive difference in edge stretch compared to advanced trimming conditions, however at larger clearances the conventional trimming conditions generated burrs which largely reduced edge stretch response. The dull upper in the advanced trimming condition controlled fracture propagation to remove burrs at larger clearances which improved edge stretch response, but at low clearances has been qualitatively shown to cause more plastic deformation in the sheared edge, which might infer a reduced edge stretch response. Attempts to use numerical methods to simulate edge stretch mechanisms have been limited, and most authors acknowledge fairly large element sizes in their 3D model that could not capture local behavior and microstructure based factors.

Gaps in the reviewed literature on sheared edge quality and edge stretch response in typical trimming conditions are numerous and have been expressed to the best of the author's ability from studying the past literature. Most notably, there have been no statistically-driven studies on edge stretch response from a wide range of trimming conditions with interaction effects to make robust predictions of edge stretch and optimal trimming conditions, especially for 6000 series aluminum. Additionally, there has been no comprehensive, quantitative study on the effect of a wide range of trimming tool edge radii on 6000 series aluminum edge stretch. Furthermore, the experimental trimming studies in the reviewed literature exhibited either no offal support (where offal rotated freely) or complete offal support (where offal rotation was completely restricted from rotation). Neither of these situations are representative of actual offal rotation in typical blanking of large circumferential holes where axisymmetric stiffness inherently supports offal rotation to some degree, leading to offal rotations somewhere between HET, highly supported advanced trimming conditions, and unsupported conventional straight edge trimming conditions. Furthermore, there has been no detailed study on the effect of common geometrical defects in the sheared edge, other than burrs, on edge stretch, such as galling and trim tool defects.

This thesis investigated the edge stretch response of a 6000 series aluminum sheet trimmed at various conditions not previously experimentally studied in detail, namely a more representative offal support scenario, a range of upper trim edge radii, galling depths, and gap distances in lower trim tool. Additionally, statistical tools including multiple linear regression and probability distribution fitting was used to generate robust conclusions on edge stretch response from the trimming conditions tested.

CHAPTER 3

Materials and Methodology

3.1 Introduction

For all subsequent chapters, the sheet metal material used while studying the three investigated trimming parameters (upper trim tool sharpness, galling depth, and lower trim tool gap distance) was identical. Experimental methodologies were structurally similar and described in this chapter. Methodology deviated in the finer detail to accommodate variables unique to the investigated trimming parameters, in which case was described in detail in respective chapters.

3.2 Material

6000 series aluminum alloys combine several desirable properties for automobile applications, such as good corrosion resistance, good weldability, excellent surface properties, and a relatively low cost [39]. The material used in this study was 0.9 mm 6000 aluminum sheet, generically designated as 6DR1 and tempered to T4 specifications⁵. This alloy has an enhanced bake response and is typically used for outer vehicle body panels that require good formability and improved dent and ding resistance. All material used in this study was leveled⁶. The mechanical properties and chemical composition supplied from the manufacturer are shown in Table 1. 6000 series aluminum exhibits lower edge stretch response compared to steel alloys used in the automobile industry. The difference can partially be attributed to that fact that 6000 aluminum has almost no strain hardening at medium to high strain (flat stress–strain curve) compared to steel, shown in Figure 4. Lack of appreciable work hardening causes the maximum elongation to be extremely sensitive to geometrical imperfections of the sheared edge because strain localization at these locations can no longer be compensated for by strain hardening.

⁵ Solution heat treated and naturally aged to a substantially stable condition.

⁶ Although there is no forming operation prior to the blanking operation, small amount of pre-strain in the coil is introduced by leveling. Since no statistically significant difference had been found between locations within the coil (Appendix A), the leveling factor was not accounted for in the study.

Table 1: Novelis manufacturer data for coil material used in this study: (a) Coil identification including heat date to T4 temper, (b) mechanical properties for 6DR1 aluminum at front and back of coil length, and (c) chemical composition (weight percent maximum, unless shown as a range) balance Al. LD/DD/TD refer to the angle of the trim line relative to material rolling direction.

(a)		(b)		(c)	
Properties		Properties	LD/DD/TD	Elements	Wt%
Coil #	1500385001	Yield Strength Front, (MPa)	113/108/105	Si	0.50-1.00
Grade	6DR1	Yield Strength Back, (MPa)	113/108/107	Fe	0.30
Heat Date	7/5/2015	Tensile Strength Front, (MPa)	223/221/216	Cu	0.20
Test Date	7/7/2015	Tensile Strength Back, (MPa)	224/223/219	Mn	0.15
Lube Date	7/5/2015	Uniform Elongation Front, (%)	22/25/23	Mg	0.40-0.80
		Uniform Elongation Back, (%)	22/24/ -	Cr	0.10
		Properties		Zn	0.10
		r_0 Front	0.79	Ti	0.10
		r_{45} Front	0.53	Others (each)	0.05
		r_{90} Front	0.67	Others (total)	0.15
		r_0 Back	0.66		
		r_{45} Back	0.37		
		r_{90} Back	0.64		

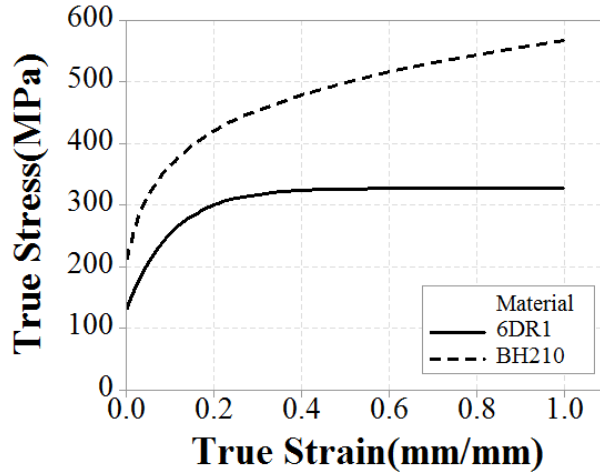


Figure 4: Comparison of true stress vs. true strain tensile testing data for 6DR1 aluminum and BH210 steel. Note that 6DR1 aluminum has flat stress-strain curve at medium to high strain. Stress and strain values are extrapolated with power law equation beyond total elongation from standard tensile test.

The material properties were valid for a period of 30 to 90 days following T4 heat treatment due to negative formability effects of natural age hardening⁷. All experimental processes have been completed within the allowed natural age hardening window of the 6DR1 material. All material not in immediate experimental use was stored at sub-zero (< -30°C) temperatures to delay age hardening and to make sure tested material was of consistent age.

⁷ Natural age hardening occurs at room temperature where hardening in material properties, like increased yield strength, is caused by metallurgical changes. More specifically, hardening is caused by precipitation of fine particles in the aluminum microstructure which dislocation theory explains that the strain field associated with precipitates resists deformation by impeding dislocation motion [39].

3.3 Methodology

The general experimental methodology followed in each subsequent chapter on the investigative trimming parameters is outlined in this section. In summary, prescribed tensile test specimens extracted from a 6DR1 aluminum coil were trimmed in a laboratory press with custom modular trimming tools that could be adjusted to accurately meet the criteria for specific trimming parameters. Trimmed specimens were then pulled to failure under tension using a universal testing machine. For each tested specimen, the total elongation to fracture data was recorded. Microscopic and metallographic pictures were used when necessary to investigate and support findings. Total elongation data were analyzed with statistical tools to provide statistically significant conclusions to optimal trimming parameters that maximize edge stretch.

3.3.1 Specimen shape and dimensions

In accordance with the designed experiment, half-dog bone specimens were electro discharge machined (EDM'd) from a coil of 0.9 mm thick 6DR1 aluminum. The specimen geometry used in this study, shown in Figure 5, was designed by Le [40] to ensure fracture within the gauge⁸. The notches on either side of the specimen matched the alignment pins on the lower trim tool to ensure consistent trimming alignment.

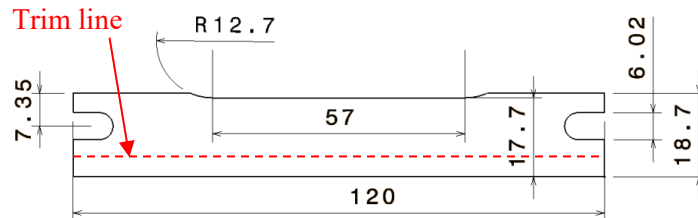


Figure 5: Dimensions (in mm) of the half-dog bone specimen. Thickness was 0.9mm.

Inner, closed loop sheared edges in blanking are typically the focus for evaluating panel formability due to high potential for large magnitudes of edge stretch along the inner in subsequent forming operations. However, unlike the curved sheared edge of the inner closed loop sheared edge, the half-dog bone specimen used in this study has a straight sheared edge. The use of straight edge, half-dog bone specimens to evaluate edge stretch in blanking can be justified as a conservative metric for evaluating edge stretch. Specifically, the alternative hole expansion test

⁸ The specimen geometry was based on ASTM E8 and designed from an iterative method to ensure fracture initiates either as a result of localization throughout the width of the sample, or from crack initiation at the sheared edge.

(HET) with curved sheared has been shown to exhibit substantial non-uniform strain distribution during edge stretching operations. In this instance, multiple localizations occur causing a large elongation result that may over estimate capability of the much larger diameter blanked holes in production. Therefore, the straight edge half-dog bone test has been shown to be a more conservative estimate of edge stretch than the HET [32].

3.3.2 Trimming operation

The experiment included three investigatory trimming parameters (upper edge sharpness, galling depth, and lower gap distance) in combination with other baseline trimming conditions (clearance, material direction, and support). Since the focus of this study was on the blanking process, the blanking die trimming standards of 90° trim angle and no shear angle were strictly adhered to. A sharp ($<0.05\text{mm}$ radius) lower trim tool was used in this study. The lower trim tools are always designed sharp but can be poorly manufactured, worn out in use, or damaged. These effects were not considered and will be a subject of a future study. The baseline trimming parameters included in this study are described in Figure 6 below.

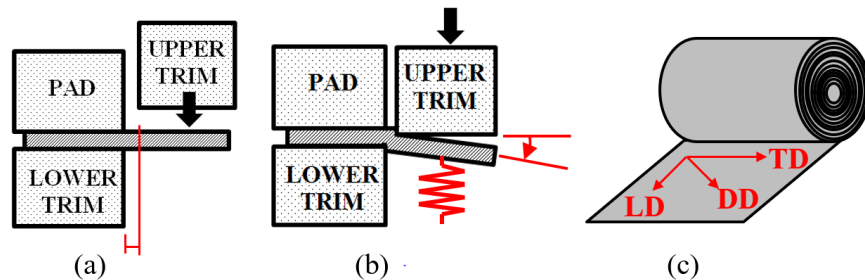


Figure 6: Three baseline trimming conditions (a) clearance (% of sheet thickness), (b) support (degrees of offal rotation), and (c) trimming direction relative to material direction.

Clearance, shown in Figure 6 (a), is the distance between the upper and lower trim tools, reported in % of the sheet thickness. Offal support, shown in Figure 6 (b), describes the amount of offal rotation allowed before the complete fracture of a trimmed sheet. Although the inner closed loop offal is not supported externally in a blanking die⁹, it is inherently stiffer than the straight offal of the half-dog bone samples. The half-dog bone samples used in this study without support do not have the same bending stiffness, and will rotate substantially more before trimming is complete. Therefore, a supporting force was necessary to control rotation of the half-dog bone offal to mimic inner slug punching during blanking. Trimming action relative to the grain direction

⁹ An external support would make slug evacuation very difficult in this case.

of the coil, shown in Figure 6 (c), is defined in three discrete directions: longitudinal direction (LD), diagonal direction (DD), and transverse direction (TD).

Experimental D2 steel (60 HRC) trimming tools were fabricated in a die shoe providing sufficient tooling alignment for uniform clearance during installation and maintaining consistent clearance with stiff guiding strategies to prevent increase of clearance during operation. The order of events of the laboratory trimming press was as follows: (1.) A half-dog bone specimen was inserted into the lower trim tool guide pins, (2.) the pad contacted the half-dog bone specimen and compressed it against the lower trim tool, and (3.) the upper trim tool continued downward and trimmed the half-dog bone specimen, shown in Figure 7. Shims were placed behind the lower trim tool to control trimming clearance between the upper and lower trim tools. The support block, shown in Figure 7 (a), was made out of two grades of polyurethane that had different stiffness, allowing for control of offal rotation. Figure 7 (b) (c) and (d) shows controlled offal rotations of partially trimmed specimens from different levels of support. The stiffer, high support block shown in Figure 7 (b) allowed for 0° of offal rotation. The softer, low support block shown in Figure 7 (c) allowed for approximately 8° of offal rotation. The no support condition, shown in Figure 7 (d), freely allowed offal to rotate before fracture, resulting in maximum offal rotation.

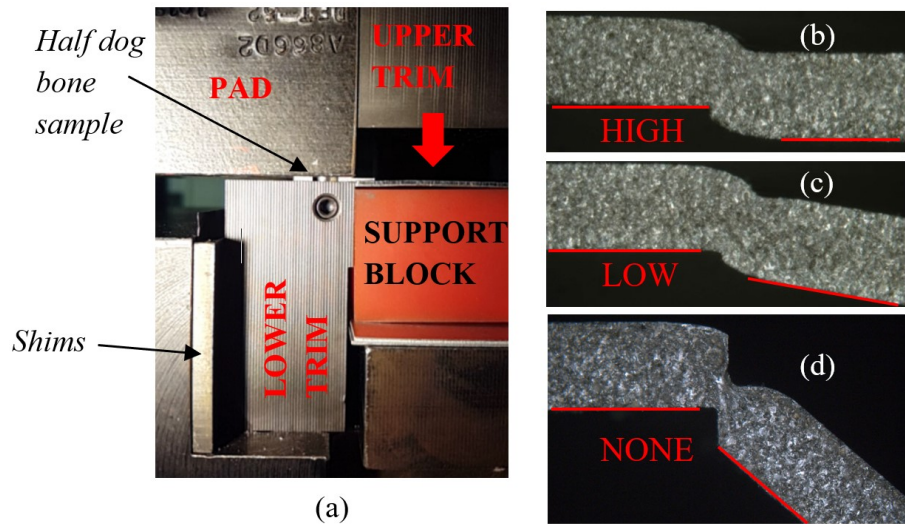


Figure 7: (a) Experimental press side view showing main operational trimming tools: pad, lower & upper trim, and support block. Press has pad closed on a half-dog bone specimen and the upper trim tool is in motion downward to complete a trimming operation. Shims behind the lower trim tool control clearance by positioning the lower trim tool relative to a fixed upper trim tool. (b) (c) & (d) shows microscopic images of partially trimmed aluminum sheet metal at the onset of fracture, showing different levels of offal rotation due to offal support with urethane blocks: (b) high, (c) low, and (d) no support.

3.3.3 Tensile testing procedure

The half-dog bone specimen, trimmed in accordance to the design of experiment, were stretched to failure in an Instron 5982 universal testing machine. A video extensometer with a base of 2" (50.8 mm) was used to measure the major strain. The resulting total elongations were computed using Equation 1 and reported as a percentage of extension to original base length, shown in Figure 8. It should be stated that total elongation measured in this way is a more conservative, global metric for analyzing strain in the sheared edge during tensile test. Local strain in 6000 series aluminum can be much higher [41].

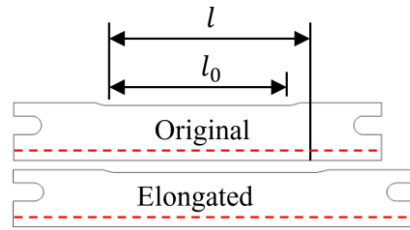


Figure 8: Original and elongated (immediately before fracture) half-dog bone length used to calculate total elongation.

$$\text{elongation (\%)} = \frac{l - l_0}{l_0} * 100\% \quad (1)$$

3.3.4 EDM trimming baseline

Untrimmed EDM half-dog bone specimens were used to establish the total elongation baseline for undamaged (untrimmed) material. For each direction, 5 EDM specimens were stretched to failure in a tensile test to measure the total elongation. Total elongation values were averaged for each condition. Figure 9 shows that the mean elongation percentages for DD, LD, and TD were 27.18 ± 0.45 , 24.98 ± 0.86 , and 25.82 ± 1.75 , respectively.

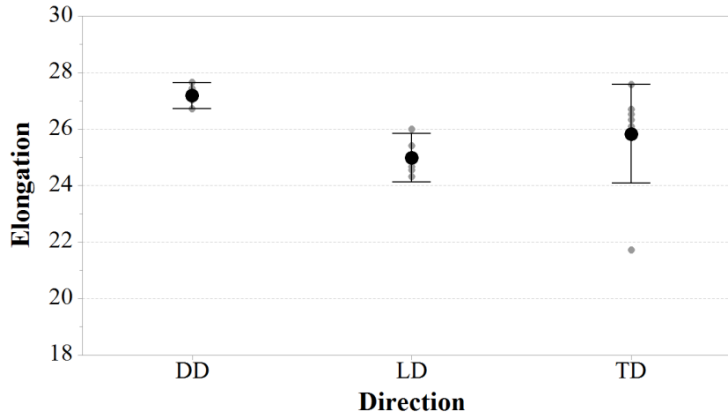


Figure 9: Mean elongation of EDM samples in the three directions. Intervals represent the 95% confidence interval on the mean elongation value.

3.3.5 Data analysis procedure

All data analysis was performed in Minitab v17. Elongation data from the half-dog bone specimens were the primary metrics for determining edge stretch performance. Analysis methodology for each chapter followed a similar procedure:

1. The relationship between elongation to fracture and each of the trimming parameters was inspected visually based on the generated scatterplot.
2. The stepwise forward selection¹⁰ linear regression analysis [42] [43] was used to select only the most significant parameters and interactions which maximized adjusted R^2 value¹¹.
3. The best model selected in step 2 was then built for a detailed investigation of the relationships between elongation and the significant trimming parameters. The residuals from the linear regression model were verified¹².
4. Optimal trimming conditions were established. The aim was to find a robust range of trimming conditions maintainable from an engineering feasibility perspective that maximize elongation.
5. The best-fit probability distribution was identified for the optimal elongation data from a list of 14 distributions¹³. This distribution was then used to estimate lower bound elongation limit.

¹⁰ Many interaction terms were included in the stepwise forward selection regression model where multicollinearity effects were present and could negatively affect results. Large multicollinearity can reduce the accuracy of the coefficient estimates where coefficients are estimated with higher standard errors thus more uncertainty. To provide a more straightforward interpretation of the regression terms, the mean centering procedure was implemented where the mean value for each continuous predictor variable was subtracted from each variable data points. [45]

¹¹ The linear regression model accounted for variance in elongation values; reported as the coefficient of determination, R^2 . These values may be low (< 50%), where accurate extrapolations cannot be made, however with statistically significant predictors present we can still assess the changes in predictor values with changes in the response value.

¹² The residuals from this linear regression model should be normally distributed, have equal variance, and be random throughout observations in order for statistical computations and p-value driven conclusions to be valid [44]

¹³ The list considered distribution included: normal, lognormal, 3-parameter lognormal, exponential, 2-parameter exponential, Weibull, 3-parameter Weibull, largest extreme value, smallest extreme value, gamma, 3-parameter gamma, logistic, loglogistic, 3-parameter loglogistic.

CHAPTER 4

Investigative Study #1: Optimal upper trim tool edge geometry

4.1 Introduction

Due to a multitude of possible causes; such as tool wear, hand-working of trim tools, and damage during blanking operation, dulling of the upper trim tool can occur. Additionally, prior experimental research into aluminum edge stretch has only investigated dull upper trim tools with constant 0.1 mm radius. However, this radius is not feasible to accurately and cost-effectively fabricate for full scale trim tools. The only methodology currently used by die manufacturing shops to alter the shape of the upper trim tool is to manually stone grind sharp trim tools, which results in inconsistent tool edge geometry (size and shape). An investigation of cross sectional tool imprints in partially trimmed blanks from a production blanking die revealed a substantial variation in the shape and size of both the upper and lower trim tool edges as can be seen in Figure 10.

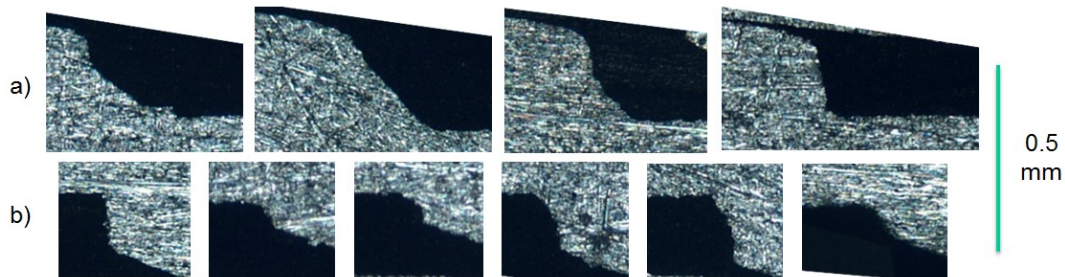


Figure 10: Multiple microscopic view of upper and lower trim tool edge imprints in 0.9mm blank in production blanking die, showing variation in tool sharpness. (a) Upper trim tool edge imprints. (b) Lower trim tool edge imprints.

The lower trim tools are always designed to have sharp radii that can be poorly manufactured, worn out in use, or damaged. These effects were not considered in this study and could be the subject of a future study. The effects of trim edge geometry in the upper trim edges of production blanking dies on edge stretch had not been reported in the literature. Therefore, the purpose of this chapter is to investigate the effect of upper trim edge geometries on edge stretch response of the trimmed edge across typical blanking die trimming conditions, with two specific objectives: (1) identify significant trimming parameters to edge stretch response, and (2)

subsequently find a range of edge radii combined with other significant trimming parameters that maximizes total elongation of the trimmed half-dog bone specimens.

4.2 Methodology

An experimental investigation was performed to examine the effect of upper trim tool edge radius on the trimmed sheet edge stretch. In summary, half-dog bone specimens that were machined from a 6DR1 aluminum coil were trimmed in the laboratory press with adjustable tooling to modulate trimming parameters, mainly accommodating multiple upper trim tools with various trim edge radii. Trimmed specimens were then stretched to failure in a tensile test machine and total elongation to fracture for each specimen was recorded. The total elongation data was analyzed with statistical tools, namely multivariate linear regression and probability distribution fitting, to provide statistically significant conclusions on edge stretch response trends and to determine if optimal trimming parameters that maximize edge stretch can be identified.

4.2.1 Trimming parameters

The trimming conditions included in this study are depicted in Figure 11. For brevity, they are referred to as clearance, support, shape, and direction. Clearance between the upper and lower trim tools, shown in Figure 11 (a), was the main process parameter, reported in percentage of the sheet thickness. Support is the amount of resistance against offal rotation, shown in Figure 11 (b). Shape refers to the geometrical radii of the upper trim tool edge, seen in Figure 11 (c). A sharp lower trim tool was used in this study. Specimen direction is the line of trimming action relative to the rolling direction of the coil, seen in Figure 11 (d).

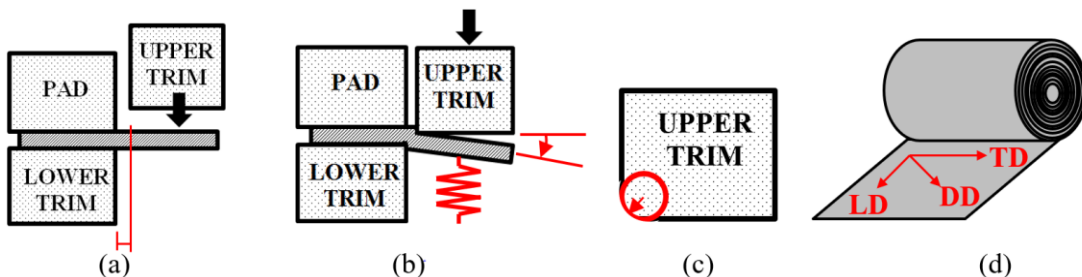


Figure 11: Investigated trimming parameters. Clearance (a), Support (b), Shape (c), Direction (d).

All half-dog bone specimens were trimmed to the procedure described in Section 3.3.2 and the components of the laboratory press operation are shown in Figure 12 (a). Unique to this study,

upper trim tools with edge radii of 0.00R, 0.10R, 0.25R, and 0.50R were interchanged accordingly to the design of experiment. Figure 12 (b) shows an isometric view of experimental trimming tools used in this study.

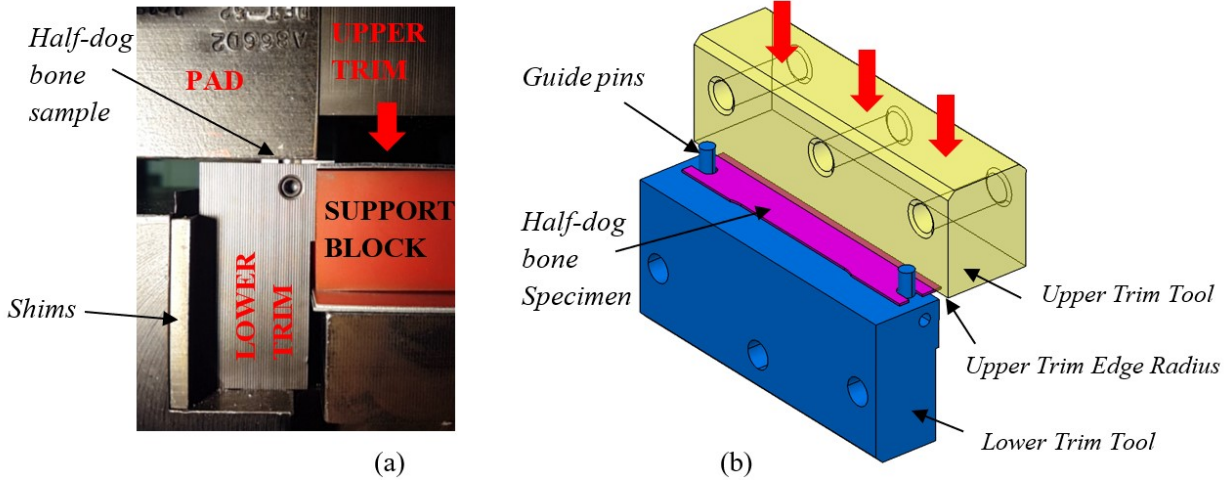


Figure 12: (a) Experimental press side view (b) isometric view of trimming operation without pad or support shown.

4.2.2 Design of experiment (DOE)

The experiment was designed as a full factorial design with four parameters, as shown in Table 2. Each combination was repeated five times for a total of 360 tests. Four shapes were selected for the upper trim tool edge: 0.00R, 0.10R, 0.25R, and 0.50R, with 0.00R representing the sharp edge level in mm. Three different clearance levels were investigated starting with the baseline clearance of 10%. The other two clearance levels, 30% and 50%, are less desirable clearances, but are often encountered in production dies. Low support replicates the baseline offal rotation of approximately 8° measured on a blanked production panel, whereas high support does not allow any offal rotation. The effect of directionality was examined by performing the trim along the longitudinal (LD), transverse (TD), and diagonal (DD) directions with respect to the rolling direction of the sheet.

Table 2: DOE matrix

Parameters	Levels
Shape (4)	0.00R, 0.10R, 0.25R, 0.50R
Support (2)	High (0°), Low (8°)
Rolling Direction (3)	LD, DD, TD
Clearance (3)	10%, 30%, 50%
Repetitions (5)	
TOTAL	360 data points

4.2.3 Design vs. actual geometry of trim tool edges

Microscopic imaging and CMM contour tracing methods were used to measure the actual edge geometry of manufactured trim tools, as presented in Figure 13. The edge measurement results of all manufactured trim tools revealed significant deviations from the design. Investigation into the manufacturing process of the trim tools revealed that the grinding practices used to generate the controlled edge radius were inconsistent, and the measurement method that validated the radius was not precise enough to meet the design intent. Table 3 shows the translation of design to actual geometry. For all following sections and data analysis, the measured (actual) geometry is used.

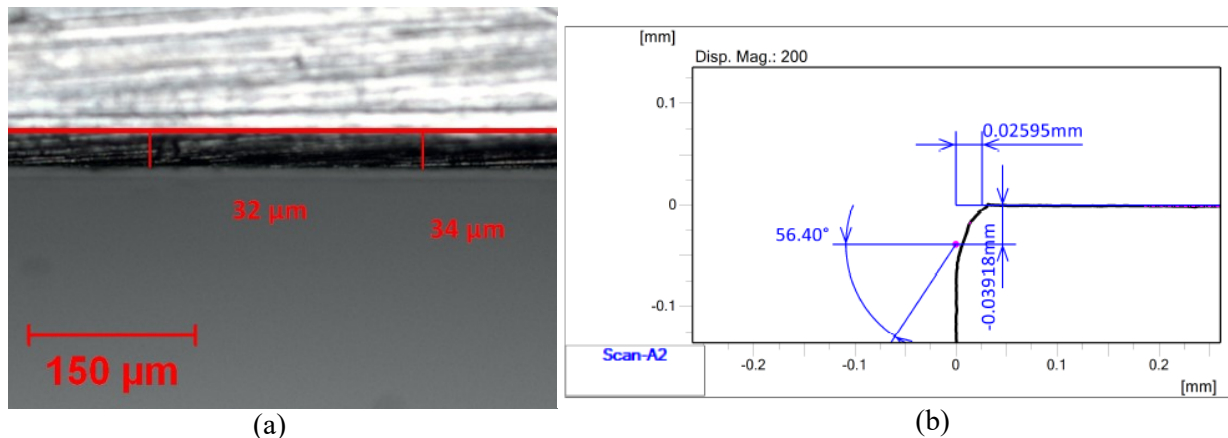


Figure 13: Both images represent the 0.00R trim tool edge by design. (a) Top view, microscopic image with actual measured trim tool edge geometry defined by contrast of lighting. (b) CMM contour tracing results showing cross-section edge profile.

Table 3: Comparison of design and actual measured geometry in trim tool edges for radius shapes.

Design	Actual
0.00R	0.040R
0.10R	0.080R
0.25R	0.140R
0.50R	0.450R

4.3 Results

4.3.1 Total elongation data analysis

In this section, elongation data for upper trim tool radii of 0.04R, 0.08R, 0.14R, and 0.45R were considered, including details on direction, clearance, and support level. In total, this dataset contained 360 elongation data points. Scatterplots were first constructed to investigate any trends in elongation response. The elongation data was separated into two graphs based on offal support level: high support shown in Figure 14 and low support shown in Figure 15.

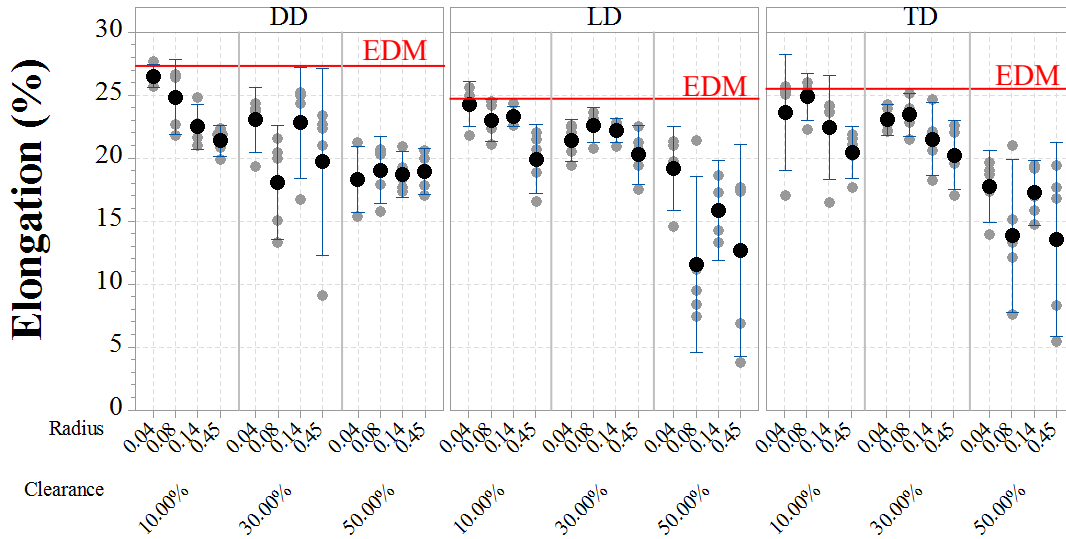


Figure 14: Elongation data for radius upper trim tool with high support trimming conditions. Mean EDM elongation shown as reference line in red. Interval lines represent 95% confidence interval on the mean elongation value.

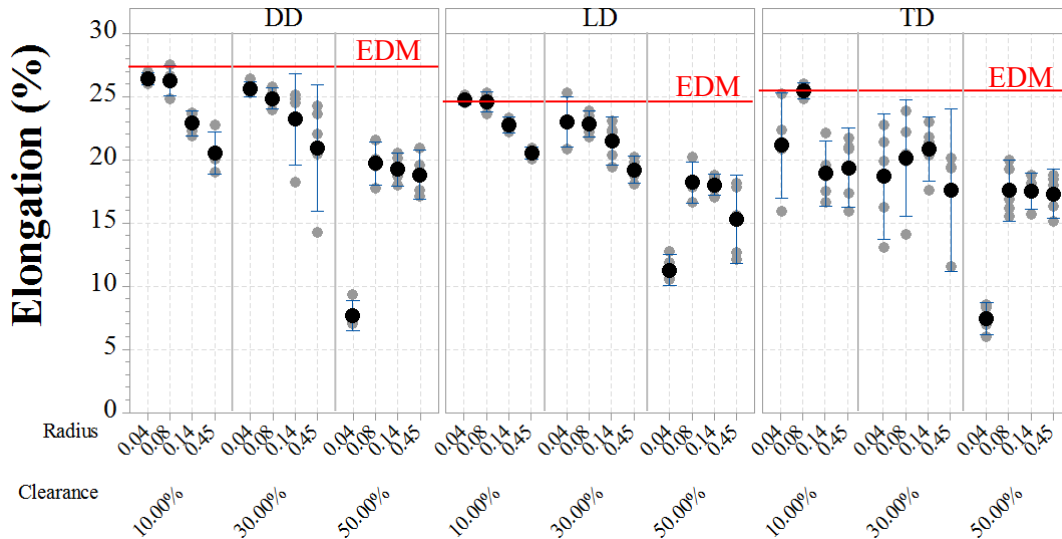


Figure 15: Elongation data for radius upper trim tool trimming with low support conditions. Mean EDM elongation shown as reference line in red. Interval lines represent 95% confidence interval on the mean elongation value.

Within each graph, three panels represent the three tested directions. Within each panel, data points are categorized by clearance and radius. One of the clearest observations common to all scatter plots is that the majority of the low elongation results originated from the 50% clearance trim condition. On the other hand, 10% clearances seemed to produce the highest elongation values. 30% clearance seemed to have slightly lower elongation values that 10% clearance.

Another observation is that as radius increased, elongation generally decreased. This trend was clearly violated by 50% clearance at low support, seen in Figure 15, which exhibited extremely

low elongation values for the 0.04R upper trim tool condition. This effect was eliminated when high support was used, seen in Figure 14, suggesting the change in the fracture initiation site and the associated change in burr size as the primary cause. Metallographic analysis of these two conditions shown in Figure 16 confirmed this initial conclusion. Sharp upper tool edge and low support promoted early fracture initiation at the upper edge resulting in formation of a large burr on the sheared edge of the specimen, as can be seen in Figure 16 (b). The large burr seen in this figure was likely large enough to have a dominant effect on the elongation response. The introduction of high support, on the other hand, was sufficient to suppress or postpone fracture initiation at the upper edge resulting in a much smaller burr as demonstrated in Figure 16 (a). The dominant burr condition at 50% clearance with low support made the elongation response highly nonlinear, and since it occurred only at one trimming condition, it has been decided to exclude it from the regression analysis.

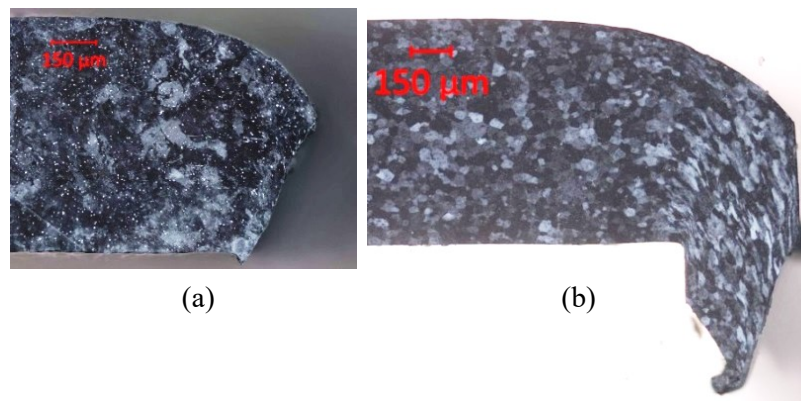


Figure 16: Cross-sectional metallographic images of trimmed edge from two trimming conditions showing the large geometrical imperfections in the low supported condition: (a) 0.04R – 50% clearance – High Support and (b) 0.04R – 50% clearance – Low Support

4.3.2 Multivariate, linear regression model

A stepwise forward selection linear regression analysis was utilized to identify statistically significant trimming parameters and interactions. The response variable was the total elongation to fracture of the sheared specimens. Predictor variables included radius and clearance as continuous variables, as well as direction, and support as categorical variables. All two and three way interaction terms between the predictor variables were included in the model. The tabulated results of the model are shown in Appendix B. According the ANOVA table generated by the last iteration of the stepwise procedure, the most significant main factors were radius and clearance. The only significant interactions were clearance*support and support*direction.

A regression model was then built that included all significant terms identified by the forward stepwise procedure. The tabulated results for this model and the fulfillment of the assumptions of linear regression¹⁴ are shown in Appendix B. The ANOVA table indicates that radius, clearance, direction, and the two-way interactions clearance*support and support*direction were still significant predictors of elongation. Support factor was not significant, but was kept in the model to maintain the hierarchical structure¹⁵. Equation 2 represents the elongation percentage as a function of significant trimming parameters generated from the linear regression model: radius (mm), clearance (decimal), and support (0 if high, 1 if low).

$$\text{Elongation (\%)} = 26.513 - 7.373 \text{ Radius} - 16.80 \text{ Clearance} - 2.512 \text{ Support} + 5.80 \text{ Clearance} * \text{Support} \quad (2)$$

Equation 2 is only valid for the transverse direction (TD) trimming, which is purposeful in representing the lowest elongation response direction, or worst case scenario commonly preferred in engineering applications.

To facilitate investigation of the trends of the elongation response, the regression equations produced by the regression model were graphed in Figure 17, along with the main effect plot in Figure 18. Only the transverse direction (TD) elongation data was presented in Figure 17 for simplicity of visualization.

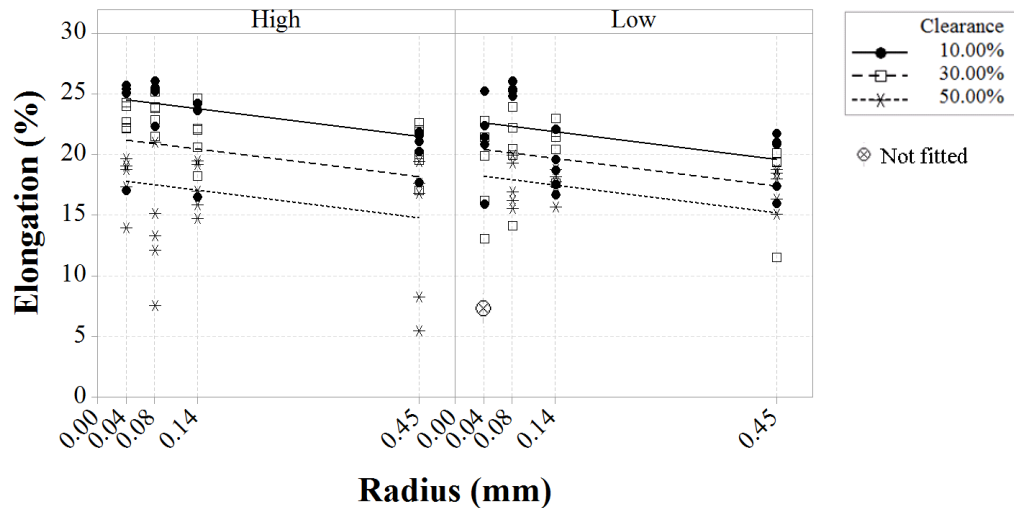


Figure 17: Scatterplot of elongation vs. radius of upper trim tool with regression lines: left pane high support, right pane low support. Only transverse direction (TD) data is shown. Data not fitted at 50% clearance, low support.

¹⁴ The residuals from this linear regression model should be normally distributed, have equal variance, and be random throughout observations in order for statistical computations and p-value driven conclusions to be valid [44].

¹⁵ A hierarchical regression model contains all lower order terms necessary to describe high order interaction terms.

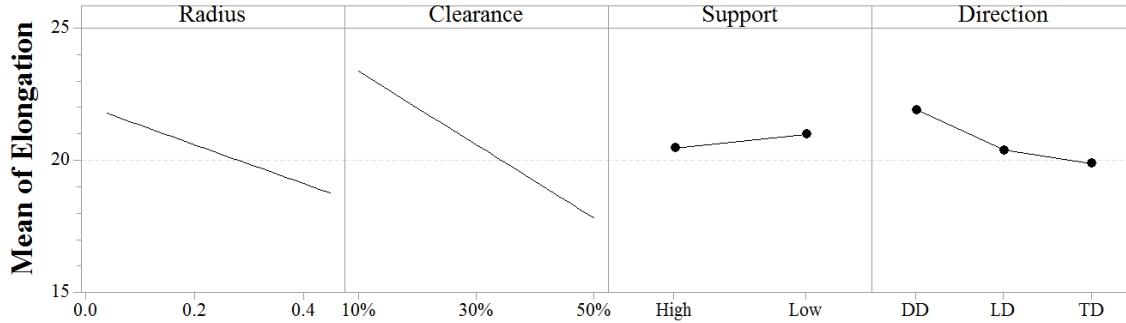


Figure 18: Main effect plot generated by regression model showing that radius of upper trim tool and clearance are significant and negatively proportional to elongation.

The plotted regression equations in Figure 17 show that as clearance increased, elongation response decreased. Additionally, as radius of upper trim tool edge increased, the elongation response decreased, excluding the 0.04R – 50% - low support condition. This was expected since increasing of the upper trim edge radius leads to an increased amount of sheared edge damage in the form of plastic deformation. The main effect plot, shown in Figure 18, confirms that increasing clearance and radius resulted in reduction of mean elongation response. Figure 18 also shown that the specimens cut in the diagonal direction had the highest elongation whereas samples cut in transverse direction had the lowest elongation. Additionally, the main effect plot, Figure 18, indicates that low support resulted in higher elongation response compared to high support. The sheared edge quality obtained with different upper tool edge radii at 10% clearance can be visually assessed from the metallographic pictures in Figure 19. The trimmed specimens from the 0.04R, 0.08R, and 0.14R tools failed to show a significant change in overall sheared edge profile geometry and grain deformation, shown in Figure 19 (a), (b), and (c) respectively. However, the trimmed specimen from the 0.45R tool resulted in significant increase in grain deformation localized near the sheared edge, as well as more irregular sheared edge profile.

From these findings, expected elongation can be optimized by minimizing radius and clearance. Since achieving a perfect, singular radius and clearance is practically infeasible in full scale blanking operations, to add engineering robustness, optimal trimming conditions were defined as a range: maintain clearance at or below 30% and upper trim tool radius at or below 0.14 mm. Under these conditions, edge stretch was robust across High/Low support and LD/DD/TD directions.

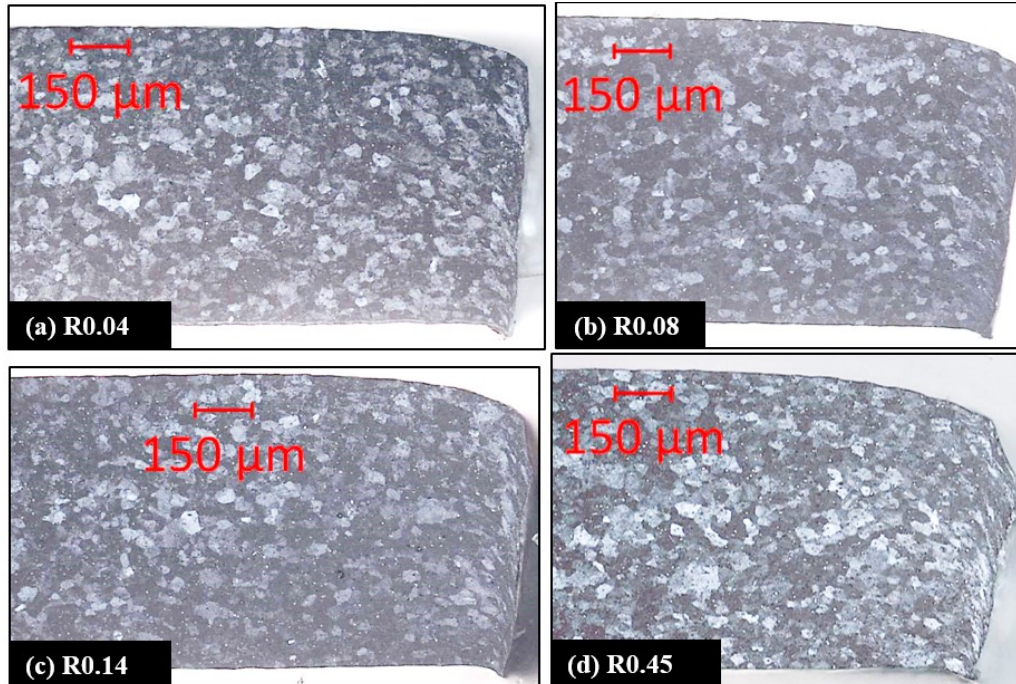


Figure 19: Microscopic pictures of trimmed edge at 10% clearance, DD, and high support showing variability in damage to the grain structure of the sheared edge. Radius in the upper trim tool was (a) 0.04R (b) 0.08R (c) 0.14R (d) 0.45R. The largest distribution of damage was clearly visible for dulllest edge at R0.45 in (d).

4.3.3 Probability distribution of optimal parameters

The combined elongation data for the optimal trimming conditions was graphed in a frequency distribution plot and probability plot, shown in Figure 20. The elongation data resulted in a good fit for a left-skewed 3-parameter Weibull distribution curve, as seen in Figure 20 (a) and (b). Based on the three parameters of the Weibull distribution, the mean and standard deviation of each data set can be calculated¹⁶. The identified distribution was used to determine the lower bound elongation limits for various levels of risk as shown in Table 4. The skewness of the Weibull distribution resulted in much greater risk of failure than can be expected with normally distributed data at any elongation limit. Even at six standard deviations from the mean, 300 defects per million (DPM) would be expected compared to 3.4 DPM for a normal process. The skewness also indicates that the elongation limits, with any reasonable risk, are much lower than the mean.

¹⁶ The mean and standard deviation of a skewed-left Weibull probability distribution function differ from typical mean and standard deviation computation that assumes normally distributed data.

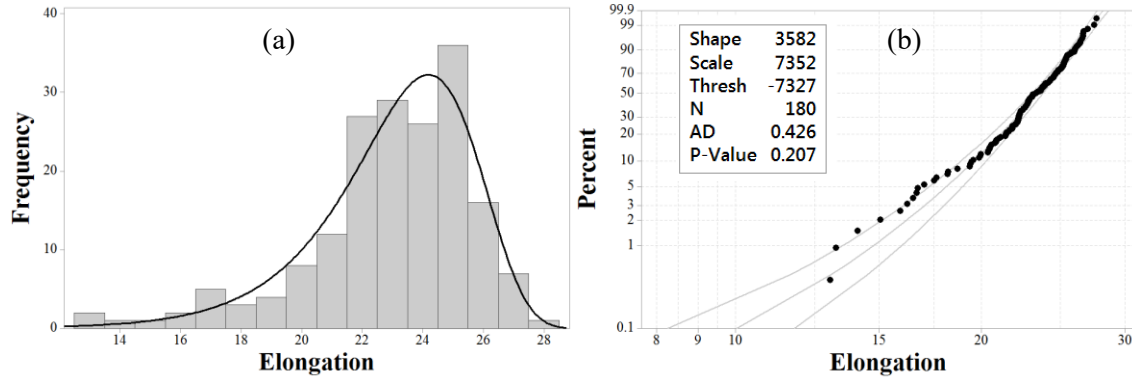


Figure 20: (a) Histogram of optimal radius elongation data with fitted 3-parameter Weibull distribution. (b) The corresponding probability plot with lower and upper bound 95% confidence intervals.

Table 4: Elongation limits for optimal radius trimming conditions and various levels of risk

Mean	Std. Dev.	Probability Density Function (PDF)		
23.8158	2.6314	<p>Density</p> <p>X</p>		
Std. Dev. From Mean	Success Rate	Lower Bound	Total Elongation, X (%)	Defects per million (DPM)
$\mu - 1\sigma$	85.58%	21.18		144200
$\mu - 2\sigma$	95.77%	18.55		42300
$\mu - 3\sigma$	98.81%	15.92		11900
$\mu - 4\sigma$	99.67%	13.29		3300
$\mu - 5\sigma$	99.91%	10.66		900
$\mu - 6\sigma$	99.97%	8.03		300

4.4 Conclusion

The purpose of this chapter was to investigate edge stretch in a range of upper trim edge geometries across typical blanking die trimming conditions, and effectively identify which shapes maximize edge stretch of 6DR1 0.9 mm aluminum. Findings are summarized below:

1. The most significant trimming parameter to affect edge stretch was clearance: as clearance increased, elongation decreased. The majority of the low elongation results originated from the 50% clearance trim condition.
2. For all investigated radius upper trim tool shapes, findings showed that generally as radius increased, elongation decreased. The exception to this trend was extremely low elongation values at 50% clearance with low support and sharp upper trim tool conditions. Elongation

was maximized by maintaining clearance at or below 30% and upper trim tool radius at or below 0.14 mm.

3. Trimmed edge elongations for this material followed left-skewed Weibull distribution with much greater risk of failure than can be expected based on normally distributed data. For this reason, the elongation limit for this material was much lower than the mean elongation.
4. For a failure risk of 0.03%, the limits were 8% elongation for optimal radius upper trim tool conditions.

CHAPTER 5

Investigative Study #2: Galling Study

5.1 Introduction

A common, undesirable effect in shear trimming operations of aluminum is galling. A gall mark is defined as the notch-like geometrical imperfection on the material sheared edge that occurs during the trimming operation. Figure 21 shows magnified views of gall marks occurring in aluminum trimmed edges.

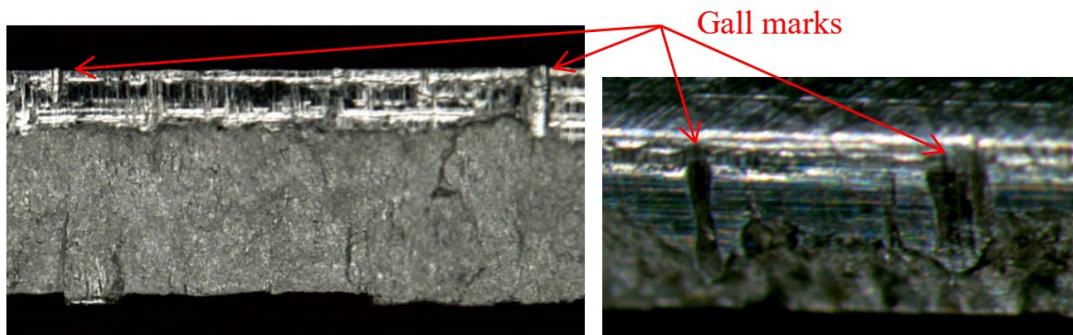


Figure 21: Gall marks occurring in the trimmed edge of production trimmed aluminum panels.

Galling is caused by a localized accumulation of material on the working surfaces of the upper trim tool that effectively notches the sheared edge of the subsequently trimmed sheet. These gall marks may become stress concentration zones during edge stretching operations, limiting overall edge stretch. A detailed study on the effect galling on edge stretch of aluminum has not been reported in the literature. Therefore, the purpose of this chapter is to investigate the edge stretch response of specimens galled at controlled depths in a variety of trimming conditions, with two specific objectives: (1) identify significant trimming parameters to edge stretch response, and (2) subsequently find a range of galling depths combined with other significant trimming parameters that maximizes total elongation of the trimmed half-dog bone specimens.

5.2 Methodology

The experimental methodology studied the effect of gall depth on edge stretch. In summary, half-dog bone specimens that were machined from a 6DR1 aluminum coil were trimmed in the

laboratory press with adjustable tooling to modulate trimming parameters, mainly variable galling depths in the upper trim tool. Trimmed specimens were then stretched to failure in a tensile test machine and total elongation to fracture data was recorded. The total elongation to fracture data was analyzed with statistical tools to identify, with statistical significance, the optimal trimming parameters that maximize edge stretch.

5.2.1 Trimming parameters

The trimming conditions included in this study are depicted in Figure 22. For brevity they are referred to as clearance, support, shape, gall depth, and direction.

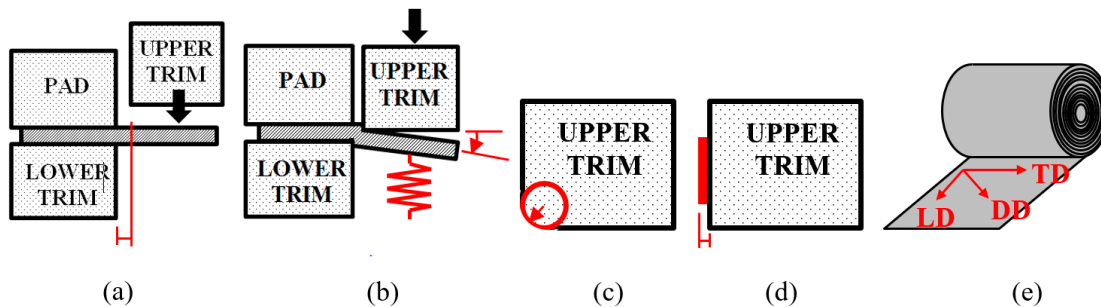


Figure 22: Investigated trimming parameters. Clearance (a), Support (b), Shape (c), Gall Depth (d), and Direction (e).

Clearance between the upper and lower trim tools, shown in Figure 22 (a), was the main process parameter, reported in % of the sheet thickness. Support is the amount of resistance against offal rotation, shown in Figure 22 (b). Shape refers to the geometrical shape of the upper trim tool edge, seen in Figure 22 (c). A sharp lower trim tool was used in this study. The upper trim tool contained a variable depth galling plate, shown in Figure 22 (d), which induced a controlled notch into the trimmed sample. Specimen direction is the line of trimming action relative to the rolling direction of the coil, seen in Figure 22 (e). All half-dog bone specimens were trimmed to the procedure described in Section 3.3.2 and the components of the laboratory press operation are echoed in Figure 23.

Unique to this study, the galling depth was controlled using shims of variable thickness behind the galling plate in the upper trim tool, shown in Figure 23 (b). To ensure the galling plate remained stationary during installation and trimming operation, a set screw included the upper trim tool was tightened against the galling plate. Based on this setup, galling occurred after shear trimming initiated which is representative of actual galling that occurs in a production blanking scenario.

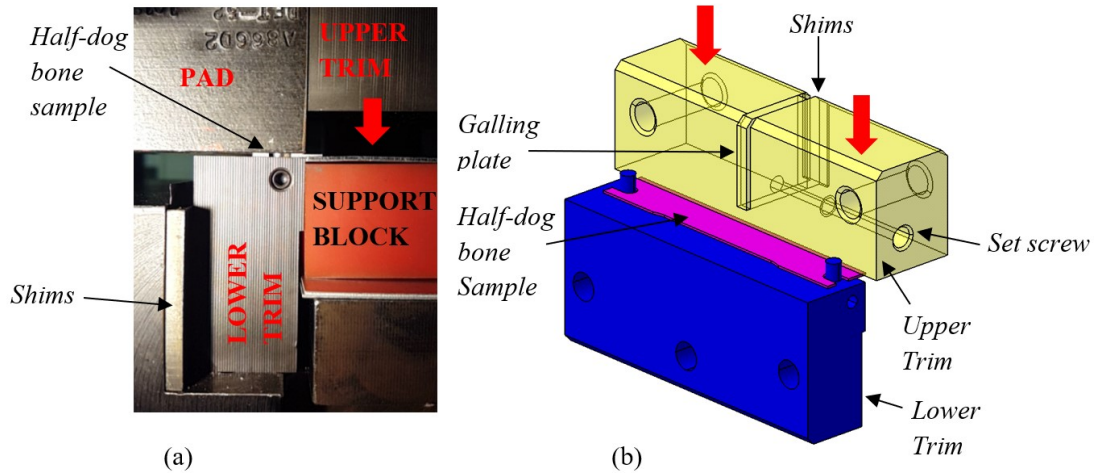


Figure 23: (a) Experimental press side view (b) isometric view of trimming operation without pad or support shown, galling plate identified.

5.2.2 Design of experiment (DOE)

The experiment was designed as a full factorial DOE with four parameters, as shown in Table 5. Each combination was repeated five times. Four gall depth levels were selected to represent minimum and maximum galling conditions commonly present in production environment: 0mm, 0.0254mm, 0.0508mm, 0.0762mm. Two upper trim edge shape and support combinations were selected: Sharp-No Support and 0.25R-High Support. No support allows offal to rotate freely, whereas high support does not allow any offal rotation. Two levels of clearance were investigated: the baseline clearance of 10% of the sheet thickness and a clearance of 30% that represents clearance levels often encountered in production dies. The specimens were shear in three different orientations relative to the rolling direction of the sheet: Longitudinal (LD), Transverse (TD), and Diagonal (DD) trimming directions.

Table 5: DOE matrix

Parameters	Levels
Gall (4)	0mm, 0.0254mm, 0.0508mm, 0.0762mm
Upper Shape-Support (2)	Sharp-No Support, 0.25R-High Support
Rolling Direction (3)	LD, DD, TD
Clearance (2)	10%, 30%
Repetitions (5)	
TOTAL	240 data points

5.2.3 Design vs. actual geometry of trim tool edges

Microscopic imaging methods were used to measure the actual edge geometry of manufactured trim tools, as exemplified in Figure 24. The edge measurement results of all manufactured trim tools revealed that the actual geometry of the trim tools varied from design

intent. Investigation into the manufacturing process of the trim tools revealed that the grinding practices used to generate the controlled edge radius were inconsistent, and the measurement method that validated the radius was not precise enough to meet the design intent. Table 6 shows the translation of design to actual geometry. For all following sections and data analysis, the actual (measured) geometry will be used.

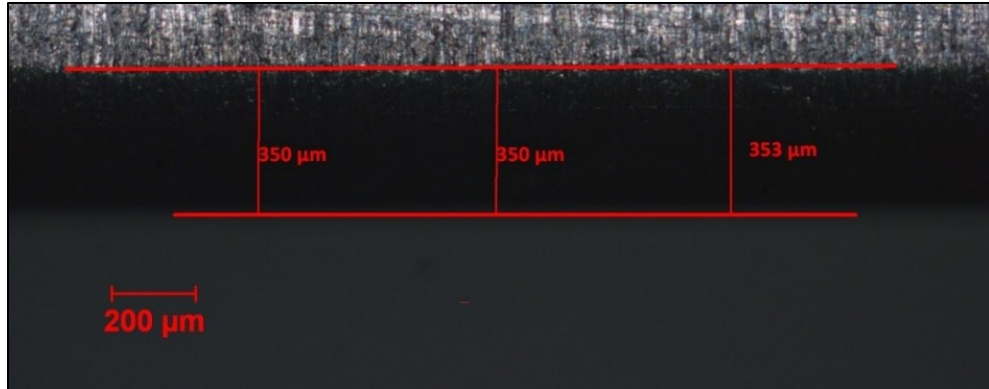


Figure 24: Top view, microscopic image with actual measured trim tool edge geometry defined by contrast of lighting showing 0.25R trim tool edge by design.

Table 6: Comparison of design and actual measured geometry in trim tool edges

Design	Actual
0.00R	0.08R
0.25R	0.33R

5.3 Results

5.3.1 Microscopic gall measurement procedure

The galling tool produced a notch in the trimmed half-dog bone specimens that could be microscopically measured, as shown in Figure 25. To ensure accurate representation of gall depth, all trimmed edges were microscopically measured and gall depths were recorded for data analysis.

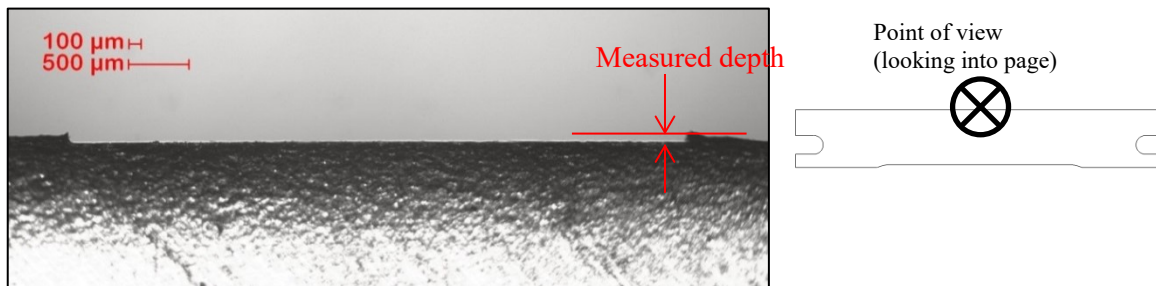


Figure 25: Microscopic view of trimmed edge with gall mark from galling tool. Measurement of gall depth was performed with microscopic images for every half-dog bone specimen.

5.3.2 Incremental edge damage

There were four incremental damage trimming conditions implemented as described in the design of experiment: 10% - 0.08R – No Support, 30% - 0.08R – No Support, 10% - 0.33R – High Support, and 30% - 0.33R – High Support. The purpose of choosing these specific trimming conditions was to generate incremental levels of plastic deformation to the trimmed edge, so as to provide information on how gall depth effects specimen total elongation across different levels of damage existing in the edge. As mentioned in the literature review, previous research widely supports that an increase of cumulative damage from plastic deformation leads to a decrease in total elongation. Also, increasing clearance and radius of upper trim tool has been found to increase sheared edge damage [22] [25] [28]. Increasing offal support, or in other words reducing the angle of offal rotation until fracture, has been found to increase cumulative plastic deformation in trimmed edge at lower clearances, thus reducing edge stretch [18]. Taking these factors into consideration, the least damaged edge was expected for the trim condition 10%-0.08R-No Support. The most damaged edge considering the same factors should be for the trim condition 30%-0.33R-High Support. To support this hypothesis, elongation values of trimmed half-dog bone specimens were analyzed to investigate the expected decrease in edge stretch as trimming conditions increased edge damage. Figure 26 shows the total elongation values for the four major trimming conditions. Elongation data validates the hypothesis, with statistical significance, that the 10%-0.08R-No Support condition reflects lowest damage and highest elongation response, while the 30%-0.25R-High Support condition reflects highest damage and lowest elongation response out of the tested conditions.

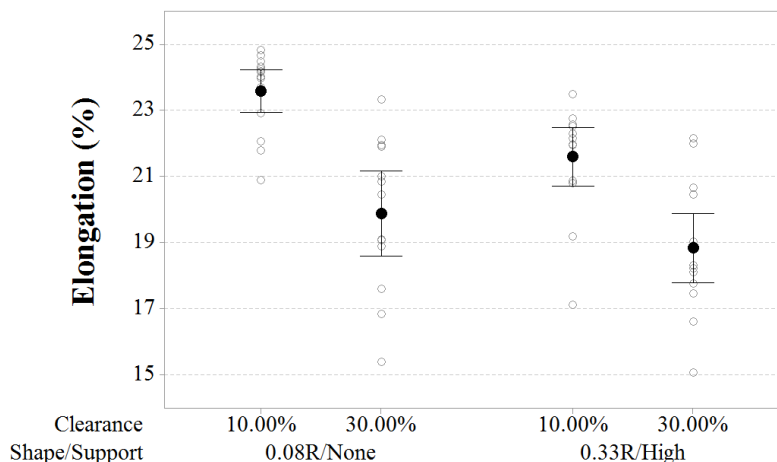


Figure 26: Interval plot of four incremental damage trimming conditions with 95% confidence interval for the mean shown. Elongation results show that 10%-0.08R-No Support condition produced the highest response and 30%-0.25R-Support condition produced the lowest response.

5.3.3 Observations of natural galling

Upon following procedures to measure the gall depth in each half-dog bone specimen, it was discovered that in addition to the artificial gall produced by the galling tool, random notching sometimes occurred along the entire trimmed edge. These random notches were defined as natural gall marks and were assumed to be an intrinsic effect based on specific trimming conditions. The majority of natural galling occurred for the 30% - 0.33R – High Support trim condition. Natural galling was not significantly present in the other trim conditions. Figure 27 provides microscopic visualization of average trimmed edge quality for the four incremental damage trimming conditions. Figure 27 (a) – (c) shows trimming conditions that produced no significant imperfections like natural galling. Figure 27 (d) clearly shows natural notches were seen in the 30% - 0.33R – High Support trim condition. In some cases, the depth of these natural notches was larger than the artificial gall depth, seen in Figure 27 (e). Since natural notch marks were discovered to occasionally exceed the depth of the artificial gall mark, it was predicted that they could dominate the elongation response and hide the effects of the controlled artificial galling.

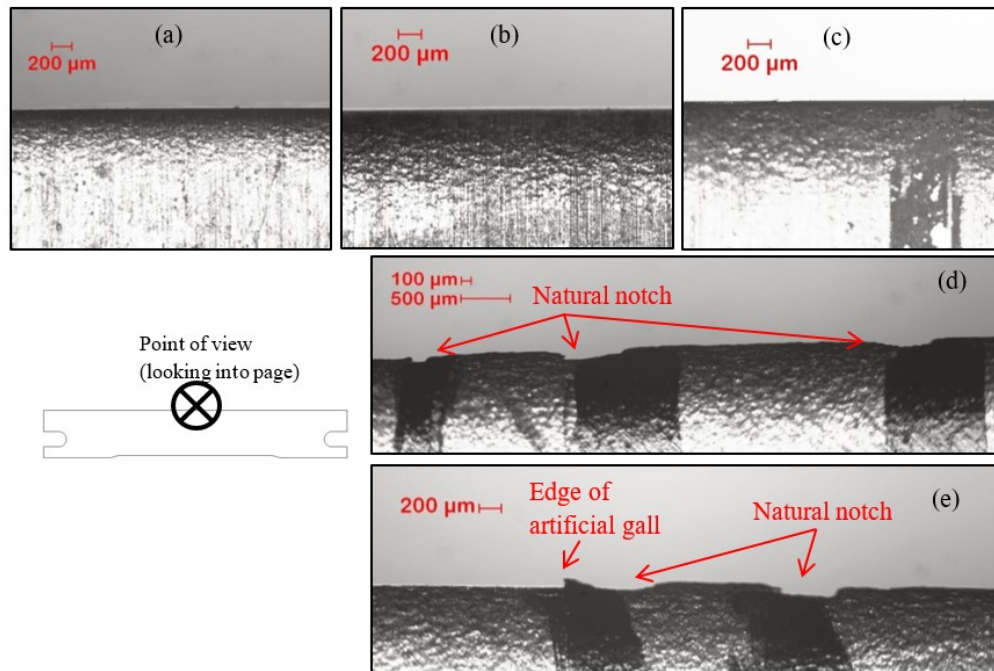


Figure 27: Microscopic pictures of trimmed half-dog bone edge, looking down the trim edge for each of the four major trimming conditions. (a) Shows the average edge quality of 10% - 0.08R – No Support trim condition with no natural galling occurring. (b) Shows the average edge quality of 30% - 0.08R – No Support trim condition with no natural galling occurring. (c) Shows the average edge quality of 10% - 0.33R – High Support trim condition with no natural galling occurring. (d) Shows the average edge quality of 30% - 0.33R – High Support trim condition with natural gall marks occurring. (e) Microscopic picture of artificial and natural galling occurring in the 30% - 0.33R – High Support trim condition, specifically showing how natural gall depth exceeded the artificial gall depth.

To further understand the geometrical effects of both the artificial and natural galling to the sheared edge, a laser profilometer measurement¹⁷ was performed along the sheared edge for each of the four incremental damage trimming conditions. Locations of artificial and natural galling were targeted and resulting data was organized and plotted to 2D and 3D contour plots in MATLAB R2017a, shown in Figure 28 through Figure 31. After investigation of the sheared edge contour plots, it was found that the extent of geometrical imperfection to the sheared edge due to artificial galling varied based on the trimming condition. Starting from inspection of the contour plots of 10% - 0.08R – No Support trimming condition shown in Figure 28, the gall mark penetration depth and length was effective through the entire thickness of the specimen. This low damage trimming condition produced negligible sheared edge rollover and fracture zone rotation which allowed for the galling tool to completely pass through the entire specimen thickness. Now considering the increased clearance condition, 30% - 0.08R – No Support, more noticeable fracture zone rotation can be observed in Figure 29. The fracture zone rotated away from trimming plane, effectively increasing the trimming clearance, which in turn reduced the galling penetration length. The result of this effect led to an effective galling penetration length of about 75% of the specimen thickness, where the unaffected areas to the gall were in the rotated fracture zone. These observations for Figure 29 can be replicated for the 10% - 0.33R – High Support trimming condition shown in Figure 30, where a larger rotation of the sheared edge fracture zone led to an approximate 50% penetration length through specimen thickness. Finally, for the 30% - 0.33R – High Support trimming condition shown in Figure 31, the extent of fracture rotation and rollover was at its greatest compared to the other three trimming conditions, which led to the smallest effective penetration length of about 30% penetration through specimen thickness. Unique to this trimming condition was the occurrence of natural gall marks, which were previously observed in Figure 27 (d) and (e). Upon closer inspection of the geometry of the natural gall marks described by the 2D contour plot in Figure 31 (b), the effective penetration depth and length through specimen thickness of the natural gall clearly exceeded that of the artificial gall mark.

¹⁷ A UBM laser profilometer was programmed to perform approximately 30 linear scans longitudinally across the sheared edge at a measurement resolution of 100 points/mm.

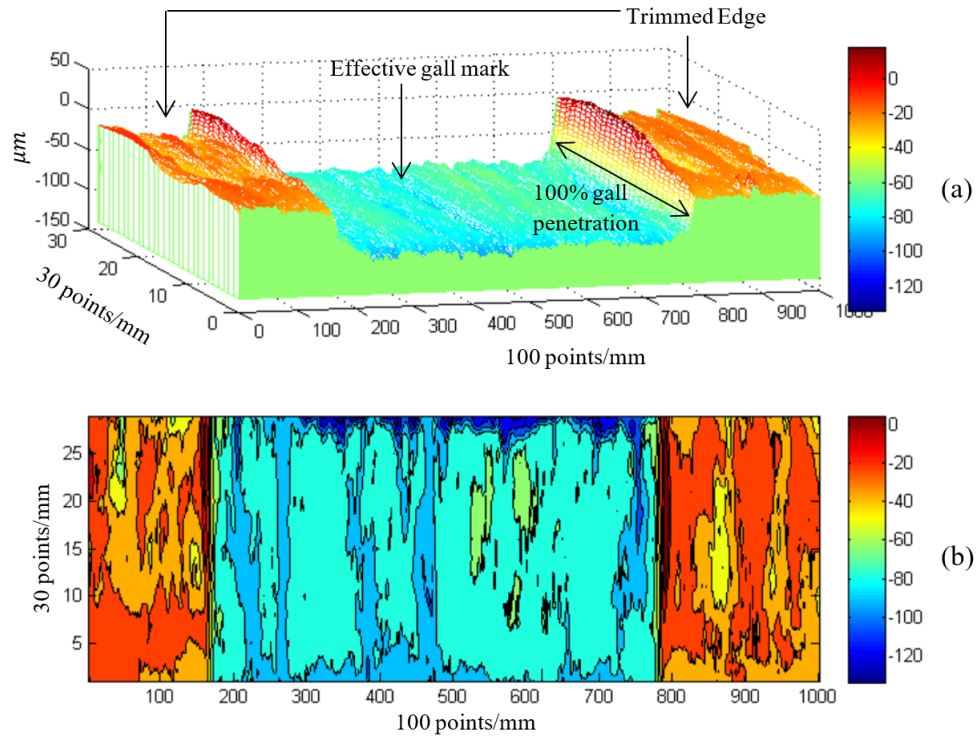


Figure 28: Visualizations of profilometer measurement data of half-dog bone sample trimmed edge at 10% - 0.08R/No Support condition. (a) 3D mesh plot and (b) contour plot clearly shows the effective gall mark penetrates entire trimmed surface.

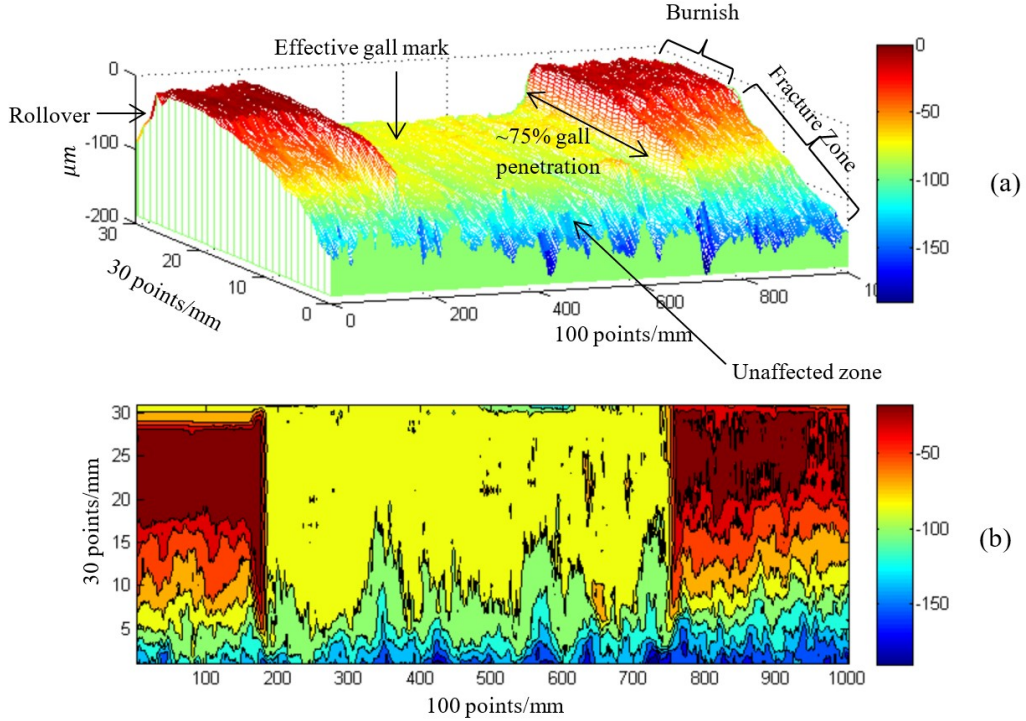


Figure 29: Visualizations of profilometer measurement data of half-dog bone sample trimmed edge at 30% - 0.08R/No Support condition. (a) 3D mesh plot and (b) contour plot shows the effective gall mark partially penetrates the trimmed surface, approximately 75% of the total thickness. The partial gall penetration is due to the rollover and the angle of the fracture zone which eventually exceeds the galling depth and creates an unaffected zone.

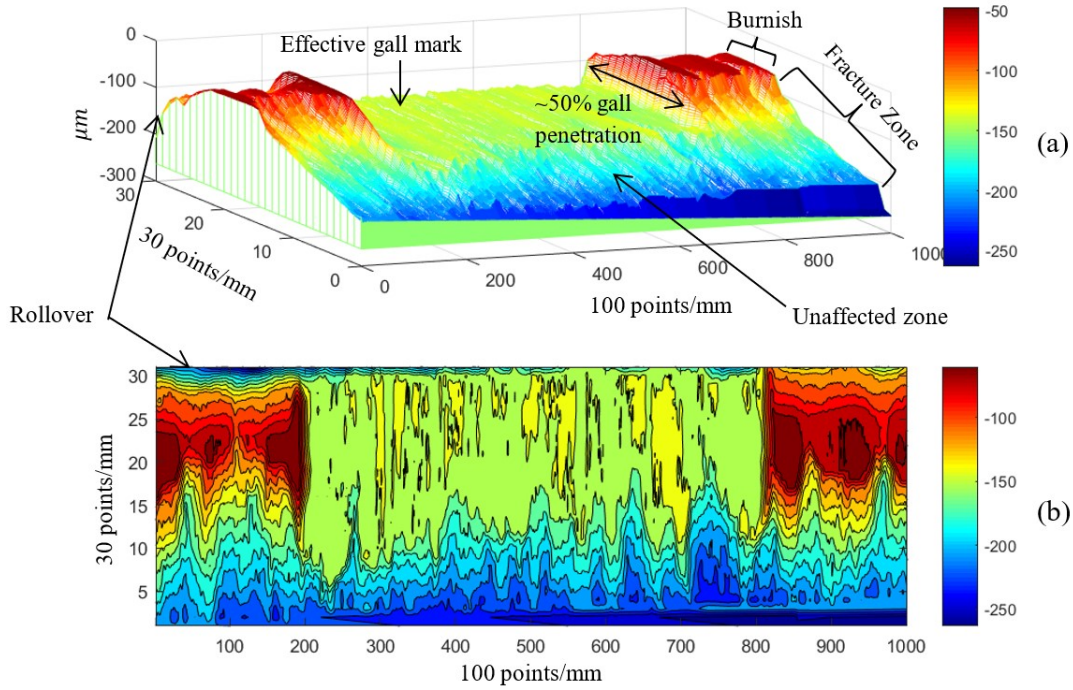


Figure 30: Visualizations of profilometer measurement data of half-dog bone sample trimmed edge at 10% - 0.33R/High support condition. (a) 3D mesh plot and (b) contour plot shows the effective gall mark partially penetrates the trimmed surface, approximately 50% of the total thickness. The partial gall penetration is due to the rollover and the angle of the fracture zone which eventually exceeds the galling depth and creates an unaffected zone.

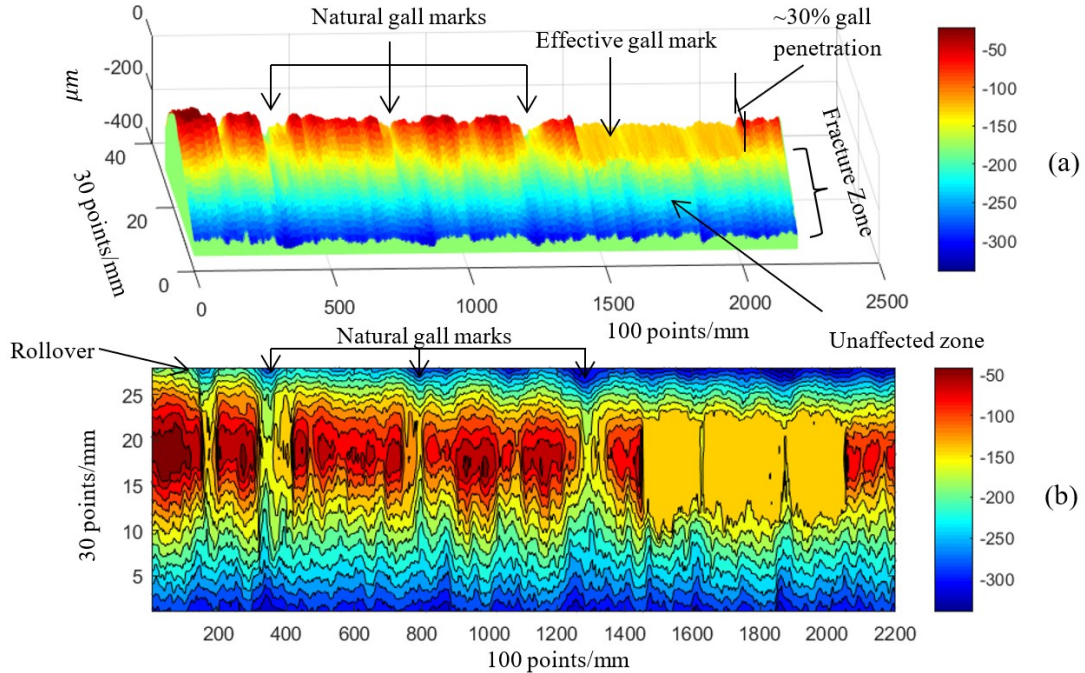


Figure 31: Visualizations of profilometer measurement data of half-dog bone sample trimmed edge at 10% - 0.33R/High support condition. (a) 3D mesh plot and (b) contour plot shows the effective gall mark partially penetrates the trimmed surface, approximately 30% of the total thickness. The partial gall penetration is due to the rollover and the angle of the fracture zone which eventually exceeds the galling depth and creates an unaffected zone. Natural gall marks are present, and can exceed the artificial gall mark both in depth and length.

To better understand the effect of artificial vs. natural galling on specimen edge stretch, both the natural and artificial notches of every half-dog bone specimen were marked by location and measured by depth, seen in Figure 32 (a). Upon tensile testing, the fracture initiation location was observed, and recorded as either at the artificial gall, natural gall, or another location not identified, seen in Figure 32 (b).

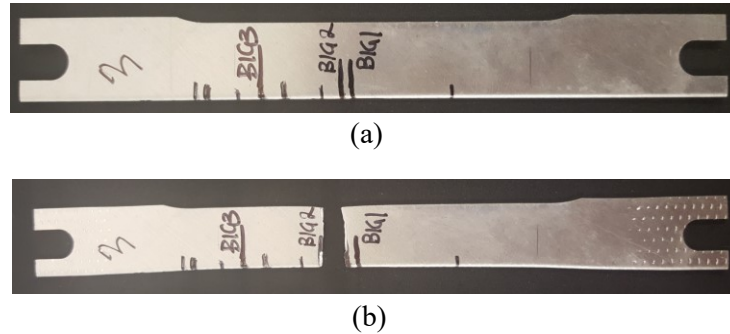


Figure 32: (a) Half-dog bone tensile specimen with significant gall marks located by black marker lines and (b) identical tensile specimen after tensile test showing fracture initiation occurred at previously identified gall mark.

The percentile breakdown of fracture initiation location at each of the four incremental trimming conditions and intended gall depths was calculated, shown in Figure 33. It can be generally observed that the tensile specimens trimmed at 0.08R/Low Support for 10% and 30% clearances more often fractured at the artificial gall mark location as gall depth increased. This result indicates that the gall marks induced by the upper trim tool had an effect on specimen during the tensile test, and therefore must have an effect on specimen edge stretch. For the 0.33R/High Support trimming condition, observations were distinct for 10% and 30% clearances. At 10% clearance, fracture location could not be predicted consistently since the majority of fractures occurred at an unidentified location outside the galling tool location. At 30% clearance, fracture location was often at natural gall marks that were previously identified and measured. Based on the observations from Figure 33, in order to best model the relationship of gall depth and edge stretch, the gall depth measurement used in future analysis will reflect artificial measured gall depth from galling tool, except in cases where fracture initiated at an identified natural gall mark, in which the natural gall depth will be used for analysis and replace the corresponding artificial gall depth.

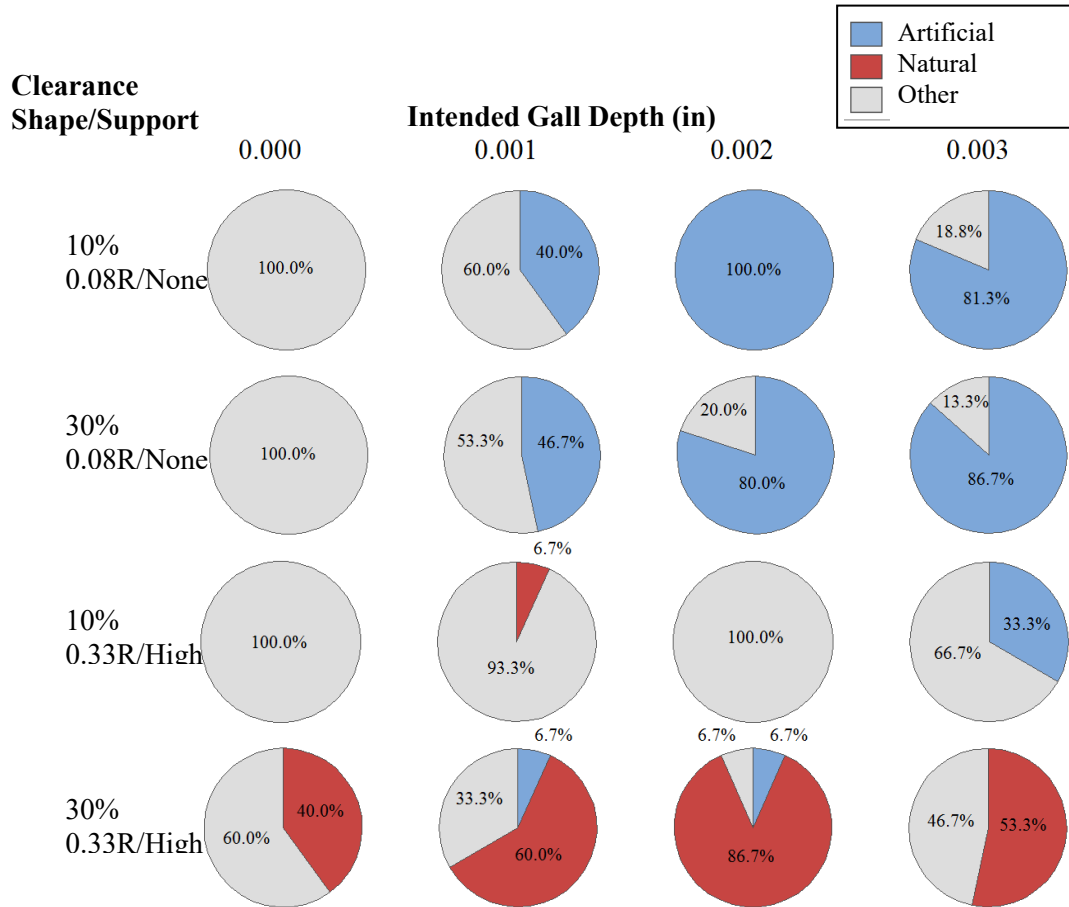


Figure 33: Pie chart percentile breakdown of fracture initiation location at four main trimming conditions: Rows represent four Clearance – Shape/Support conditions and columns represent four intended gall depths (in inches). Each pie chart is categorized by fracture location: “Artificial” represents fracture at galling tool location, “Natural ” represents fracture at a measured and identified notch outside the galling tool location, and “Other” represents fracture at unmeasured location outside the galling tool location.

5.3.4 Total elongation data analysis

According to the DOE, elongation data for gall depths of 0mm, 0.0254mm, 0.0508mm, and 0.0762mm was considered, including details on direction, clearance, upper edge shape and support level. In total, this dataset contained 240 total elongation data points. Scatterplots were constructed to investigate any prominent relationships between gall depth measurement (in micro-meters) and total elongation response, shown in Figure 34. The data points were separated into two panel columns, where each column represented the respective support and upper trim tool shape condition: 0.08R – No Support (left) and 0.33R – High Support (right). The rows in each panel column reflect the three material rolling directions: DD, LD and TD. Each panel data points were categorized by clearance: 10% and 30% clearance. By high level assessment of the data points in

Figure 34, increasing gall depth can generally be observed to reduce elongation response for most trim conditions except 10% - 0.33R/High which seemed to have a null relationship.

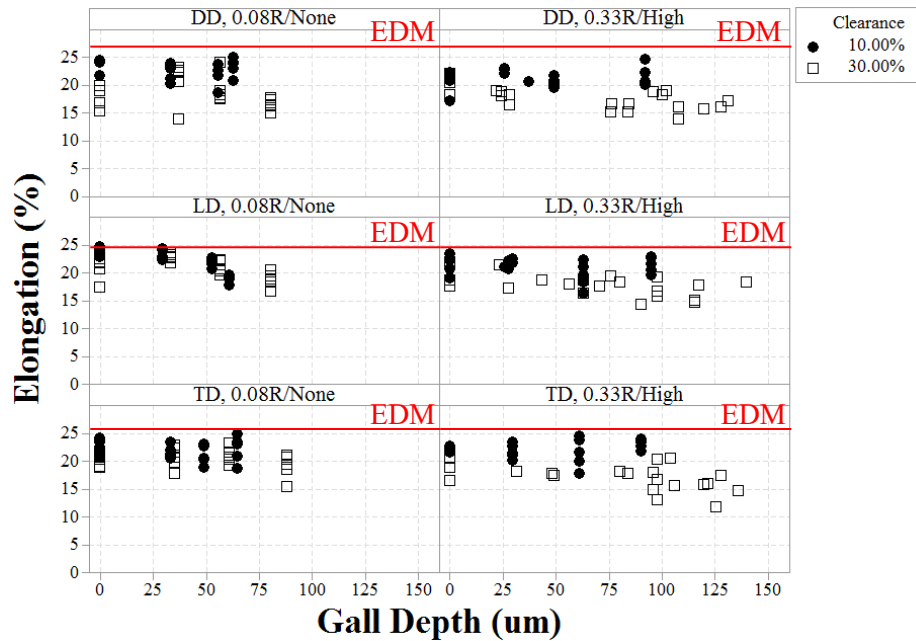


Figure 34: Elongation data for all measured gall depths (micro-meters). Each panel represents a combination of support/upper trim tool shape and rolling direction conditions. Data points are categorized by clearance. Mean EDM elongation shown as reference line in red.

5.3.5 Multivariate, linear regression model

A stepwise forward selection linear regression analysis was utilized to identify statistically significant trimming parameters and interactions. The response variable was the total elongation to fracture of the sheared specimens. Predictor variables included clearance and gall depth as continuous variables, as well as direction and shape/support as categorical variables. All two and three way interaction terms between the predictor variables were included in the model. The tabulated results of the model are shown in Appendix C. According the ANOVA table generated by the last iteration of the stepwise procedure, the most significant main factors were clearance, gall depth, and shape/support. The significant interactions were clearance*shape/support and galldepth* clearance*shape/support.

A regression model was built that included all significant terms previously identified by the forward stepwise procedure. The tabulated results for this model and the fulfillment of the assumptions of linear regression¹⁸ are shown in Appendix C. The ANOVA table indicates that

¹⁸ The residuals from this linear regression model should be normally distributed, have equal variance, and be random throughout observations in order for statistical computations and p-value driven conclusions to be valid [44].

clearance, gall depth, and, shape/support, and the interactions terms clearance*shape/support and galldepth* clearance*shape/support were still significant predictors of elongation. Galldepth*clearance and galldepth*shape/support were not significant, but were kept in the model to maintain the hierarchical structure¹⁹. Equation 3 and 4 represent the elongation response as a function of significant trimming parameters generated from the linear regression model for 0.08R/No Support and 0.33R/High Support conditions respectively: gall depth (μm) and clearance (decimal form).

Shape/Support

$$0.08\text{R/No Support} \quad \text{Elongation (\%)} = 24.782 - 0.0362 \text{ Gall Depth} - 13.34 \text{ Clearance} + 0.0567 \text{ Gall Depth} * \text{Clearance} \quad (3)$$

$$0.33\text{R/High Support} \quad \text{Elongation(\%)} = 22.568 + 0.0161 \text{ Gall Depth} - 10.72 \text{ Clearance} - 0.1395 \text{ Gall Depth} * \text{Clearance} \quad (4)$$

To facilitate investigation of the trends of the elongation response, the regression equations produced by the regression model are graphed in Figure 35, along with the main effect plot in Figure 36.

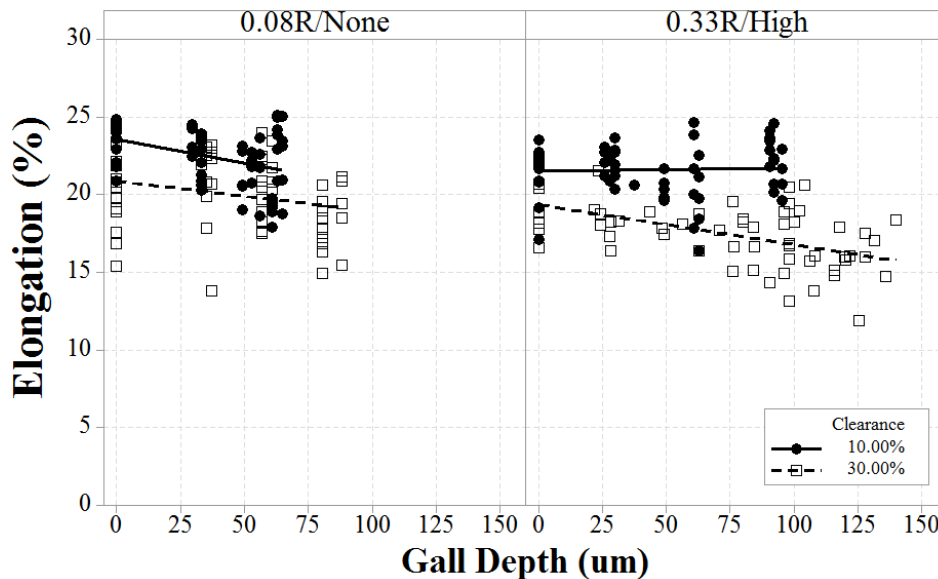


Figure 35: Scatterplot of elongation vs. gall depth with regression lines from regression model. Each panel represents shape/support trimming condition. Data within each panel categorized by clearance.

¹⁹ A hierarchical regression model contains all lower order terms necessary to describe high order interaction terms.

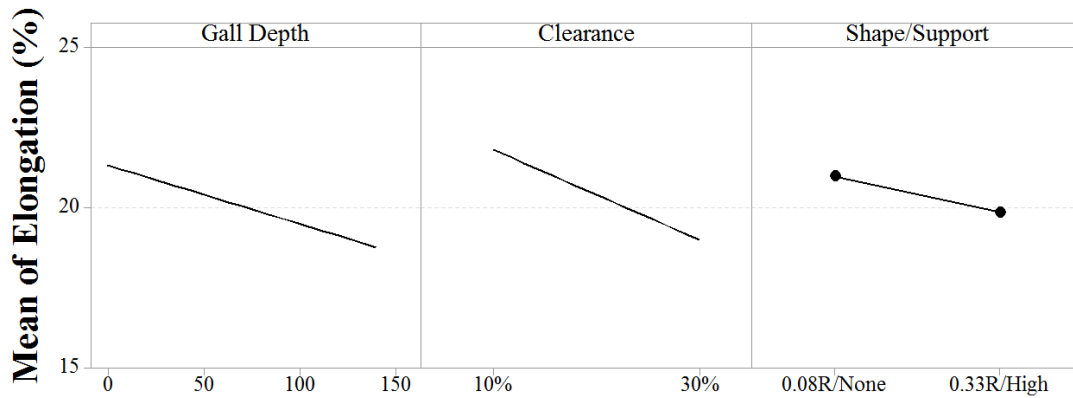


Figure 36: Main effect plot of individual trimming conditions, generated by regression model.

The plotted regression equations in Figure 35 show that as clearance increased, elongation response decreased. Additionally, as gall depth increased, elongation generally decreased except for 0.33R/High Support – 10% clearance condition where elongation response was not affected by gall depth. The mean effect plot in Figure 36 reaffirms that increasing gall depth and clearance reduces elongation response.

A proposed explanation for the difference of elongation response based on shape/support and clearance condition could be described by starting with the findings from Figure 28 through Figure 31, whereas trimming conditions increased cumulative damage, fracture zone rotation increased and artificial gall penetration length decreased. A perceptible conclusion could be that the magnitude of galling effect on edge stretch (represented by regression slopes in Figure 35) reduced as the effective artificial gall penetration length reduced. In other words, as gall penetration length increased, this most likely generated a larger stress concentration zone which led to larger negative effects on edge stretch response. Of course, looking at Figure 35 this trend seemed to be violated by the 30%-0.33R High Support where gall depth had a significant negative effect on edge stretch, even though it had the smallest artificial gall penetration length from Figure 31. However the majority of plotted points in Figure 35 are from the natural gall phenomenon since the majority of fracture initiation was at recorded at natural gall marks seen in Figure 33. Natural galling likely overshadowed the effect of artificial galling on edge stretch response because findings from Figure 31 showed that natural gall marks often exceed the penetration depth and length of artificial gall marks. Since natural galling seemed to dominate over artificial galling geometrically, it would have contributed to an increase in magnitude of the negatively sloped elongation response, which is precisely what is observed in Figure 35. From these findings, expected elongation can be optimized by minimizing clearance and galling depth. Since achieving a complete absence of

galling is practically infeasible in full scale blanking operations, to add engineering robustness, optimal trimming conditions were defined as a range: galling depth at or below 50 μm . To add robustness across different levels of damage in the sheared edge, the optimal galling depth data included elongation from low to medium damage trimming conditions tested: 10% - 0.08R – No Support, 30% - 0.08R – No Support, 10% - 0.33R – High Support. As an exception, the high damage trimming condition, 30% - 0.33R/High Support, was removed from consideration of optimal galling conditions because it produced an unstable, random occurrence of natural gall marks that nearly reached depths of 150 μm and produced the lowest elongation response. Under these conditions, edge stretch was robust across LD/DD/TD directions.

5.3.6 Probability distribution of optimal parameters

The combined elongation data for optimal trimming conditions was graphed in a frequency distribution plot and probability plot, shown in Figure 37. The elongation data resulted in a good fit for a left-skewed 3-parameter Weibull distribution curve, as seen in Figure 37 (a) and (b).

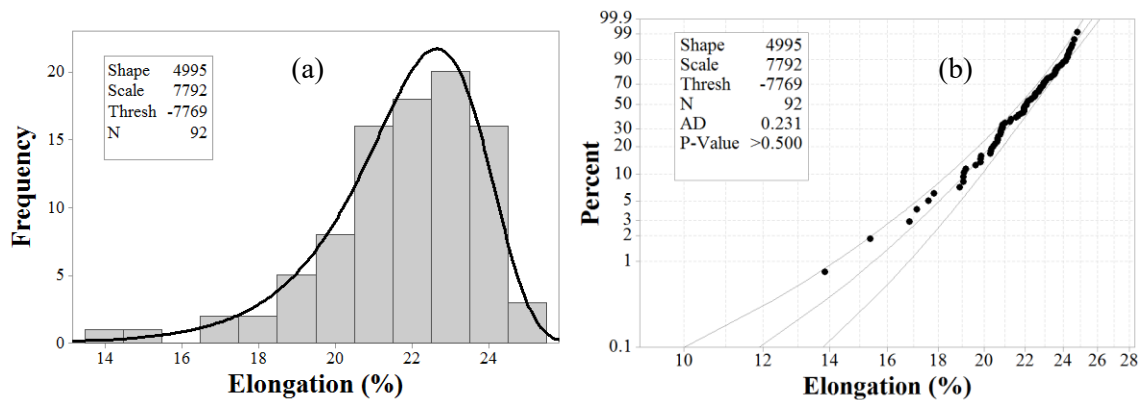


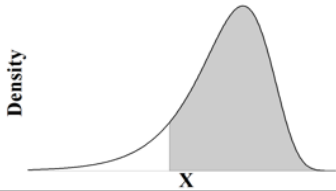
Figure 37: (a) Histogram of optimal gall elongation data with fitted probability distribution (3-parameter Weibull). (b) The corresponding probability plot with lower and upper bound 95% confidence interval.

Based on the three parameters of the Weibull distribution, the mean and standard deviation of each data set can be calculated²⁰. The identified distribution was used to determine the lower bound elongation limits for various levels of risk, as shown in Table 7. The skewness of the Weibull distribution resulted in much greater risk of failure than can be expected with normally distributed data at any elongation limit. Even at six standard deviations from the mean, 300 defects per million

²⁰ The mean and standard deviation of a skewed-left Weibull probability distribution function differ from typical mean and standard deviation computation that assumes normally distributed data.

(DPM) would be expected compared to 3.4 DPM for a normal process. The skewness also indicates that the elongation limits, with any reasonable risk, are much lower than the mean.

Table 7: Elongation limits for optimal radius trimming conditions and various levels of risk

Mean	Std. Dev.	Probability Density Function (PDF)		
22.10	2.00			
Std. Dev. From Mean	Success Rate	Lower Bound Total Elongation, X (%)	Defects per million (DPM)	
$\mu - 1\sigma$	85.59%	20.10	144100	
$\mu - 2\sigma$	95.77%	18.10	42300	
$\mu - 3\sigma$	98.81%	16.10	11900	
$\mu - 4\sigma$	99.67%	14.10	3300	
$\mu - 5\sigma$	99.91%	12.10	900	
$\mu - 6\sigma$	99.97%	10.10	300	

5.4 Conclusion

The purpose of this chapter was to investigate edge stretch in a range of galling depths across typical blanking die trimming conditions, and effectively identify which conditions maximize edge stretch of 6DR1 0.9 mm aluminum. Findings are summarized below:

1. Four major trimming conditions were studied, reflecting incrementally distinct damage in the sheared edge. Elongation data indicated that the 10%-0.08R-No Support condition reflected lowest damage, highest elongation response while the 30%-0.33R-Support condition reflected highest damage, lowest elongation response.
2. Galling penetration depth and length through material thickness have a significant effect on elongation response. More specifically, as penetration depth and length increases, the elongation response decreased
3. Artificial galling had the largest penetration length on sheared edge at the lower damage trimming conditions with small rollover and fracture zone rotation, 10%-0.08R-No Support and 30%-0.08R-No Support. Fracture initiation located at artificial gall for these trimming conditions occurred frequently. Artificial galling had the smallest magnitude of penetration on sheared edge at the higher damage trimming conditions with large rollover and fracture zone rotation, 10%-0.33R-High Support and 30%-0.33R-High Support. Fracture initiation located at artificial gall for these trimming conditions occurred infrequently.

4. Natural gall marks occurred unintentionally at random depths in the highest damaging trimming condition 30% - 0.33R/High Support. Natural gall marks often had larger gall penetration depth and length through material thickness when compared to the geometry of the artificial gall marks. Fracture initiation of tensile test specimens often were located at natural gall marks in the 30% - 0.33R/High Support trimming condition.
5. Elongation was maximized by maintaining galling depth at or below 50 μm . As an exception, the trimming condition 30% - 0.33R/High Support was removed from consideration of optimal trimming conditions because it produced an unstable, random occurrence of natural gall marks.
6. Edge stretch response followed left-skewed Weibull distribution with much greater risk of failure than can be expected based on normally distributed data. For this reason, the elongation limit for this material was much lower than the mean elongation.
7. For a failure risk of 0.03%, the limits were 10.1% elongation for optimal galling depth trimming conditions.

CHAPTER 6

Investigative Study #3: Lower trim tool gap study

6.1 Introduction

The design of conventional blanking die trim tools may contribute to edge damage that would reduce edge stretch. Specifically, the trim line of the door opening in body-side panel, Figure 38(a), is not trimmed by a continuous tool edge, but rather by an array of smaller trim tool inserts with gaps in between that collectively form the entire trim line, as can be seen in Figure 38(b). There are two main reasons why large, continuous trim tool inserts are not traditionally used: (1) it is difficult to maintain dimensional integrity of trim line after heat treatment and (2) due to uneven wear on the trim edge in a production tool, it is difficult to service and replace one large trim edge compared to multiple smaller inserts. Assembly procedures of the segmented trim tools require a small gap between the trim inserts to compensate for dimensional and fitted tolerances. The effect this gap on edge stretch of aluminum has not been reported in the open literature. Therefore, the purpose of this chapter is to investigate the edge stretch response of specimens trimmed with tools exhibiting a range of gap levels, with two specific objectives: (1) identify significant trimming parameters to edge stretch response, and (2) subsequently find a range of tool gap distances combined with other significant trimming parameters that maximizes total elongation of the trimmed half-dog bone specimens.

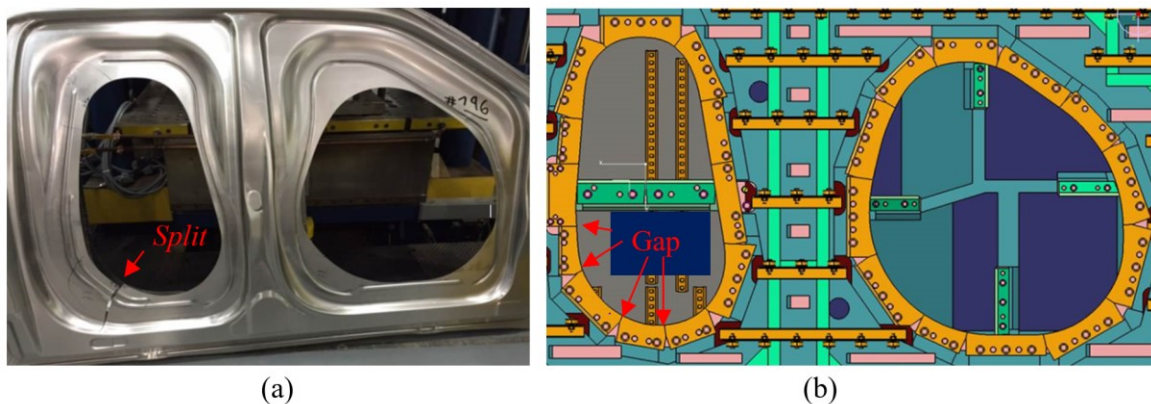


Figure 38: (a) DOP drawn shell with pre-mature split and (b) CAD model of trim tool inserts for blanking window opening with designed gaps shown.

6.2 Methodology

The experimental methodology studied the effect of lower trim tool gap on edge stretch. In summary, half-dog bone specimens that were machined from a 6DR1 aluminum coil were trimmed in the laboratory press with adjustable tooling to modulate trimming parameters, mainly variable gap distances in the lower trim tool. Trimmed specimens were then pulled to failure in a tensile test machine where total elongation data was recorded. Total elongation data was analyzed with statistical tools to provide statistically significant conclusions to optimal trimming parameters that maximize edge stretch.

6.2.1 Trimming parameters

The trimming conditions included in this study are depicted in Figure 39. For brevity they are referred to as clearance, support, shape, gap distance, and direction.

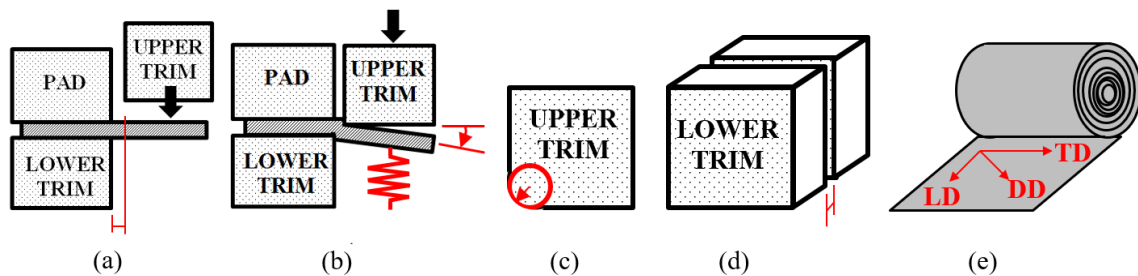


Figure 39: Five major categories of trimming conditions. Clearance (a), Support (b), Shape (c), Lower trim tool gap (d), and Direction (e).

Clearance between the upper and lower trim tools, shown in Figure 39 (a), was the main process parameter, reported in % of the sheet thickness. Support is the amount of resistance against offal rotation, shown in Figure 39 (b). Shape refers to the geometrical shape of the upper trim tool edge, seen in Figure 39 (c). A sharp lower trim tool was used in this study. Gap refers to the distance between a split lower trim tool that leads to a gap in the trim line, shown in Figure 39 (d). Sample direction is the line of trimming action relative to the rolling direction of the coil, seen in Figure 39 (e).

All half-dog bone specimens were trimmed to the procedure described in Section 3.3.2 and the components of the laboratory press operation are echoed in Figure 40. Unique to this study, the gap depth was controlled using shims of variable thickness in between the split lower trim tool, shown in Figure 40 (b).

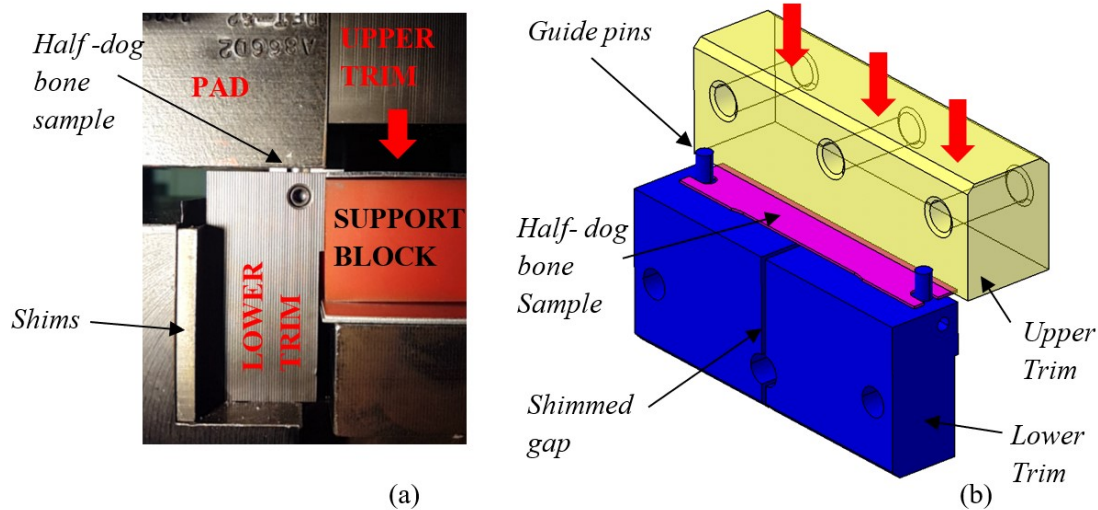


Figure 40: (a) Experimental press side view (b) Isometric view of laboratory trim tools with the gap in the lower tool and arrows indicating trimming operation.

6.2.2 Design of experiment (DOE)

The experiment was designed as a full factorial DOE with four parameters, as shown in Table 8. Each combination was repeated five times. Four gap distance levels were selected to represent minimum and maximum gap condition commonly present in production dies: 0.075mm, 0.085mm, 0.1mm, 0.15mm. Two upper trim edge shape and support combinations were selected: Sharp-No Support and 0.25R-High Support. No support allows for free rotation of offal, whereas high support did not allow any offal rotation. Two levels of clearance were investigated: the baseline clearance of 10% of the sheet thickness and a clearance of 30% that represents clearance levels often encountered in production dies. The specimens were shear in three different orientations relative to the rolling direction of the sheet: Longitudinal (LD), Transverse (TD), and Diagonal (DD) trimming directions.

Table 8: Description of all conditions in full factorial DOE

Parameter	Level
Gap (4)	0.075mm, 0.085mm, 0.1mm, 0.15mm
Upper Shape-Support (2)	Sharp-None, 0.25R-High
Rolling Direction (3)	LD, DD, TD
Clearance (2)	10%, 30%
Repetitions (5)	
TOTAL	240 data points

6.2.3 Design vs. actual geometry of trim tool edges

Microscopic imaging methods were used to measure the actual edge geometry of manufactured trim tools, as shown in Figure 41. The edge measurement results of all manufactured trim tools revealed that the actual geometry of the trim tools varied from design intent.

Investigation into the manufacturing process of the trim tools revealed that the grinding practices used to generate the controlled edge radius were inconsistent, and the measurement method that validated the radius was not precise enough to meet the design intent. Table 9 shows the translation of design to actual trim tool edge geometry. For all following sections and data analysis, the actual (measured) geometry will be used.

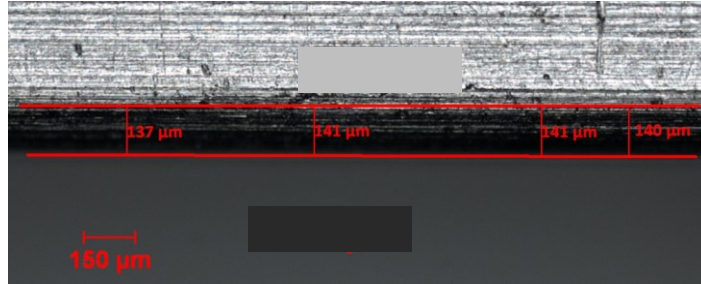


Figure 41: (a) Trim tool with radius geometry shown with two arrows that represent the two directions that microscopic pictures were taken and measured. (b) Top view, microscopic image with actual measured trim tool edge geometry defined by contrast of lighting showing 0.25R trim tool edge by design.

Table 9: Comparison of design and actual measured geometry in trim tool edges

Design	Actual
0.00R	0.04R
0.25R	0.14R

6.3. Results

6.3.1 Microscopic gap measurement

To account for any variability in the gap setup, the observed gap width in each trimmed half-dog bone specimen, was microscopically imaged, as can be seen in Figure 42, and subsequently measured. A total of three measurements along the length of the gap witness mark were made, and the average of the three measurements was then recorded for data analysis.

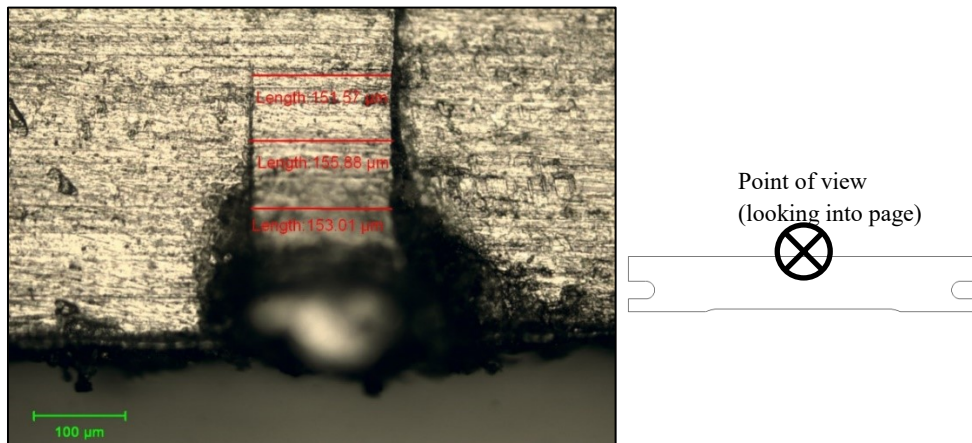


Figure 42: Microscopic view of gap width witness in the trimmed half-dog bone specimen with three measurements along the gap width shown.

6.3.2 Incremental edge damage

There were four incremental damage trimming conditions implemented as described in the design of experiment: 10% - 0.04R – No Support, 30% - 0.04R – No Support, 10% - 0.14R – High Support, and 30% - 0.14R – High Support. The purpose of choosing these specific trimming conditions was to generate incremental levels of plastic deformation to the trimmed edge, so as to provide information on how gap distances effects specimen total elongation across different levels of damage existing in the edge. More details on the reasoning on this theory was provided in the previous chapter, section 5.3.2. Elongation values of trimmed half-dog bone specimens were analyzed to investigate the expected decrease in edge stretch as trimming conditions due to increased edge damage. Figure 43 shows the total elongation values against the four trimming conditions. Elongation data shows, with statistical significance, that the 10%-0.04R-No Support condition experienced the lowest damage with the highest elongation response, while the 30%-0.14R-Support condition experienced the highest damage with the lowest elongation response.

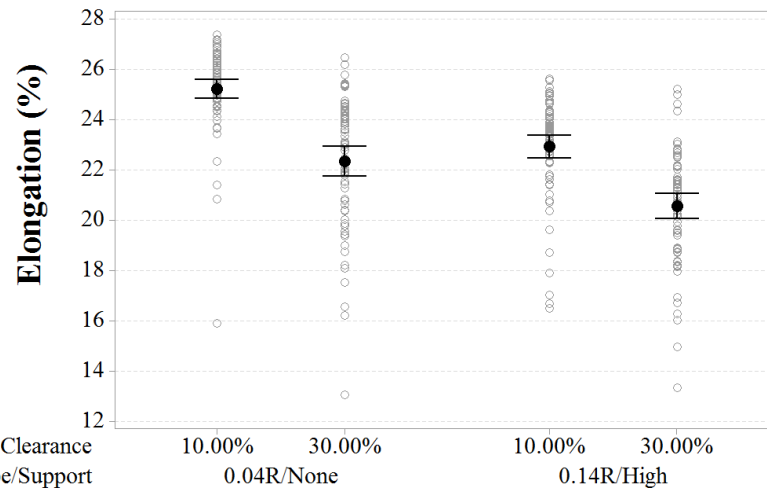


Figure 43: Interval plot of four main trimming conditions with 95% confidence interval for the mean shown. Elongation results show that 10%-0.04R-No Support condition produced the highest response and 30%-0.14R-Support condition produced the lowest response.

6.3.3 Total elongation data analysis

According to the DOE, elongation data for gap distances of 0.075mm, 0.85mm, 0.1mm, and 0.15mm was considered, including details on direction, clearance, upper edge shape and support level. In total, this dataset contained 240 elongation data points. Scatterplots were constructed to investigate any prominent relationships between gap measurement in the lower trim tool and elongation response, shown in Figure 44. The data points were separated into three panel

columns that represented each of the three material rolling directions: DD, LD, and TD. Within each column, there were two groupings of graphs that represented the two clearance conditions: 10% (top) and 30% (bottom). Within each grouping of graphs, data was separated into the two levels of shape/support parameters: 0.04R/None (top) and 0.14R/High (bottom). By high level assessment of the data points in Figure 44, there was no clear correlation between gap measurement and elongation response.

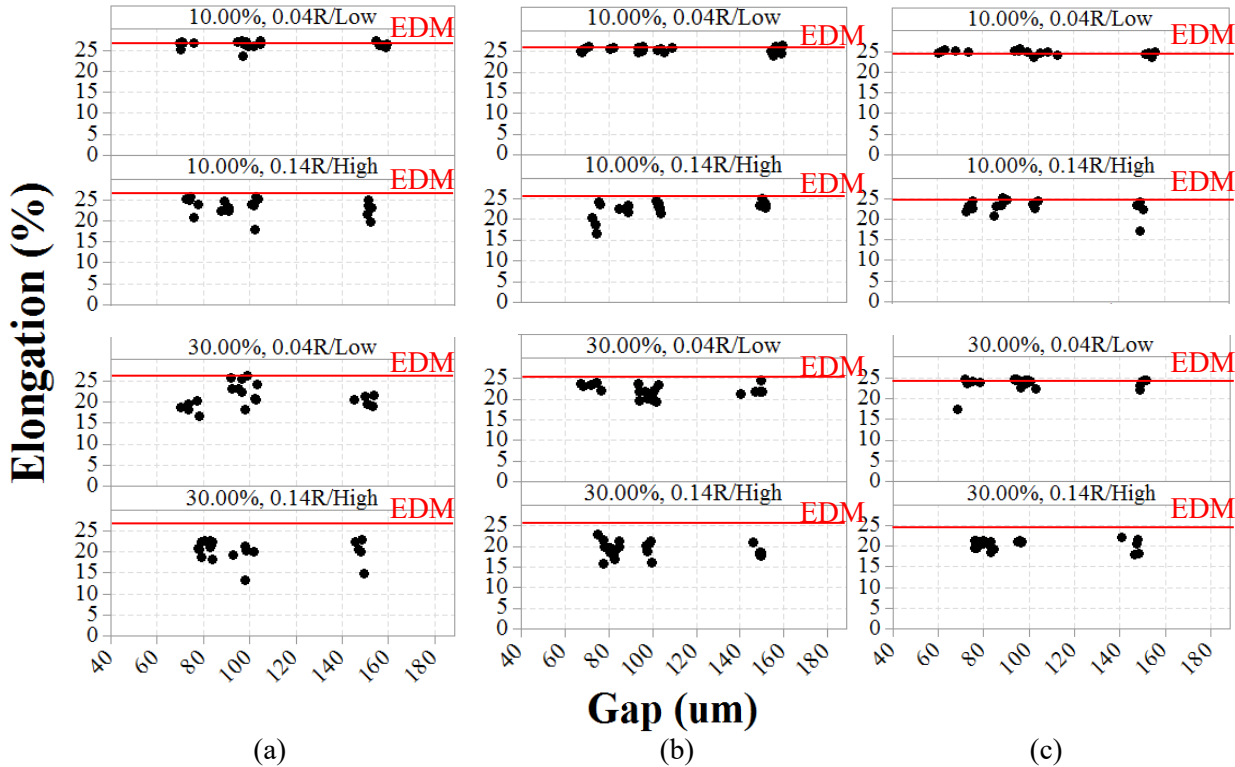


Figure 44: Scatter plot of total elongation and gap distance based of trimming conditions. Panel columns represent rolling direction: (a) DD, (b), TD, and (c) LD. Rows of panels represent clearance and shape/support conditions.

6.3.4 Multivariate, linear regression model

A stepwise forward selection linear regression analysis was utilized to identify statistically significant trimming parameters and interactions. The response variable was the total elongation to fracture of the sheared specimens. Predictor variables included clearance and gap distance as continuous variables, as well as direction and shape/support as categorical variables. All 2 and 3 way interaction terms between the predictor variables were included in the model. The tabulated results of the model are shown in Appendix D. According the ANOVA table generated by the last iteration of the stepwise procedure, the most significant main factors were clearance and

shape/support. Gap distance and direction were not added in the stepwise procedure since they were not found to be significant predictor of elongation.

A regression model was built that included all significant terms previously identified by the forward stepwise procedure. The tabulated results for this model and the fulfillment of the assumptions of linear regression²¹ are shown in Appendix D. The ANOVA table indicates that clearance and shape/support were still significant predictors of elongation. Equation 4 and 5 represent the elongation response as a function of significant trimming parameters generated from the linear regression model for 0.04R/No Support and 0.14R/High Support conditions respectively: gall depth (μm) and clearance (decimal form).

Shape/Support

$$0.04\text{R/No Support} \quad \text{Elongation (\%)} = 26.900 - 14.92 \text{ Clearance} \quad (4)$$

$$0.14\text{R/High Support} \quad \text{Elongation(\%)} = 24.550 - 14.92 \text{ Clearance} \quad (5)$$

To facilitate investigation of the trends of the elongation response, the regression equations produced by the regression model are graphed in Figure 45, along with the main effect plot in Figure 46.

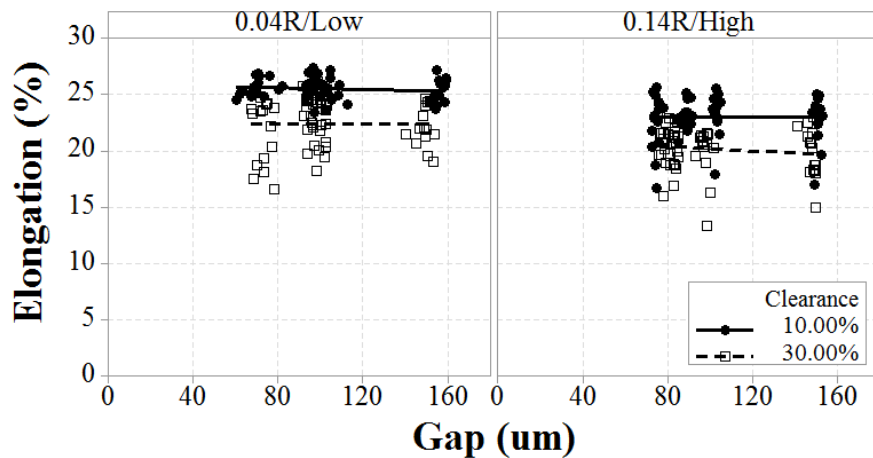


Figure 45: Scatterplot of elongation vs. gap distance with regression lines from regression model. Each panel represents shape/support trimming condition. Data within each panel categorized by clearance.

²¹ The residuals from this linear regression model should be normally distributed, have equal variance, and be random throughout observations in order for statistical computations and p-value driven conclusions to be valid [44].



Figure 46: Main effect plot of individual trimming conditions, generated by regression model.

The plotted regression equations in Figure 45 and main effect plot in Figure 46 show that as clearance increased, elongation response decreased. They also showed that the gap distance in the lower trim tool had no significant effect on total specimen elongation.

Further investigation into the apparent null gap effect on total elongation led to the investigation of microscopic images of trimmed edge of specimens near gap location. Microscopic imagery of trimmed edge geometry at gap location, shown in Figure 47, revealed that for all trimming conditions, a geometrical imperfection was observed at the gap location in the lower trim tool, primarily in the form of a burr. The burr generated at the location of the gap varied in shape and size based on trimming conditions, as can be seen in Figure 47. With the low to high damage trimming conditions of 10% - 0.04R – No Support, 10% - 0.14R – High Support, and 30% - 0.14R – High Support, the burr length along the trimmed edge was approximately the same size as the gap distance while burr height tended to increase, seen from Figure 47 (a), (c), and (d) respectively. In these cases, the burr was located directly at the location of the gap in the lower trim tool. The 30% - 0.04R – No Support trimming condition produced the largest burr height, shown in Figure 47 (b), however, unlike the other trimming conditions, the burr length existed outside the bounds of the gap location, shown in Figure 47 (b). Although an apparent burr was observed to form in the sheared edge at the gap location for all trimming conditions, observations of the same images from Figure 47 (a)-(d) showed that there were no visible imperfections that penetrated through the entire thickness of the trimmed edge, above the generated burr at the gap location. The absence of any penetration of geometrical imperfections through the sheared edge thickness might have contributed to the null gap effect because in the previous chapter on galling, geometrical imperfections with smaller penetration lengths through the sheared edge were found to have limited to null effect on edge stretch.

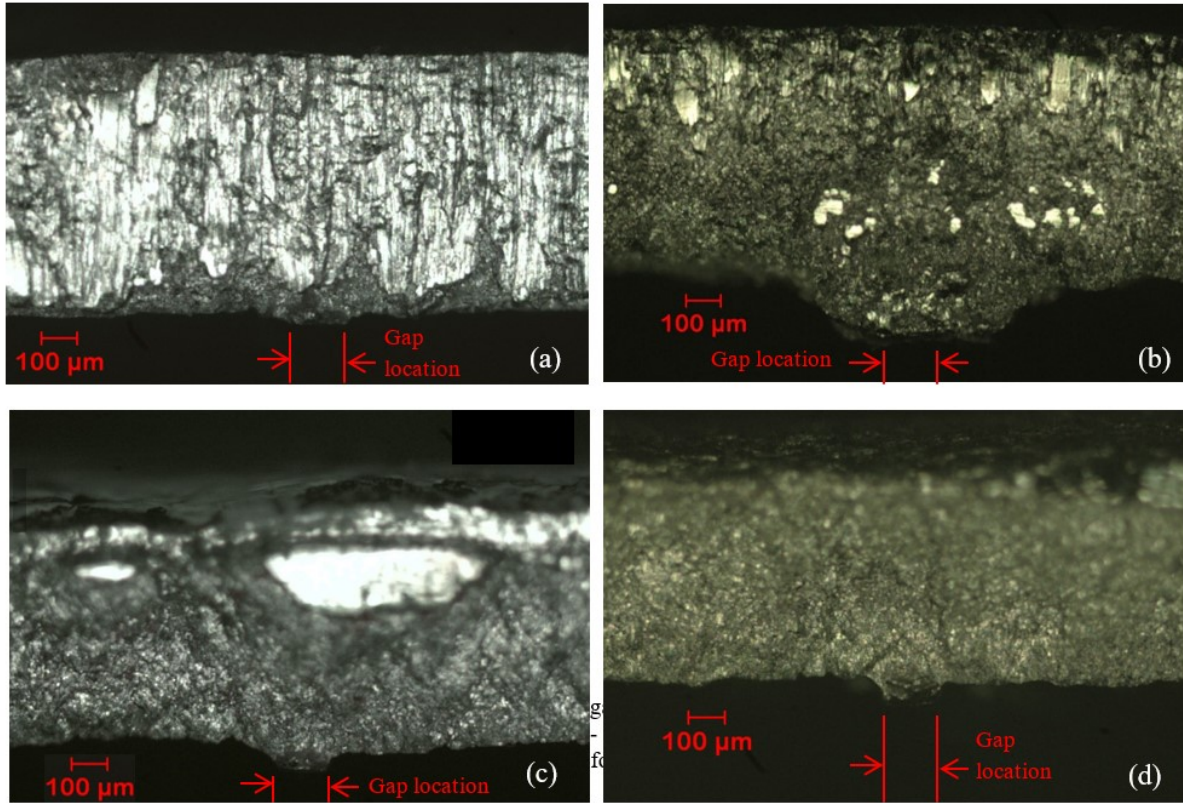


Figure 47: Microscopic images of trimmed edge at gap location for each of the four major trimming conditions: (a) 10% - 0.04R – No Support, (b) 30% - 0.04R – No Support (c) 10% - 0.14R – High Support, and (d) 30% - 0.14R – High Support. Gap distance for all images were at maximum value of 0.004”

Even further investigation into the null gap effect on total elongation led to the data collection on the fracture locations for all stretched to failure half-dog bone specimens. The foundational assumption would be that if the gap in the lower trim tool had a direct effect on specimen elongation, then the fracture initiation in the half-dog bone specimen should be witnessed at the location of the gap in the tool in a significant number of cases. Findings showed that the percent of fracture initiations located at the gap in the lower tool was null at 10% clearance and marginally appeared at 30% clearances, shown in Figure 48. For the instances that fracture did initiate at the gap location, the total elongation values were compared to specimens that fractured at other locations with a two sample t-test, however no statistically significant difference was found.

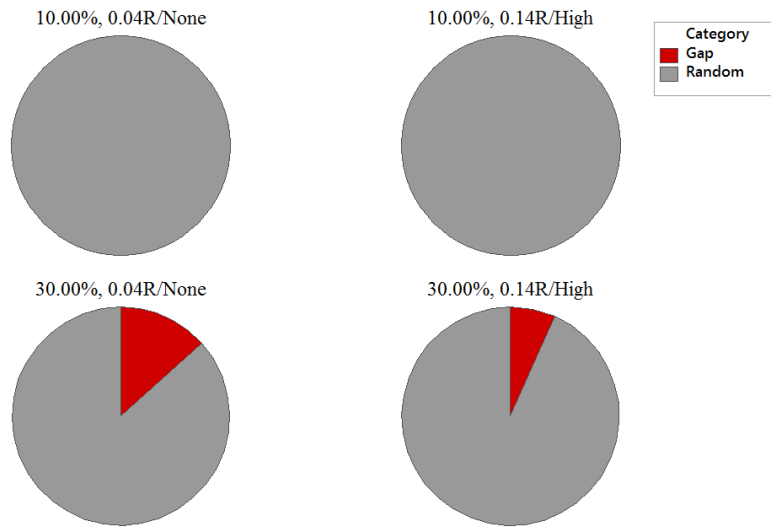


Figure 48: Percentage of fracture initiation located at gap in lower trim tool in half-dog bone specimen, shown in red, compared to random location outside gap.

From these findings, expected elongation can be optimized by minimizing clearance and maintaining the gap distance in the lower trim tool within experimented limits. Since common blanking die practices incorporate trim tool inserts with gap conditions, to add engineering robustness, optimal trimming conditions were defined as a range: gap distance less than 0.15mm. To add robustness across different levels of damage in the sheared edge, the optimal gap conditions included elongation from the low to high damage trimming conditions tested: 10% - 0.04R – No Support, 30% - 0.04R – No Support, 10% - 0.14R – High Support, and 30% - 0.14R – High Support. Under these conditions, edge stretch was robust across LD/DD/TD directions. Unlike the previous chapter on galling, the high damage 30% - 0.14R/High support condition was decided to be included in the optimal gap condition consideration because no natural galling was observed, most likely due to the sharper 0.14R edge compared to the 0.33R in the previous chapter.

6.3.5 Probability distribution of optimal parameters

The combined elongation data for optimal trimming conditions was graphed in a frequency distribution plot and probability plot, shown in Figure 49. The elongation data resulted in a good fit for a left-skewed 3-parameter Weibull distribution curve, as seen in Figure 49 (a) and (b). Based on the three parameters of the Weibull distribution, the mean and standard deviation of each data

set can be calculated²². The identified distribution was used to determine the lower bound elongation limits for various levels of risk, as shown in Table 10.

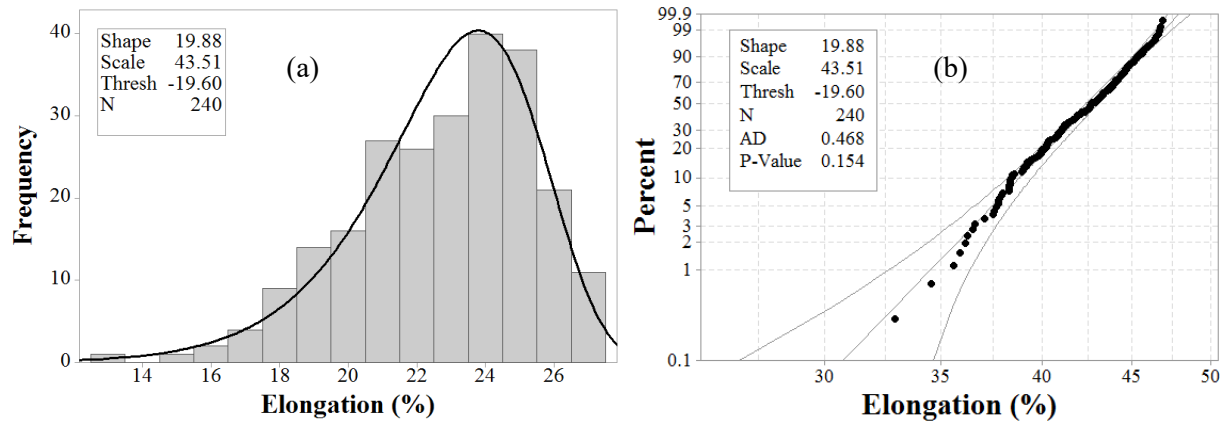
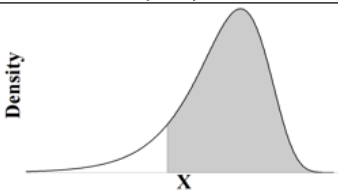


Figure 49: (a) Histogram of optimal gall elongation data with fitted probability distribution (3-parameter Weibull). (b) The corresponding probability plot with lower and upper bound 95% confidence interval.

Table 10: Elongation limits for optimal radius trimming conditions and various levels of risk

Mean	Std. Dev.	Probability Density Function (PDF)	
22.75	2.64		
Std. Dev. From Mean	Success Rate	Lower Bound Total Elongation, X (%)	Defects per million (DPM)
$\mu - 1\sigma$	85.00%	20.11	150000
$\mu - 2\sigma$	95.94%	17.47	44600
$\mu - 3\sigma$	99.05%	14.83	9500
$\mu - 4\sigma$	99.81%	12.19	1900
$\mu - 5\sigma$	99.97%	9.55	300
$\mu - 6\sigma$	99.995%	6.91	50

The skewness of the Weibull distribution resulted in much greater risk of failure than could be expected with normally distributed data at any elongation limit. Even at six standard deviations from the mean, 50 defects per million (DPM) would be expected compared to 3.4 DPM for a normal process. The skewness also indicates that the elongation limits, with any reasonable risk, are much lower than the mean.

²² The mean and standard deviation of a skewed-left Weibull probability distribution function differ from typical mean and standard deviation computation that assumes normally distributed data.

6.4 Conclusion

The purpose of this chapter was to investigate edge stretch in a range of gap distances in the lower trim tool across typical blanking die trimming conditions, and effectively identify which conditions maximize edge stretch of 6DR1 0.9 mm aluminum. Findings are summarized below:

1. Four major trimming conditions were studied, reflecting incrementally distinct damage in the sheared edge. Elongation data indicated that the 10%-0.04R-No Support condition experienced the lowest damage and the highest elongation response, while the 30%-0.14R-Support condition experienced the highest damage and the lowest elongation response.
2. Gap distance in the lower trim tool had no statistically significant effect on aluminum edge stretch. However, investigation of microscopic images showed that geometrical imperfections in the form of burrs existed in various magnitudes at the gap location.
3. Optimal trimming conditions were defined by maintaining gap distance at or below 0.15mm.
4. Edge stretch response followed left-skewed Weibull distribution with much greater risk of failure than can be expected based on normally distributed data. For this reason, the elongation limit for this material was much lower than the mean elongation.
5. For a failure risk of 0.005%, the limits were 6.91% elongation for optimal galling depth trimming conditions.

CHAPTER 7

Conclusion

7.1 Summary

The purpose of the undertaken investigation in this thesis was to study 6DR1 aluminum edge stretch response of the three investigatory trimming parameters (upper edge sharpness, galling depth, and lower gap distance) in combination with other baseline trimming conditions (clearance, material direction, and support), and to statistically determine a robust range of optimal trimming conditions feasible from an engineering perspective that maximize material edge stretch. The most significant findings are listed below:

1. Clearance between upper and lower trim tools had the most significant influence on material elongation: as clearance increased, material elongation decreased. Optimal clearances were defined at clearances below 30% of the thickness of the trimmed sheet.
2. The edge radius of the upper trim tool had a significant effect on material elongation: as radius increased, elongation decreased. Optimal radius in upper trim tool was identified to be a radii below 0.14 mm.
3. Gall depth had a significant reduction effect on material elongation. Generally, as gall penetration depth and length increased, the elongation response decreased. More specifically, when gall penetration length was maximized in lower damage trimming conditions where sheared edge rollover and fracture angle were small, the increase of galling depth significantly reduced the edge stretch response. Alternatively, when gall penetration length was minimized in higher damage trimming conditions where sheared edge rollover and fracture angle were large, the increase of galling depth marginally reduced the edge stretch response. Additionally, at the high damage trimming conditions, undesirable natural galling occurred with randomly distributed penetration depth and length. Optimal gall depth in the sheared edge was defined as less than $50\mu m$.
4. Gap distance in the lower trim tool had no statistically significant effect on material elongation.

Overall, the measured elongations from all investigative studies followed a left-skewed Weibull distribution with greater statistical probability of low elongation to failure than that predicted with a normal distribution.

7.2 Implications

The results of this analysis has wide ranging practical applications in the field of automotive sheet metal stamping that includes, but not limited to, providing an appropriate discriminant on edge stretch in FEA formability evaluation, supporting stamping die design standards, and developing die maintenance schedules.

7.3 Limitations

There are several limitations of the methods and findings discussed in this paper. First, the linear regression models that drove the conclusions on optimal trimming conditions are only valid to discuss general effects within the range of the experimented trimming parameters and may not be valid for predictions outside of those ranges. This is because the model R^2 values were generally low (~ 50%). Second, only one material and gauge was used throughout this study: 0.9mm 6DR1 aluminum sheet; there was no investigation preformed that provided evidence that the findings presented in this paper were valid across different 6000 series aluminum alloys and across different gauges.

7.4 Future work

Following the methods and findings throughout this paper, additional research into investigating the wear geometry of trim tools as a function of trimming cycles would prove valuable. This study assumed the wear profile of the trim tool edge as a uniform radius; however, it is quite plausible that the actual wear profile geometry is variable in shape. Determining the wear function of trim tools would be valuable in developing stamping die maintenance schedules, and in specifically determining when tools are outside the optimal parameters. Another useful study would investigate the geometry and rate of accumulation of galling as a function of trimming cycles. This information would also prove useful in stamping die maintenance schedules, by determining the point when galling exceeds the optimal limits discussed in this paper.

Additionally, this study could be repeated for multiple materials or thicknesses to determine if the observed extend to other alloys and thicknesses.

REFERENCES

- [1] K. Lange, Handbook of Metal Forming, McGraw-Hill, 1985.
- [2] E. Izod, "Behavior of Materials of construction under pure shear," *Proceedings Of The Institution Of Mechanical Engineers*, pp. 5-55, 1906.
- [3] G. Anthony, "Pressure-recording indicator for punching machinery," *Transactions of the ASME*, pp. 215-31, 1911.
- [4] T. Chang and H. Swift, "Shearing of Metal Bars," *Journal of the Institute of Metals*, pp. 119-146, 1950.
- [5] R. Slater and W. Johnson, "The effects of temperature, speed, and strain-rate on the force and energy required in blanking," *Inst. J. Mech. Sci.*, vol. 9, pp. 271-305, 1967.
- [6] C. Noble and P. Oxley, "Crack formation in blanking and piercing," *Int. J. Prod. Res.* , vol. 2, pp. 265-274, 1963.
- [7] W. Jouri and N. Jones, "The impact behavior of aluminium alloy and mild steel double-shear specimens," *Int. J. Mech. Sci.*, vol. 30, pp. 133-172, 1988.
- [8] A. Atkins, "On Cropping and Related Processes," *International Journal of Mechanical Sciences*, vol. 22, 1980.
- [9] Q. Zhou and T. Wierzbicki, "A tension zone model of blanking and tearing of ductile metal plates," *Int. J. Mech. Sci.*, vol. 38, pp. 303-324, 1996.
- [10] W. Johnson, R. Sowerby and R. Venter, Plane Strain Slip Line Fields, Pergamon Press Inc., 1982.
- [11] T. Jimma, " The Theoretical Research on the Blanking of a Sheet Material," *Bulletin of JSME*, vol. 6, pp. 568-576, 1963.
- [12] D. Broek, "A study on ductile fracture," *Ph.D. Thesis*, 1971.

- [13] F. McClintock, "A criterion for ductile fracture by the growth of holes," *Journal of Applied Mechanics*, pp. 363-371, 1968.
- [14] M. Cockcroft and D. Latham, "Ductility and the Workability of Metals," *Journal of the Institute of Metals*, vol. 96, pp. 33-39, 1968.
- [15] J. Rice and D. Tracey, "On the Ductile Enlargement of Voids in Triaxial Stress Fields," *J. Mech. Phys. Solids*, vol. 17, pp. 201-217, 1969.
- [16] Z. Chen, C. Tang, T. Lee and L. Chan, "Numerical simulation of fine-blanking process using a mixed finite element method," *International Journal of Mechanical Sciences*, vol. 44, pp. 1309-1333, 2002.
- [17] S. Golovashchenko, "A study on trimming of aluminum autobody sheet and development of a new robust process eliminating burrs and slivers," *International Journal of Mechanical Sciences*, vol. 48, pp. 1384-1400, 2006.
- [18] X. Hu, K. Choi, X. Sun and S. Golovashchenko, "Edge Fracture Prediction of Traditional and Advanced Trimming Processes for AA6111-T4 Sheets," *Journal of Manufacturing Science and Engineering*, vol. 136, 2014.
- [19] E. Taupin, J. Breitling, W. Wu and T. Altan, "Material fracture and burr formation in blanking results of FEM simulations and comparisons with experiments," *Journal of Materials Processing Technology*, vol. 59, pp. 68-78, 1996.
- [20] D. Brokken, "Numerical modelling of ductile fracture in blanking," Technische Universiteit Eindhoven, 1999.
- [21] Y. Stegeman, A. Goijaerts, D. Brokken, W. Brekelmans, L. Govaert and F. Baaijens, "An experimental and numerical study of a planar blanking process," *Journal of Materials Processing Technology*, vol. 87, pp. 266-276, 1999.
- [22] K. Wang, G. L and T. Wierzbicki, "FE Simulation on Edge Fracture Considering Pre-damage from Blanking Process," Massachusetts Institute of Technology, Cambridge, MA, 2014.
- [23] F. Faura, A. Garcia and M. Estrems, "Finite element analysis of optimum clearance in the blanking process," *Journal of Materials Processing Technology*, Vols. 80-81, pp. 121-125, 1998.

- [24] R. Hambli, "Design of Experiment Based Analysis for Sheet Metal Blanking Processes Optimisation," *Int. J. Adv. Manuf. Tech.*, vol. 19, pp. 403-410, 2002.
- [25] X. Hu, X. Sun and S. Golovashchenko, "Predicting tensile stretchability of trimmed AA6111-T4 sheets," *Computational Materials Science*, pp. 409-419, 2014.
- [26] M. Li, "An experimental investigation on cut surface and burr in trimming aluminum autobody sheet," *International Journal of Mechanical Sciences*, vol. 42, pp. 889-906, 2000.
- [27] S. Golovashchenko and A. Ilinich, "Analysis of Trimming Processes for Advanced High Strength Steels," *SAE International*, 2008.
- [28] X. Hu, X. Sun and S. Golovashchenko, "An integrated finite element-based simulation framework: From hole piercing to hole expansion," *Finite Elements in Analysis and Design*, vol. 109, pp. 1-13, 2016.
- [29] S. Golovashchenko, A. Ilinich, B. N. and L. Smith, "Analysis of Trimming Processes for Advanced High Strength Steels," *SAE International*, 2009.
- [30] S. Golovashchenko, "Quality of trimming and its effect on stretch flanging of automotive panels," *Journal of Materials Engineering and Performance*, vol. 17, pp. 316-325, 2008.
- [31] A. Konieczny and T. Henderson, "On Formability limitations in stamping involving Sheared edge stretching," *SAE Technical Paper Series*, 2007.
- [32] C. Chiriac, "A Study of the Plastic Deformation of Sheared Edges of Dual Phase 780 Steel," *SAE International*, 2010.
- [33] Q. Le, J. deVries, S. Golovashchenko and J. Bonnen, "Analysis of sheared edge formability of aluminum," *Journal of Materials Processing Technology*, vol. 214, pp. 876-891, 2014.
- [34] J. Chintamani and S. Sriram, "Sheared Edge Characterization of Steel Products used for Closure Panel Applications," *SAE International*, 2006.
- [35] N. Wang and S. Golovashchenko, "Mechanism of fracture of aluminum blanks subjected to stretching along the sheared edge," *Journal of Materials Processing Technology*, vol. 233, pp. 142-160, 2016.
- [36] T. Lee, L. Chan and B. Wu, "Straining Behaviour in Blanking Process - Fine Blanking Vs. Conventional Blanking," *Journal of Materials Processing Technology*, vol. 48, pp. 105-111, 1995.

- [37] S. Yu, X. Xie, J. Zhang and Z. Zhao, "Ductile fracture modeling of initiation and propagation in sheet-metal blanking processes," *Journal of Materials Processing Technology*, pp. 169-172, 2007.
- [38] A. Ilinich, S. Golovashchenko and L. Smith, "Material anisotropy and trimming method effects on total elongation in DP500 sheet steel," *Journal of Materials Processing Technology*, vol. 211, pp. 441-449, 2011.
- [39] I. Polmear, *Light Alloys*, Butterworth-Heinemann, 2017.
- [40] Q. Le, "Analysis of Sheared Edge Formability of Aluminum," Ford Research Laboratory Technical Reports, 2013.
- [41] A. Beese, M. Luo, Y. Li, Y. Bai and T. Wierzbicki, "Partially couple anisotropic fracture model for aluminum sheets," *Engineering Fracture Mechanics*, vol. 77, pp. 1128-1152, 2010.
- [42] M. Fritz and P. D. Berger, *Improving the User Experience Through Practical Data Analytics*, Morgan Kaufmann, 2015.
- [43] "Basics of stepwise regression," [Online]. Available: <http://support.minitab.com/en-us/minitab/17/topic-library/modeling-statistics/regression-and-correlation/basics/basics-of-stepwise-regression/>. [Accessed 2016].
- [44] K. M. Ramachandran and C. P. Tsokos, *Mathematica Statistics with Applications in R*, Academic Press, 2nd edition, 2015.
- [45] G. Shieh, "Clarifying the role of mean centering in multicollinearity of interaction effects," *British Journal of Mathematical and Statistical Psychology*, vol. 64, pp. 462-477, 2011.

Appendix A

The following graph shows elongation of half-dog bone specimens cut by EDM machining at different locations along coil length. No statistically significant difference had been found between locations within the coil.

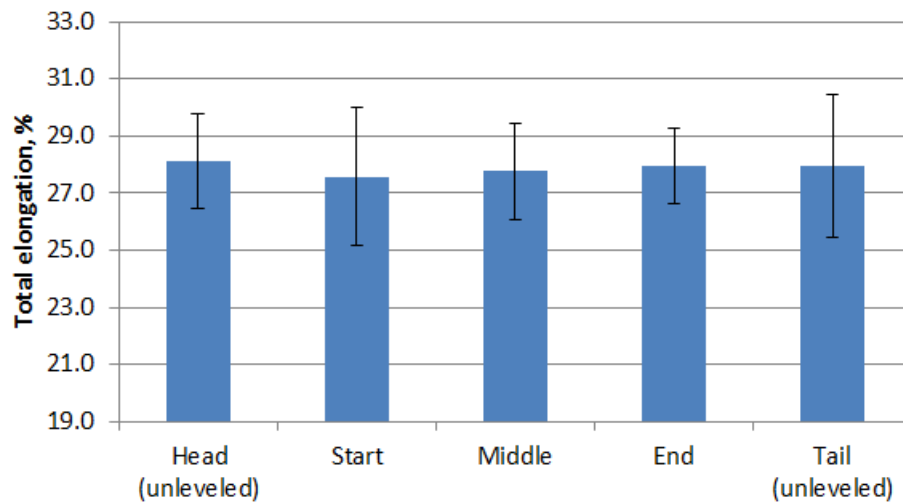


Figure 50: Total elongation (%) for EDM'd edge at different locations along coil in diagonal direction (DD).

Appendix B

Results of forward stepwise linear regression analysis for the radius upper trim steel shapes are shown in Figure 51. The significant regression terms are indicated with a p-value < 0.05.

	-----Step 1-----		-----Step 2-----		-----Step 3-----		-----Step 4-----	
	Coef	P	Coef	P	Coef	P	Coef	P
Constant	24.907		27.213		27.789		27.452	
Clearance	-14.52	0.000	-14.182	0.000	-16.78	0.000	-16.80	0.000
Radius			-6.78	0.000	-7.00	0.000	-7.09	0.000
Direction			-2.095	0.002	-2.097	0.001	-1.157	0.138
Radius*Direction			-1.68	0.610	-1.67	0.599	-1.65	0.558
Support					-1.167	0.070	-0.425	0.581
Clearance*Support					5.79	0.003	5.80	0.003
Support*Direction							-2.095	0.009
Radius*Clearance								
Clearance*Direction								
Radius*Clearance*Direction								
Radius*Support								
Radius*Clearance*Support								
Radius*Support*Direction								
Clearance*Support*Direction								
Radius*Clearance*Support*Direction								
S		3.23645		2.91782		2.87693		2.84467
R-sq		34.53%		47.57%		49.33%		50.75%
R-sq(adj)		34.34%		46.63%		48.11%		49.27%
R-sq(pred)		33.75%		45.15%		46.41%		47.25%
Mallows' Cp		112.29		32.42		24.27		18.44

Figure 51: Results of forward stepwise linear regression analysis for the radius upper trim steel shapes. Significant terms were considered when p-value < 0.05.

Tabulated results of the final linear regression model for the radius upper trim steel shapes are shown in Figure 52. The significant regression terms are indicated with a p-value < 0.05. The residual chart for this regression model is shown in Figure 53. The residual variance was fairly constant across the fitted values satisfying the assumption of equal variance. Independence assumption was also satisfied as there were no obvious trends in the observation sequence of residual values. However, the distribution of residuals was not normal. In attempt to alleviate the problem, the elongation data was transformed by applying a Box-cox transformation. Box-cox transformation showed a slight improvement in R^2 value, equality of residual variance, and normality of residuals. However, compared to the non-transformed model, the box-cox transformation did not significantly affect the decoded regression coefficients or significance. Therefore, a non-transformed model was chosen to simplify the analysis.

Analysis of Variance

Source	DF	Adj SS	Adj MS	F-Value	P-Value
Regression	8	2759.49	344.94	42.73	0.000
Radius	1	485.94	485.94	60.20	0.000
Clearance	1	1342.87	1342.87	166.36	0.000
Support	1	2.44	2.44	0.30	0.583
Direction	2	65.46	32.73	4.05	0.018
Clearance*Support	1	74.42	74.42	9.22	0.003
Support*Direction	2	76.85	38.43	4.76	0.009
Error	334	2696.06	8.07		
Lack-of-Fit	60	939.72	15.66	2.44	0.000
Pure Error	274	1756.34	6.41		
Total	342	5455.55			

Model Summary

S	R-sq	R-sq(adj)	R-sq(pred)
2.84113	50.58%	49.40%	47.86%

Coefficients

Term	Coef	SE Coef	T-Value	P-Value	VIF
Constant	27.503	0.562	48.97	0.000	
Radius	-7.373	0.950	-7.76	0.000	1.01
Clearance	-16.80	1.30	-12.90	0.000	1.88
Support					
Low	-0.422	0.767	-0.55	0.583	6.24
Direction					
LD	-1.450	0.521	-2.78	0.006	2.56
TD	-0.989	0.519	-1.91	0.057	2.54
Clearance*Support					
Low	5.80	1.91	3.04	0.003	4.95
Support*Direction					
Low LD	-0.168	0.752	-0.22	0.823	3.23
Low TD	-2.090	0.752	-2.78	0.006	3.19

Regression Equation

Support	Direction	Equation
High	DD	Elongation = 27.503 - 7.373 Radius - 16.80 Clearance
High	LD	Elongation = 26.053 - 7.373 Radius - 16.80 Clearance
High	TD	Elongation = 26.513 - 7.373 Radius - 16.80 Clearance
Low	DD	Elongation = 27.081 - 7.373 Radius - 10.99 Clearance
Low	LD	Elongation = 25.463 - 7.373 Radius - 10.99 Clearance
Low	TD	Elongation = 24.001 - 7.373 Radius - 10.99 Clearance

Figure 52: Tabulated results of the final linear regression model for the radius upper trim steel shapes including ANOVA table, R^2 value, and regression equations.

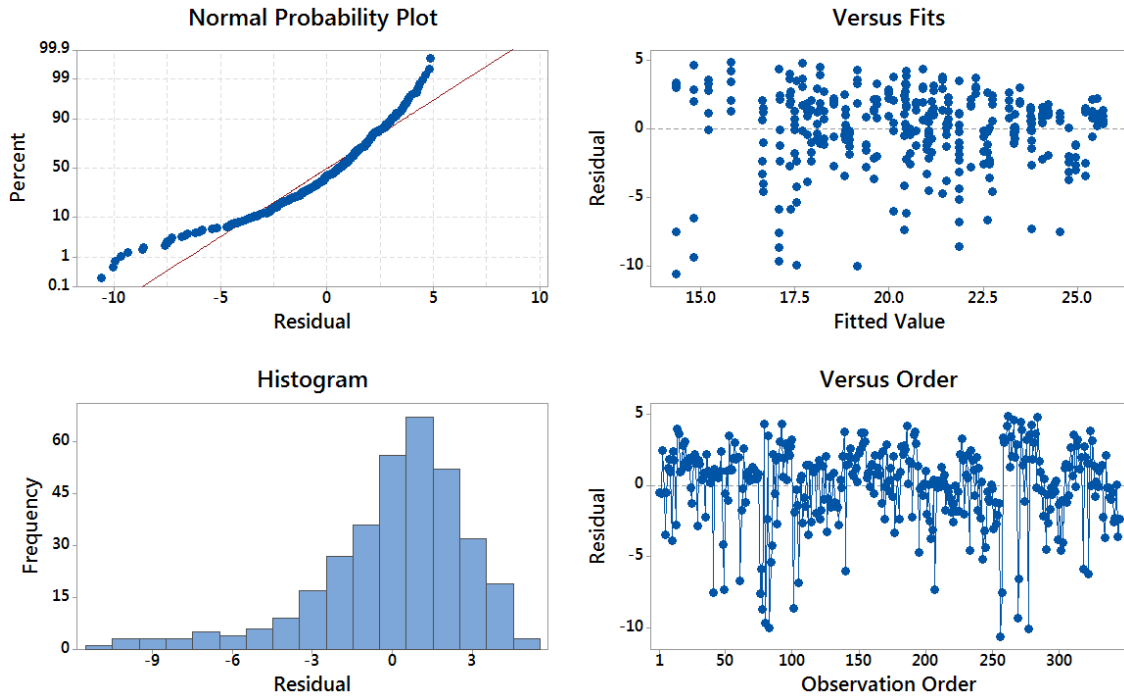


Figure 53: Diagnostic graphs of the residuals from the final linear regression model for the radius upper trim steel shapes.

Appendix C

Results of forward stepwise linear regression procedure for the radius upper trim steel shapes are shown in Figure 54. The significant regression terms are indicated with a p-value < 0.05.

	-----Step 1-----		-----Step 2-----		-----Step 3-----		-----Step 4-----	
	Coef	P	Coef	P	Coef	P	Coef	P
Constant	20.383		20.383		21.043		20.975	
Clearance	-16.29	0.000	-14.18	0.000	-14.53	0.000	-10.52	0.000
Gall Depth			-0.02385	0.000	-0.01927	0.000	-0.02495	0.000
Shape/Support					-1.321	0.000	-1.123	0.000
Gall Depth*Clearance							0.0567	0.392
Gall Depth*Shape/Support							0.01327	0.102
Clearance*Shape/Support							-7.13	0.008
Gall Depth*Clearance*Shape/Support							-0.1962	0.016
Direction								
Clearance*Direction								
Shape/Support*Direction								
Clearance*Shape/Support*Direction								
Gall Depth*Direction								
S	2.25185		2.09177		1.99424		1.93681	
R-sq	34.55%		43.77%		49.10%		52.81%	
R-sq(adj)	34.28%		43.29%		48.46%		51.38%	
R-sq(pred)	33.45%		42.33%		47.36%		49.54%	
Mallows' Cp	111.05		64.20		37.90		26.26	

Figure 54: Results of forward stepwise linear regression analysis for the radius upper trim steel shapes. Significant terms were considered when p-value < 0.05.

Tabulated results of the final linear regression model for the radius upper trim steel shapes are shown in Figure 55. The significant regression terms are indicated with a p-value < 0.05. The residual chart for this regression model is shown in Figure 56. The residual variance was fairly constant across the fitted values satisfying the assumption of equal variance. Independence assumption was also satisfied as there were no obvious trends in the observation sequence of residual values. However, the distribution of residuals was not normal. In attempt to alleviate the problem, the elongation data was transformed by applying a Box-cox transformation. Box-cox transformation showed a slight improvement in R^2 value, equality of residual variance, and normality of residuals. However, compared to the non-transformed model, the box-cox transformation did not significantly affect the decoded regression coefficients or significance. Therefore, a non-transformed model was chosen to simplify the analysis.

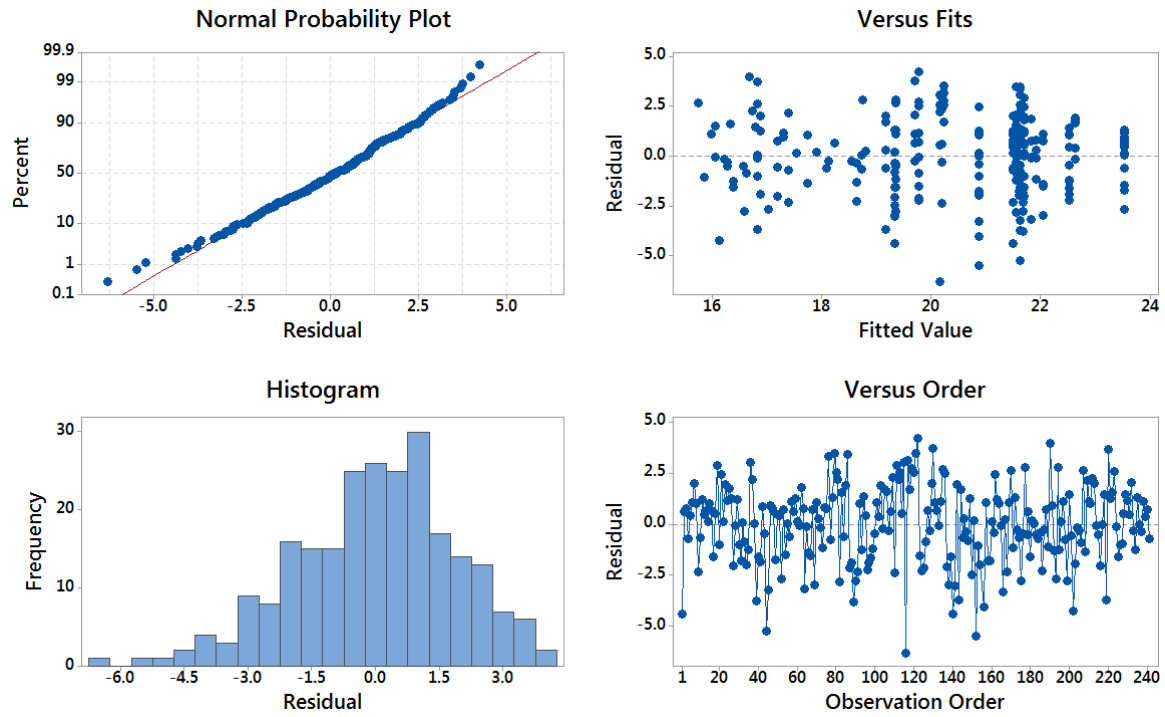


Figure 56: Diagnostic graphs of the residuals from the final linear regression model for the radius upper trim steel shapes.

Appendix D

Results of forward stepwise linear regression procedure for the radius upper trim steel shapes are shown in Figure 57. The significant regression terms are indicated with a p-value < 0.05.

	-----Step 1-----		-----Step 2-----	
	Coef	P	Coef	P
Constant	22.741		23.915	
Clearance	-14.92	0.000	-14.92	0.000
Shape/Support			-2.349	0.000
Direction				
Clearance*Direction				
Gap (um)				
Gap (um)*Clearance				
Gap (um)*Direction				
Gap (um)*Clearance*Direction				
S		2.17675		1.83330
R-sq		32.15%		52.07%
R-sq(adj)		31.86%		51.67%
R-sq(pred)		31.00%		50.85%
Mallows' Cp		135.00		28.06

Figure 57: Results of forward stepwise linear regression procedure for the radius upper trim steel shapes. Significant terms were considered when p-value < 0.05.

Tabulated results of the final linear regression model for the radius upper trim steel shapes are shown in Figure 58. The significant regression terms are indicated with a p-value < 0.05. The residual chart for this regression model is shown in Figure 59. The residual variance was fairly constant across the fitted values satisfying the assumption of equal variance. Independence assumption was also satisfied as there were no obvious trends in the observation sequence of residual values. However, the distribution of residuals was not normal. In attempt to alleviate the problem, the elongation data was transformed by applying a Box-cox transformation. Box-cox transformation showed a slight improvement in R^2 value, equality of residual variance, and normality of residuals. However, compared to the non-transformed model, the box-cox transformation did not significantly affect the decoded regression coefficients or significance. Therefore, a non-transformed model was chosen to simplify the analysis.

Analysis of Variance

Source	DF	Adj SS	Adj MS	F-Value	P-Value
Regression	2	865.47	432.737	128.75	0.000
Clearance	1	534.33	534.335	158.98	0.000
Shape/Support	1	331.14	331.140	98.52	0.000
Error	237	796.56	3.361		
Lack-of-Fit	235	796.20	3.388	18.75	0.052
Pure Error	2	0.36	0.181		
Total	239	1662.03			

Model Summary

S	R-sq	R-sq(adj)	R-sq(pred)
1.83330	52.07%	51.67%	50.85%

Coefficients

Term	Coef	SE Coef	T-Value	P-Value	VIF
Constant	26.900	0.290	92.80	0.000	
Clearance	-14.92	1.18	-12.61	0.000	1.00
Shape/Support					
0.14R/High	-2.349	0.237	-9.93	0.000	1.00

Regression Equation

Shape/Support
0.04R/Low Elongation (%) = 26.900 - 14.92 Clearance

0.14R/High Elongation (%) = 24.550 - 14.92 Clearance

Figure 58: Tabulated results of the final linear regression model for the radius upper trim steel shapes including ANOVA table, R^2 value, and regression equations.

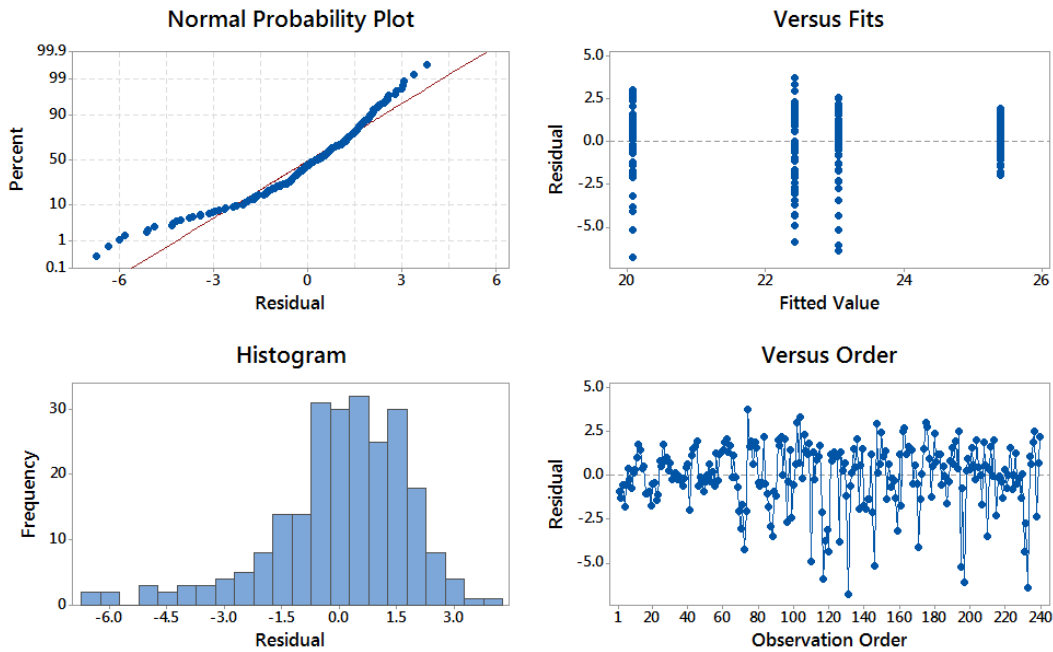


Figure 59: Diagnostic graphs of the residuals from the final linear regression model for the radius upper trim steel shapes.